

**Deposition and Comparative Wear
Study of Thin Film Coatings**

A thesis for the degree of M. Eng.

Presented to

Dublin City University

by

Md. Abdul Azim, M.Sc.(Eng.)

School of Mechanical & Manuf. Engg.

Dublin City University

Research Supervisors

Professor M.S.J. Hashmi

Dr. D.C. Cameron

November, 1994.

Acknowledgements

I wish to express my sincere thanks to my supervisor, Professor M.S.J. Hashmi who provided me the opportunity to undertake this research project for M. Eng. degree. Throughout the course of this thesis, he has been a constant source of advice, support and encouragement, which is and will always be much appreciated.

I wish to express my sincere thanks to Dr. David C. Cameron, School of Electronic Engineering, Dublin City University, for his guidance and tuition in doing deposition of molybdenum nitride films and their characterization.

Special thanks to Mr. Michael J. Murphy, Research Officer, Advanced Materials Processing Centre, D.C.U, for his assistance throughout this research work. I am also grateful to Mr. David M. Kennedy, Department of Mechanical Engineering, Carlow RTC, who kindly allowed me to carry out the wear tests using his test rig.

My sincere thanks to the staff of the workshop in the School of Mechanical and Manufacturing Engineering who helped in the fabrication work of the test rigs.

Finally, I wish to thank all for their suggestions and help at various stages of this research work and in the preparation of this thesis.

Deposition and Comparative Wear Study of Thin Film Coatings.

Md. Abdul Azim

Abstract

As a part of a group project a magnetron deposition system was designed, constructed and commissioned for producing thin film coatings. Deposition of molybdenum nitride films has been carried out using reactive magnetron sputtering for characterization. The films were characterized in terms of their thickness, hardness and adhesion. The films were reasonably hard but poorly adherent to the steel flats.

A wear test rig designed, constructed and commissioned by another research student to carry out impact wear tests was adapted for adhesive wear tests. Progressive wear tests have been done on titanium carbide (5% titanium) coated, titanium nitride coated and uncoated specimens of four substrate materials. The substrate materials are: i) D2 tool steel, ii) D3 tool steel, iii) Vanadis 4 and iv) Vanadis 10. Titanium carbide coatings proved to have good wear resistance but titanium nitride coatings did not. Different coatings imparted different wear resistance to the substrate. The substrate materials have a profound effect on the wear resistance of the coated surfaces.

Contents

	Page
Acknowledgements	i
Abstract	ii
Contents	iii
List of Abbreviations	vi
List of Notations	vii
Chapter 1 Introduction	
1.1 Introduction	1
1.2 Surface Engineering Technology	1
1.2.1 Introduction	1
1.2.2 Magnetron Sputtering	2
1.2.2.1 Introduction	2
1.2.2.2 Magnetrons	9
1.2.2.3 Film Microstructures	10
1.2.2.4 Ion Bombardment	16
1.2.2.5 Internal Stress	17
1.2.2.6 Substrate Effects	18
1.2.2.7 Hysteresis Effect	18
1.3 Study of Wear	20
1.3.1 Introduction	20
1.3.2 Adhesive Wear	22
1.3.3 Reduction of Adhesive Wear	24
1.4 Literature Review	25
1.4.1 Introduction	25
1.4.2 Sputtering	25
1.4.3 Wear	27
1.5 Objective of the Present Study	30
Chapter 2 Experimental Equipment	
2.1 Introduction	31
2.2 Equipment for Deposition	31
2.2.1 Deposition Chamber	31
2.2.2 Magnetrons	38

2.2.3	Cooling System	39
2.2.4	Pumping Stack	43
2.2.5	Gas Supply System	43
2.2.6	Substrate Biasing	44
2.2.7	Substrate Preheating	44
2.2.8	Residual Gas Analyzer	46
2.2.9	Substrate Table Assembly	46
2.3	Equipment for Characterization	47
2.3.1	Interferometer	47
2.3.2	Microhardness Tester	49
2.3.3	Scratch Tester	52
2.4	Equipment for Wear Generation	53
2.4.1	Substrate Table	53
2.4.2	Wear Tools	53
2.4.3	Sliding Mechanism	53
2.4.4	Revolution Counter	55
2.5	Equipment for Wear Measurement	55

Chapter 3 Experimental Procedure

3.1	Introduction	58
3.2	Deposition of Films	58
3.2.1	Commissioning with Ti Film Deposition	58
3.2.2	Commissioning with TiN Film Deposition	63
3.2.3	Deposition of MoN _x Films	64
3.3	Deposition of Ti _x C and TiN Films by External Supplier	68
3.4	Characterization of Films	68
3.4.1	Thickness	68
3.4.2	Hardness	69
3.4.3	Adhesion	70
3.5	Generation of Wear	70
3.6	Measurement of Wear	71

Chapter 4 Results and Discussions

4.1	Introduction	72
4.2	Deposited MoN _x Films	72

4.2.1	Effect of Substrate Bias	72
4.2.1.1	Deposition Rate	73
4.2.1.2	Hardness	73
4.2.2	Effect of Deposition Pressure	73
4.2.2.1	Deposition Rate	73
4.2.2.2	Hardness	74
4.2.3	Effect of Magnetron Current	74
4.2.3.1	Deposition Rate	74
4.2.3.2	Hardness	75
4.3	Wear Tests on Specimens Coated by External Supplier	88
4.3.1	Profiles Across the Wear Track	88
4.3.2	Effect of Number of Cycles on Wear	93
4.3.3	Wear of Coated and Uncoated Surfaces	118
4.3.4	Comparative Wear of Different Coatings	118
4.3.5	Effect of Substrate Materials on Wear	127
4.3.6	Effect of Coating Hardness and Adhesion on Wear	130

Chapter 5 Conclusions and Suggestions for Further Work

5.1	Introduction	133
5.2	Conclusions	133
5.2.1	Deposition of MoN _x Films	133
5.2.2	Wear Tests on Specimens Coated by External Supplier	134
5.3	Suggestions	134
5.3.1	Deposition of MoN _x Films	134
5.3.2	Wear Tests on Specimens Coated by External Supplier	135

References	136
------------	-----

Appendix A	A1
------------	----

List of Abbreviations

d.c.	direct current
MFC	mass flow controller
PES	plasma emission spectrometer
PTFE	polytetrafluoroethylene
PVD	physical vapour deposition
r.f.	radio frequency
rpm	revolution per minute
sccm	standard cubic centimeter per minute
VM	vertical magnification

List of Notations

α_f	thermal expansion of the film
α_s	thermal expansion of the substrate
Ar	argon
d_{ts}	target to substrate distance
G	gauss
λ	1.wavelength of emission, 2.wavelength of light
Mo	molybdenum
MoN_x	molybdenum nitride
Mo_2O_3	molybdenum oxide
N_2	nitrogen
P	power
p	pressure
SiN	silicon nitride
Ti	titanium
Ti_2C	titanium carbide
TiN	titanium nitride

Chapter 1

Introduction

1.1 Introduction

The importance of materials for the evolution of human society is incalculable. The demands on the performance of components are ever increasing and homogeneous materials are often unable to meet all the necessary requirements. Dating from Egyptian times, the enhancement of performance of materials by the application of coatings has an ancient history, when marble coffins were covered in gold to increase aesthetic properties. Such enhanced properties resulted in the development of coatings for the following applications: thermal barrier properties, corrosion resistance, biocompatible applications, electronic applications, tribological properties, optical use, decorative use etc.

1.2 Surface Engineering Technology

1.2.1 Introduction

Surface Engineering technology encompasses the techniques and processes which are used to induce, modify and enhance the performance of surfaces. It also covers the characterization of such surfaces and interfaces. It designs a composite system of coating and substrate for desired performance which cannot be achieved by either the coating or substrate alone. The expanding use of surface coating technologies has generated a need to understand the interrelationship between the mechanical, physical and chemical properties of the coating substrate system and so enhance performance in many engineering applications. It undertakes to assess the basic quality of a coating and to determine if the properties of a particular coating are suitable for the intended application. There is strong economic justification for improving surfaces e.g. the wear and corrosion resistance properties imparted by coatings to a substrate may increase the life of different parts of machinery.

Many coating deposition techniques and surface treatments are available for the modification of surface characteristics. Selection of the coating deposition or surface treatment technique depends on the functional requirements, shape, size and metallurgy of the substrates, availability of the coating materials for the technique, level of

adhesion desired, availability of coating equipment and cost. This selection of a suitable coating deposition or surface treatment technique often becomes difficult. It requires a thorough understanding of the merits and limitations of each technique. The methods of deposition technology are classified as shown in Fig.1.1.

1.2.2 Magnetron Sputtering

1.2.2.1 Introduction

Sputtering is a process whereby coating material is dislodged and ejected from the solid or liquid surface due to the momentum exchange associated with surface bombardment by energetic particles as shown in Fig.1.2. The high energy particles are usually positive ions or energetic neutrals of a heavy inert gas. The sputtered material is ejected primarily in atomic form from the source of the coating material, called the target. The substrate is positioned in front of the target so as to intercept the flux of sputtered atoms as shown in Fig.1.3. The sputtering momentum exchange occurs primarily within a region extending only about 1nm below the surface. The basic processes involving sputtering are: i) glow discharge and ii) ion beam.

In the glow-discharge sputtering process, a target is placed into a vacuum chamber which is evacuated to 10^{-7} to 10^{-5} torr and then back filled with a working gas, such as an inert gas (say Ar), to a pressure (5×10^{-3} to 10^{-1} torr for conventional planar diode processes) adequate to sustain a plasma discharge. A negative bias (0.5 to 5 kV for a d.c. device) is then applied to the target so that it is bombarded by positive ions from the plasma. Ions accelerated by this voltage impact on the target and cause ejection sputtering of the target materials. Glow-discharge sputtering technology is limited in the sense that the target current density and voltage cannot easily be independently controlled except by varying the working gas pressure or using coils instead of permanent magnets. The following are the categories of glow-discharge sputtering: i) diode sputtering, ii) triode sputtering and iii) magnetron sputtering.

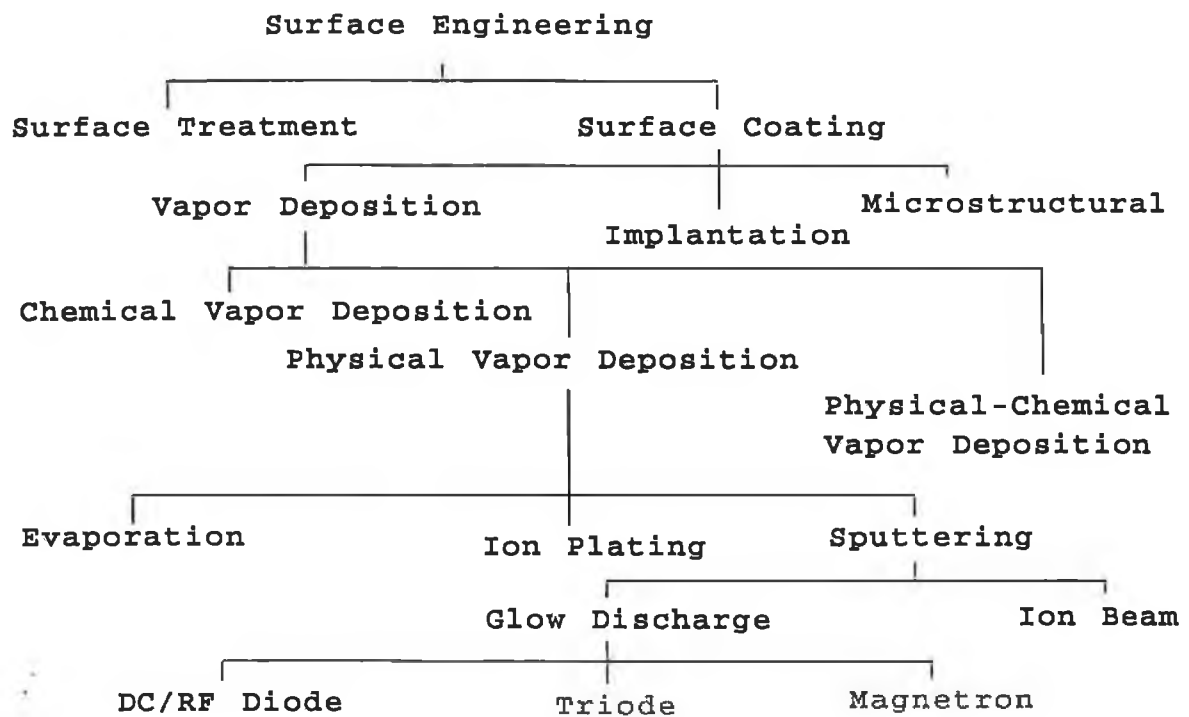
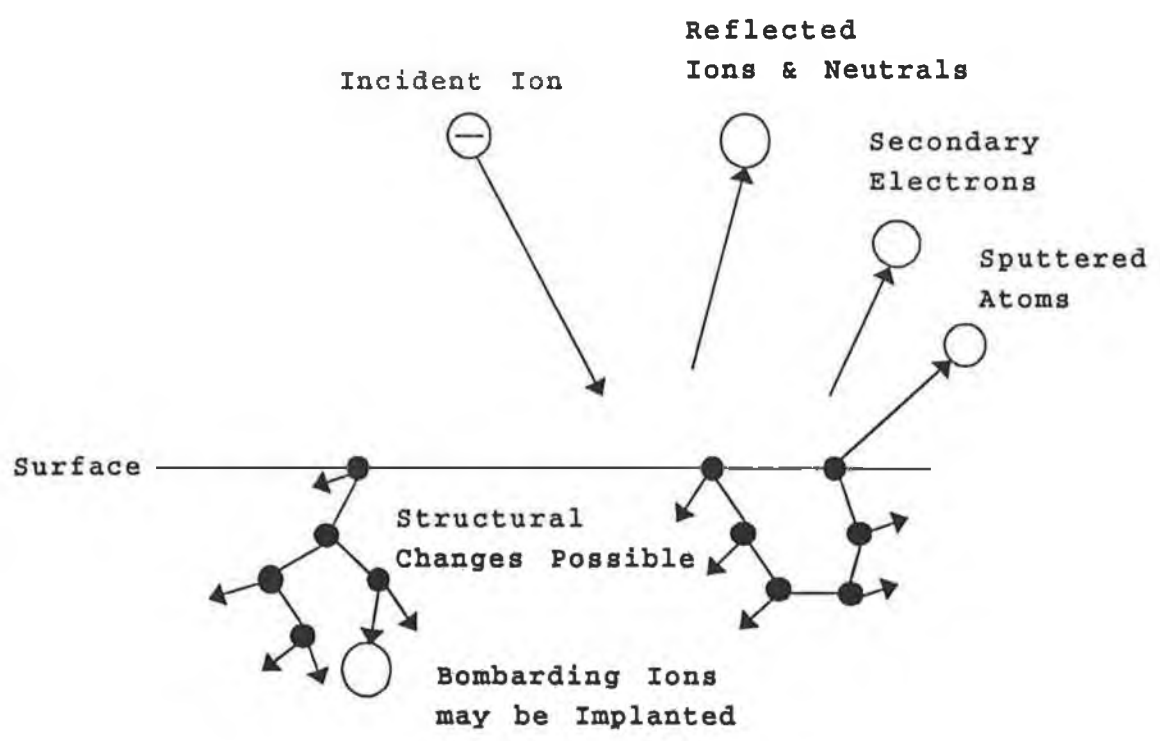


Fig.1.1 Various surface engineering techniques.



Collision Sequences:
may Terminate within
the Target

or

Result in the Ejection of
a Target Atom (Sputtering)

Fig.1.2 Sputtering process [85].

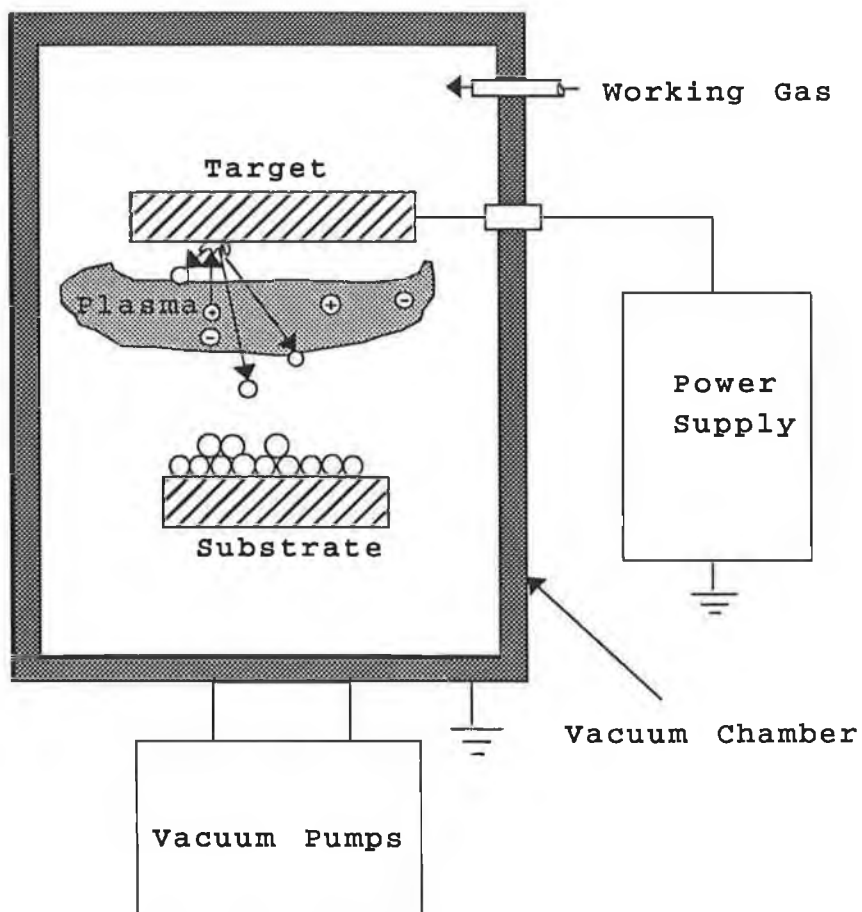


Fig.1.3 Schematic diagram of sputter coating process [47].

The magnetically assisted glow-discharge sputtering process is called magnetron sputtering. This process provides 1) relatively high deposition rates, 2) large deposition areas and 3) little substrate heating, which is revolutionizing the sputtering process by greatly expanding the range of feasible applications. In the present study, magnetron sputtering is used to grow films. In magnetron sputtering, the ionization efficiency of the available electrons is increased by a magnetic field. This allows sputtering at a lower pressure and provides greater current for a given applied voltage at constant pressure. One effect of the magnetic field B in conjunction with the electric field E is to form an electron trap which is configured so that an $E \times B$ drift current closes on itself as shown in Fig.1.4(a). Also the electrons must travel over a longer path (along which they continue to cause ionization) to advance a given distance from the cathode as shown in Fig.1.4(b). In this way, the magnetic field acts as though the gas pressure had been increased. Another effect of the magnetic field is the hindrance of radial diffusion of the electrons out of the glow, so that the loss of electrons which would otherwise be available for ionization is reduced. The intense ionization is responsible for rapid sputtering and rates of deposition up to $2 \mu\text{m}/\text{min}$ are possible. The intense energies used in sputtering generates much heat. This must be dissipated by water cooling of the magnetrons.

The major sources of gaseous impurities in sputtering systems are residual gases (mainly H_2O) left after initial pump out, wall desorption due to bombardment, the surface of the target (gases adsorbed when the system is vented), occluded gases in the sputtering target, backstreaming of pump fluids, leaks, and impurities in the gas supply itself. Many of these can be eliminated by a combination of good vacuum practice and extensive presputtering before coating deposition. Reactive impurities in the inert gas sources can be reduced by passing the gas through hot titanium sponge before introducing it to the process chamber. A significant improvement in the purity level of coatings during sputtering can be obtained by bias sputtering or getter sputtering. In a getter sputtering system, the sputtering gas is made to pass over an area of freshly deposited coating material. Any impurity atoms in the sputtering gas would have made a large number of collisions with depositing coating material before reaching the central region. This resulted in very high probability of the impurity atoms of being removed. However, no methods are currently available to prevent nongaseous impurities present in the cathode from finding their way into the coatings.

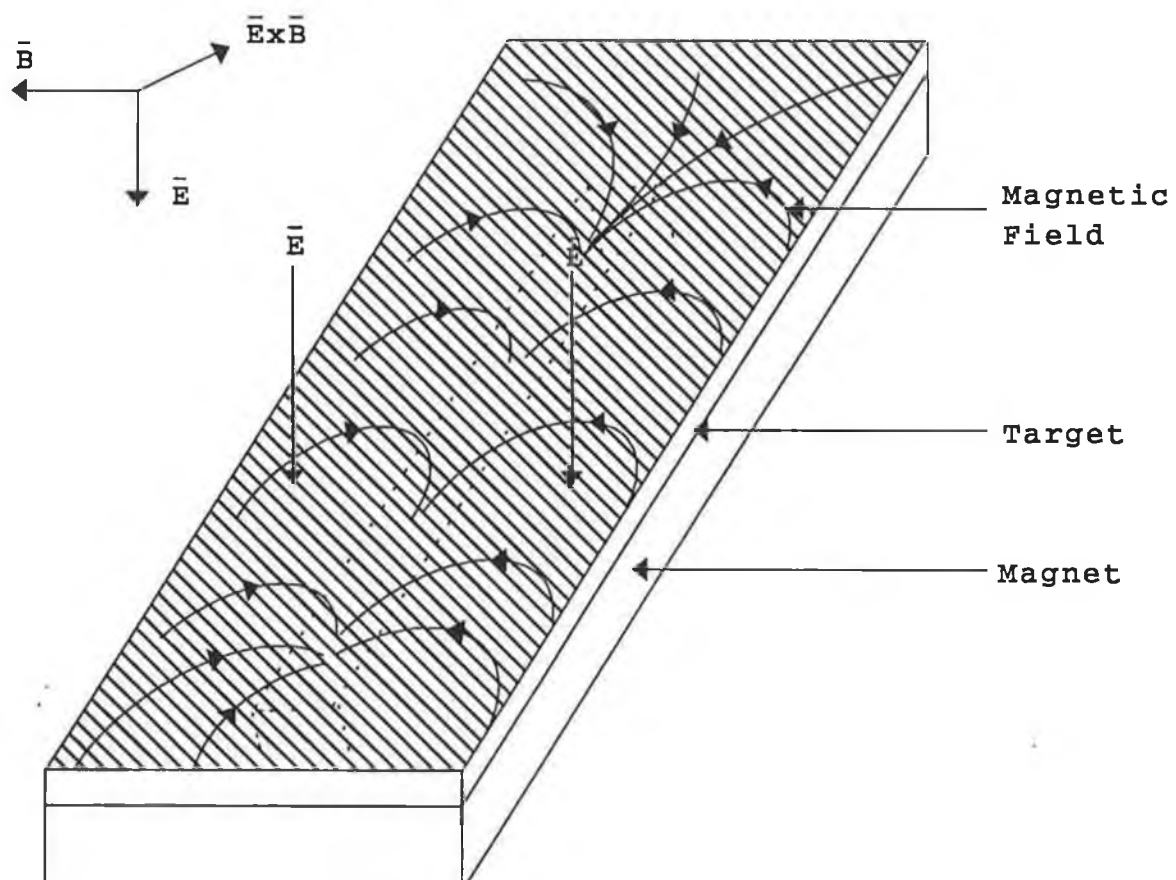


Fig.1.4(a) Planar magnetron configuration [85].

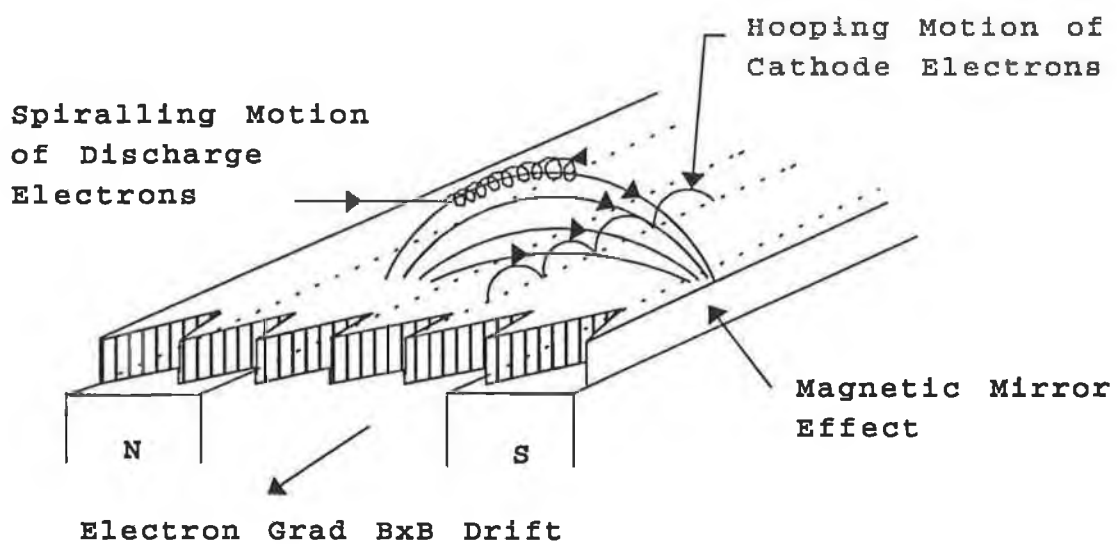


Fig.1.4(b) Electron motions in planar magnetron configuration [85].

1.2.2.2 Magnetrons

Magnetrons are a class of cold cathode discharge devices which are generally used in a diode mode. The plasma is initiated between the cathode and the anode at pressure in the mtorr range by the application of a high voltage, which can be either d.c. or r.f. A variety of geometric arrangements give efficient performance such as the long rectangular planar magnetron, cylindrical magnetron with post or hollow cathodes, and plasma ring sources. The most widely used is the planar magnetron, because of the simplicity of target manufacture.

In essence, the planar magnetron is the classic d.c. or r.f. diode sputtering arrangement consisting of a planar (cathode) and its surrounding dark-space field with the essential addition of permanent magnets directly behind the cathode. Magnet arrangements can be varied substantially; all have in common a closed path or region where the magnetic field lines are parallel to the cathode surface. For instance, the paths may be single or multiple circles or ovals, concentric circles or ovals, etc. Permanent magnets, electromagnets, or a combination of both can be used. A magnetic field parallel to the cathode surface can restrain the primary electron motion and thereby increase the ionization efficiency. The disadvantage of the planar magnetron is that the target erodes only in the transverse magnetic field region, which leads to a V-shaped erosion profile. This reduces the life of the target considerably. To overcome this, various means have been tried, such as targets of higher thickness, oscillating magnetic field, mechanical movement of magnets. Another disadvantage is coating thickness non-uniformity.

When the target material is in direct contact with the cooling water, a directly cooled magnetron results. For expensive materials, or ones in which rigidity is insufficient to provide adequate support, the material is attached to a backing plate by epoxy or screws. This is referred to as an indirectly cooled magnetron. Directly cooled magnetrons allow for higher deposition rates due to their more efficient heat dissipation.

The main disadvantages associated with magnetron sputtering and ways to overcome them are:

1. The sharp decrease of the substrate ion current with increasing distance of substrates from the magnetron target thus resulting in a decrease of deposition rate. This can be rectified by i) additional gas ionization e.g. by use of a hot cathode electron beam [46] or a hollow cathode arc electron source [56] or ii) by the magnetic confinement of the plasma, using an unbalanced magnetron [41,54,63,64,71].
2. Compared to other deposition processes, it has relatively poor throwing power which can be rectified by i) applying a bias to the substrate or ii) increasing the system pressure. Furthermore magnetron sputtering is fundamentally a line-of-sight type deposition process. However any limitation arising due to this fact can be overcome by i) utilizing more than one target, ii) rotating the substrate or c) confining the plasma between the substrate and target by using unbalanced magnetrons.

An unbalanced magnetron is one in which the magnetic fields of the opposing magnetic polarity are not equal as shown in Fig.1.5. This imbalance in the magnetic field strength can be achieved by either making the outer ring or inner ring of magnets stronger. Conventionally, the outer ring is made the stronger of the two. The resulting magnetic field line configuration allows some of the plasma in front of the target to leak towards the substrate so enhancing the ionization there. This leads to greater ion bombardment of the growing coating. Denser, harder coatings result. The increased ionization caused by the unbalanced magnetrons increases the sputter yield at a specific area between the two rings of magnets called racetrack as shown in Fig.1.6.

1.2.2.3 Film Microstructures

The properties of the coatings are highly dependent on the film microstructure which depends on the interdependent parameters in magnetron sputtering e.g. substrate bias, target power, total pressure and substrate temperature [70]. TiN films deposited at moderate

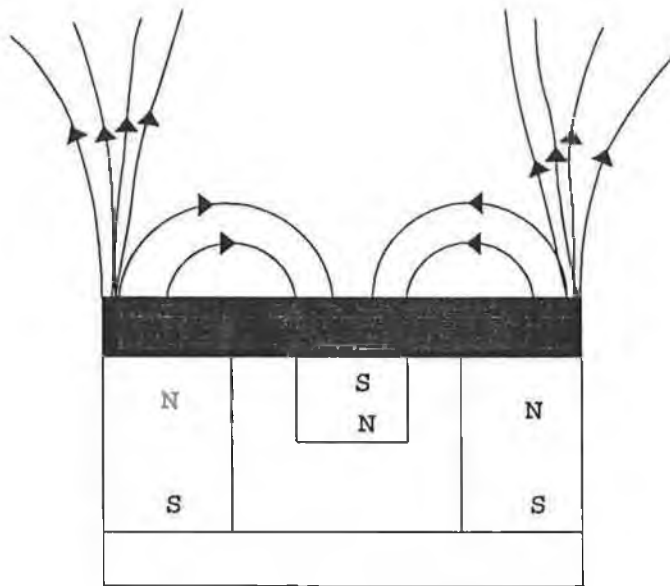


Fig.1.5 Unbalanced magnetron [85].

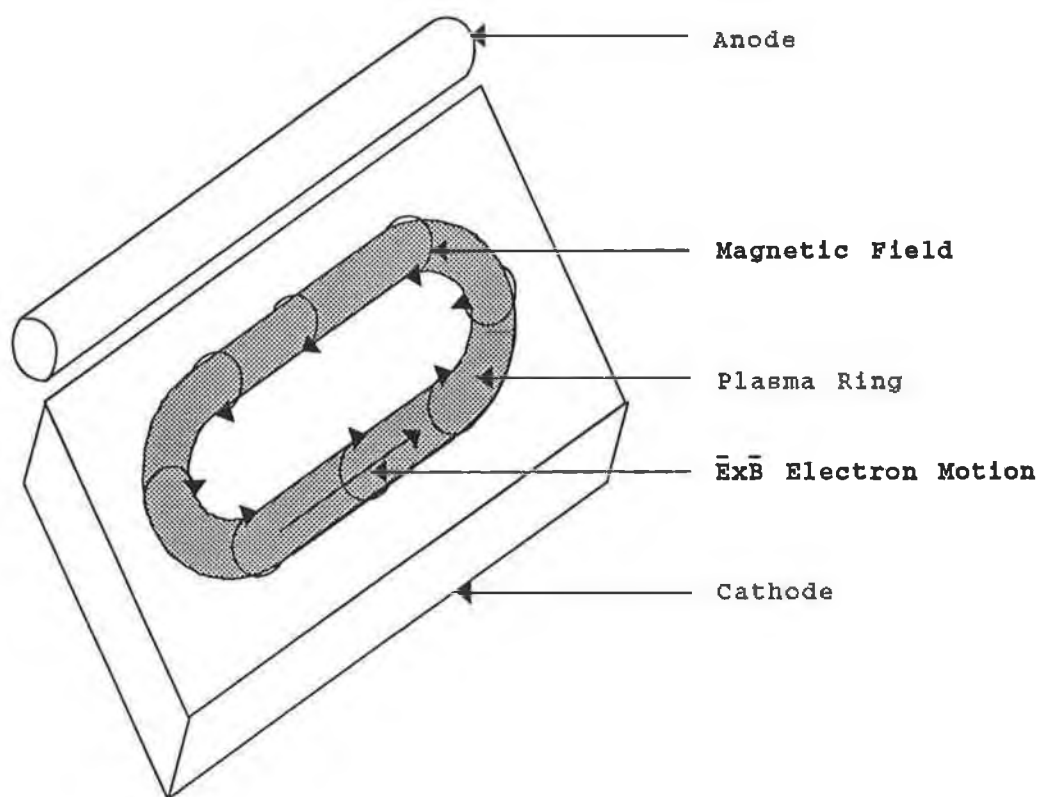


Fig.1.6 Planar magnetron with magnetic end confinement [47].

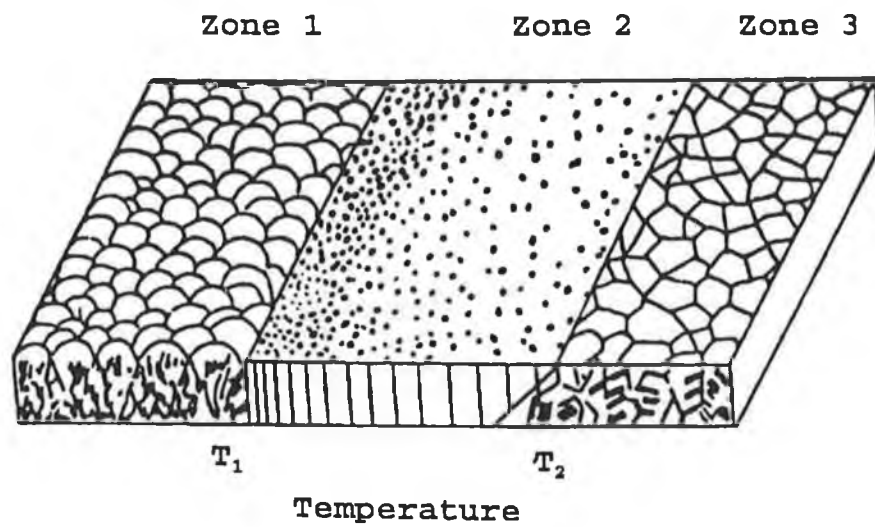
substrate bias possess a dense compact golden coloured nature. Increasing substrate temperature increases the densification of the TiN coatings while at low temperature the coatings are porous. Xing [58] found that hardness of ion plated TiN coatings varied with both the ion plating process and the base material. The hardness of the coatings increases with hardness of the base material.

In classifying thin film microstructures Movchan and Demchishin [29] were the pioneers. Results were based on their structure zone diagram as a function of T/T_m (where T is the temperature of the substrate surface and T_m is the melting temperature of the material) shown in Figs.1.7(a)&1.7(b). Low temperature Zone I structure, corresponding to low adatom mobility consisted of tapered columns with domed tops and voided boundaries. Computer simulation adds that atomic shadowing is prevalent which in combination with limited surface mobility explains the basic Zone I characteristics [32,36]. Increase in T/T_m increases the crystal diameter, implying a low activation energy and little surface diffusion. For metals $T/T_m < 0.3$ and for oxides $T/T_m < 0.26$.

Increasing temperature resulted in increased surface diffusion and a structure of straight columnar grains with a smooth topography in Zone II. Müller [60] showed that with increasing T/T_m the atomic shadowing in Zone I was dispelled. He also explained the movement of Zone I to Zone II microstructure with increasing surface diffusion. For metals $0.3 < T/T_m \leq 0.45$ and for oxides $0.26 < T/T_m \leq 0.45$.

Zone III structures are produced by further increasing the temperature. These are characterized by equiaxed grains due to recrystallization effects of such high temperatures. The coating is usually fully annealed. Typically, $0.45 < T/T_m < 1.0$ for metals and oxides.

It has been reported in reference [75] that the temperature of the substrate affects the size of the crystallites being formed. They also reported that the conditions under which the crystallization process occurs seems to affect the shape and scatter of the size of the



	Zone 1	Zone 2	Zone 3
Metals	$< 0.3 T'_m$	$0.3 - 0.45 T'_m$	$> 0.45 T'_m$
Oxides	$< 0.26 T'_m$	$0.26 - 0.45 T'_m$	$> 0.45 T'_m$

Fig.1.7(a) Structural zones in condensates[47].

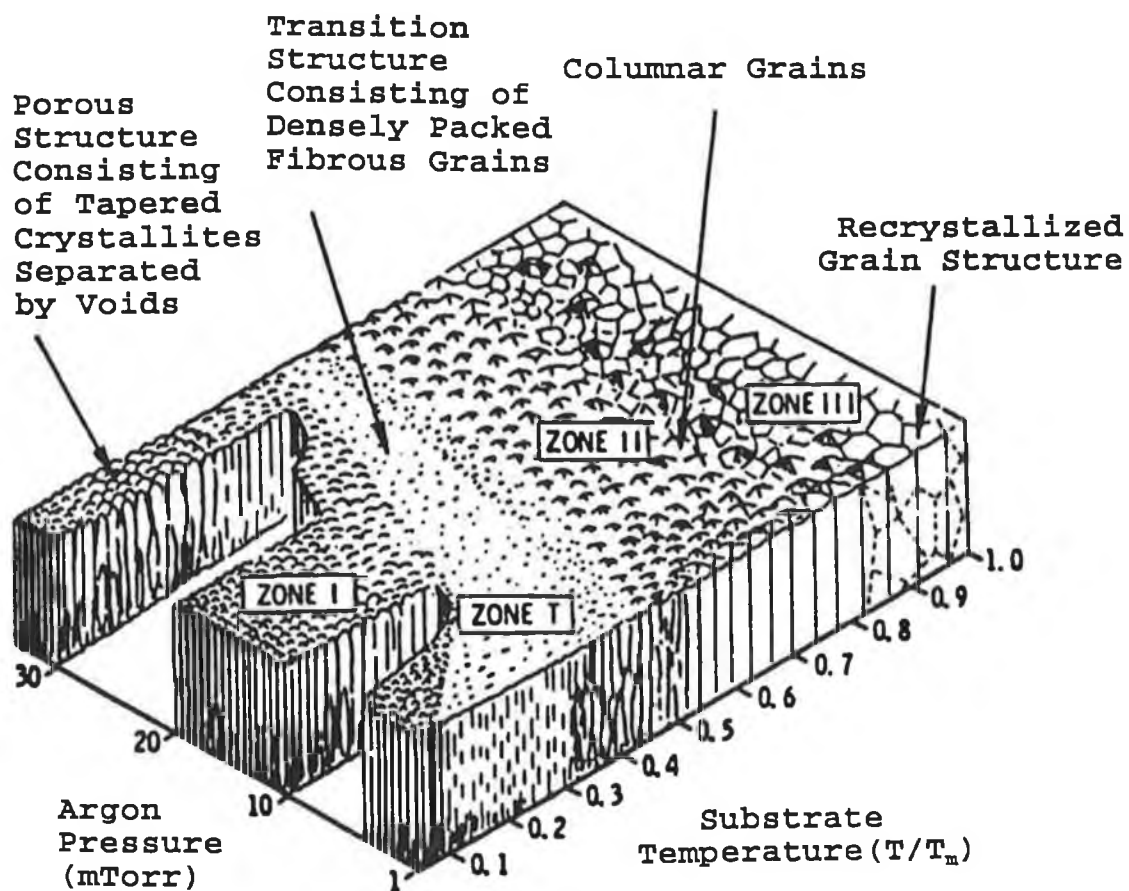


Fig.1.7(b) Structural zones in condensates [47].

crystallites. Further work undertaken by Thornton [37] necessitated the inclusion of Zone T, which is present under the effects of a sputtering gas as shown in Fig.1.7(b). Zone T consists of poorly defined fibrous grains. Zone I microstructures can shift towards Zone T by either thermally inducing greater adatom mobility or by ion bombardment. Momentum exchange then causes the coating atoms to fill the boundaries of loosely packed Zone I columns. A new model developed by Messier et al [51] accounted for both the effects. In essence, this model shows that ion bombardment promotes Zone T type dense structures.

1.2.2.4 Ion Bombardment

Physically and chemically adsorbed layers on the substrate are removed by ion bombardment prior to the deposition of films. This removal process is called sputter etching. Such layers may hinder adhesion. This process can also produce an atomistically rough surface on the substrate which renders mechanical bonding of the coatings to the samples.

During deposition ion bombardment can produce graded interfaces which provide true metallurgical bonding and reduces the effects of interfacial stress due to differences in the mechanical and thermal properties of the coatings and substrate materials [53]. Graded interfaces are most likely formed by the intermixing of the atoms at the interface due to the high energy impacts of ions and neutrals. The bombarding ions impart energy into the growing films, increase adatom mobility and forward sputter the film materials into voids and interstitial sites [74].

Ion bombardment can provide densification of films in many ways. The electrons and negative ions in the plasma accelerate towards a positively biased substrate causing ion and electron bombardment of the films. Biasing of the substrate at a small negative potential (-20 to -200 V) can also enhance further bombardment. The amount of ion bombardment is dependent on the plasma density and the bias on the substrate. The more negative the substrate bias, the greater is the bombardment. This can lead to other property modifications in addition to densification e.g. crystal growth, chemical content etc.

1.2.2.5 Internal Stress

The coatings possess inherent residual stress. The open columnar boundaries present in Zone I microstructures minimize this stress. Substantial stresses are generated in Zone T structures leading to an increase in stored elastic energy [55]. This may cause delamination of the film from the substrate.

In an investigation Rickerby et al [59] reported that variation of position affects the level of internal stress. The fine grained crystallites close to the coating-substrate interface can support high elastic stresses which indicates that yield strength is high and drops off as the coatings get thicker due to the larger grain size. Moreover, porosity increases as the coating gets thicker and stress relaxation occurs at the open columnar boundaries [67]. Hence the physical properties of the PVD coatings are directly dependent on the increased strength of grain boundaries, the application of a substrate bias to promote ion bombardment of the growing films and the correct choice of the substrate materials i.e. the coefficient of thermal expansion of the substrate should be greater than that of the films. Observations by other authors include the following:

1. Stress in films sputtered at the lowest pressures is compressive and becomes tensile at higher pressures due to thermalization of sputtered atoms and reflected energetic neutrals in collisions [74].
2. Stress in the films is compressive and its density increases with increasing ion bombardment [23,77].

PVD coatings are significantly harder when tested parallel to their growth direction compared with values derived from orthogonal directions [61].

Rudnik et al [78] indicated the possibility of a tensile residual stress in the reactively sputtered molybdenum nitride coatings for bias levels below -150 V. Such a tensile stress is unusual for reactively sputtered hard coatings. They also reported that at greater negative bias values the lattice expansion indicates a slightly compressive stress, but in these cases the bias level dramatically affects the composition of the coatings.

1.2.2.6 Substrate Effects

The growth pattern of the deposited coatings are defined by the substrate crystal. This substrate crystal affects the distribution, orientation and size of the crystallites nucleated on the growing surface [57,65]. The thermal expansivity of the substrate affects the level of the internal stress in the films. This stress in the films is compressive when $\alpha_f < \alpha_s$ and tensile when $\alpha_f > \alpha_s$ [65]. Rickerby [55,65] has suggested that compressive internal stresses may be an important factor in the determination of the porosity of PVD coatings.

1.2.2.7 Hysteresis Effect

The reactive gas combines with the sputtered atoms from the target to form a compound thin film. A higher level of reactive gas than necessary for the films to be fully reacted causes the formation of compound on the target surface. This compound formation on the target persists as the flow of reactive gas is reduced, until at a significantly lower flow level the target is exposed by physical sputtering. This general phenomenon is known as hysteresis effect.

Transitions from the first state to the second state and from the second state to the first state follow two different paths which are indicated in Figs.1.8(a)&1.8(b). In addition, deposition rate in the second state is significantly less than deposition rate in the first state. The film deposition rate also shows a hysteresis-like effect as a function of the flow of the reactive gas. In most cases the sputtering yield from the target decreases as a compound forms on the target surface and this phenomenon is called target poisoning. The use of a r.f. power supply to the magnetrons minimizes this effect. Another way of mitigating this target poisoning is to use feedback control. Rudnik et al [78] in their investigations mentioned that in the reactive sputtering of MoN_x films, there was no significant hysteresis or forbidden zone as observed with TiN films sputtering.

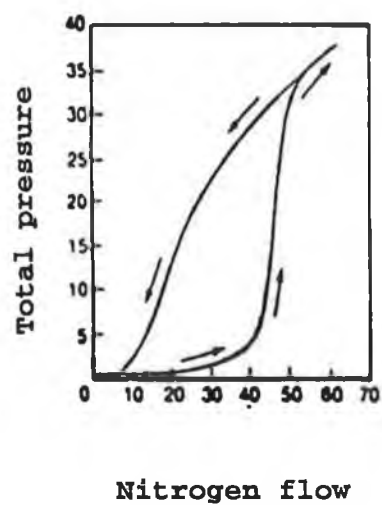


Fig.1.8(a) Hysteresis loop without feedback control [85].

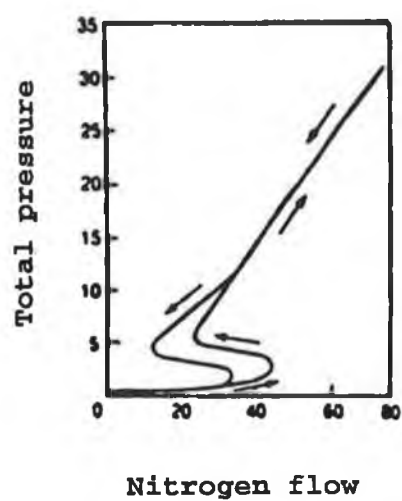


Fig.1.8(b) Hysteresis loop with feedback control [85].

1.3 Study of Wear

1.3.1 Introduction

Wear is a process in which the surface layers of a solid are ruptured as a result of the mechanical action of another body or medium. In general, wear as a function of operating time is a three-stage process as shown in Fig.1.9. The first stage is a non-equilibrium or running in stage of the wear process and represents only a small proportion of the total time of operation. The second stage is the steady state conditions of the wear process which is characterized by constant values of wear rate. This stage is the longest of the total operating time. The third stage is the catastrophic wear which is characterized by increasing wear rate and is not applicable to rubbing surfaces. In well-designed tribological systems, the removal of material is usually a very slow process, but it is very steady and continuous.

Wear is classified into six categories, which are based on quite distinct and independent phenomena. These are as follows: i) adhesive, galling or scuffing wear, ii) abrasive, scratching, scoring or gouging wear, iii) fatigue wear, iv) corrosive wear, v) erosive wear and vi) electrical arc-induced wear [66]. Another commonly encountered wear mode is fretting. This is not a distinct mechanism, but rather a combination of adhesive and abrasive forms of wear.

Wear is the main cause of material wastage and considerable savings can be made by controlling the wear. Using a suitable lubricant wear can often be controlled to an acceptable level. An understanding of various wear mechanisms is necessary for correct selection of materials, coatings, surface treatments, liquid lubricants and operating conditions for a given application. The ever increasing demand for reliability and long life of machines is one of the main problems of contemporary engineering; its economic importance is obvious. Statistical analysis shows that the main reason for the failure of machines is not breakage but wear of the moving parts resulting from rubbing stresses.

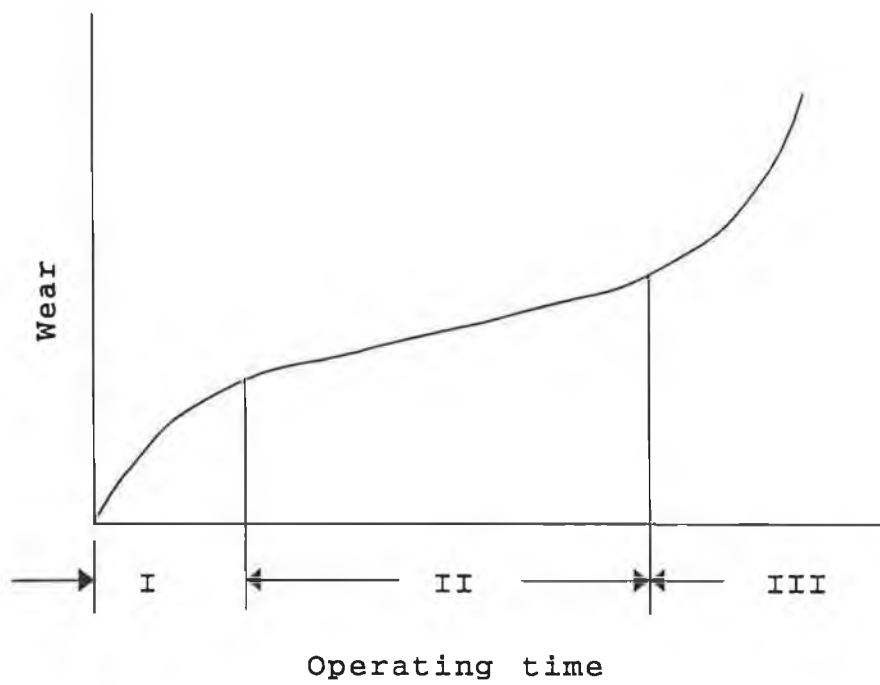


Fig.1.9 Wear as a function of operating time[43].

The following are the factors that influence wear in a sliding pair: 1) frictional properties of the materials, 2) presence of lubricants, 3) physico-mechanical properties of the materials, 4) loading conditions, 5) microgeometrical characteristics of the tool surface, 6) adhesion of the coating, 7) hardness of the materials, 8) surface roughness, 9) temperature, 10) elastic strength of the materials, 11) pressure in the rubbing process and 12) velocity of rubbing.

1.3.2 Adhesive Wear

Adhesive wear processes are initiated by the interfacial adhesive junctions that form if solid materials are in contact on an atomic scale [12]. As a normal load is applied, local pressure at the asperities becomes extremely high. In some cases, the yield stress is exceeded, and the asperities deform plastically until the real area of contact has increased sufficiently to support the applied load. In the absence of surface films, the surfaces would adhere together, but very small amounts of contaminant minimize or even prevent adhesion under purely normal loading. However, relative tangential motion at the interface acts to disperse the contaminant films at the point of contact and cold welding of the junctions can take place. If the adhesive strength of the junction is less than the cohesive strengths of the materials forming the asperities and there is no loss of material from either of the two materials, then the junction will rupture within the weaker asperity. Continued sliding causes the junctions to be sheared and new junctions to be formed. The chain of events that leads to the generation of wear particles includes the adhesion and fracture of the mating surfaces. Since both adhesion and fracture are influenced by surface contaminants and the environment, it is quite difficult to relate the adhesive wear process exclusively with the bulk properties of solid surfaces.

The following observations are generally made on adhesive wear mechanisms:

1. Interfacial metallic adhesion bonding depends on the electronic structure of the contacting bodies. It has been suggested that

strong adhesion will occur if one metal can act as an electron donor and the other as an electron acceptor [40].

2. Adhesive wear is directly related to the tendency of different mating materials to form solid solutions or intermetallic compounds with each other. The metallurgical compatibility indicated by the mutual solubility represents the degree of intrinsic attraction of the atoms of the contacting metals for each other [39].
3. Crystal structure exerts an influence on adhesive wear processes. Hexagonal metals in general exhibit lower adhesive wear characteristics than either body-centred cubic or face-centred cubic metals. This difference is believed to be related to different asperity contact deformation modes and the number of operable slip systems in the crystals [25].
4. Crystal orientation influences the adhesive wear behaviour. In general, lower adhesive wear is observed for the high atomic density, lower surface energy planes [42].
5. When dissimilar metals are in contact, the adhesive wear process will generally result in the transfer of particles of the cohesively weaker of the two materials to the cohesively stronger material [42].

The wear resulting from adhesive wear processes has been described phenomenologically by the well-known Archard equation [7]:

$$W_{ad} = V/L = K(F_N/H)$$

where W_{ad} is the wear rate, K is the wear coefficient, V is the wear volume, L is the sliding distance, F_N is the normal load and H is the hardness of the softer material.

This equation is relevant for plastic contacts which employ hardness as the only material property. However the wear coefficient K depends on various properties of the mating materials and it is not possible to describe quantitatively the influence of material properties on wear coefficient K by a simple relationship.

1.3.3 Reduction of Adhesive Wear

It is evident from the preceding discussions that wear is a complex process of material removal in which a variety of events take place independently or simultaneously. In order to prevent or reduce wear, the factors that contribute to wear should be understood. These are described below.

With increasing hardness a surface experiences less wear due to adhesion. Adhesion tends to be favoured by the presence of clean surfaces and chemical and structural similarities between the sliding metal couples.

To reduce adhesive wear of metals, the sliding metal pairs should be chosen to have a minimum tendency to form solid solutions and this could be achieved by metals having different crystal structures and chemical properties. The role of microstructure in improving adhesive wear resistance is significant. First, the microstructure influences bulk properties, including the initiation of cracks. This is generally the case when the size of microstructural features is smaller than the depth of indentation of abrasive particles. Second, the microstructural features become effective as discrete components, and their individual properties assume increasing importance. The presence of hard phases, particularly carbides, has beneficial effects on wear resistance. Composition, amount and morphology all affect the precise degree of improvement.

Adhesive wear usually results from an inadequate supply of lubricant to the contact area. It is indicated if the wear debris shows large metallic particles and the surfaces are damaged with material transferred from one surface to the other. Often for large contact areas sufficient lubrication passages are not provided and unlubricated regions result. This promotes adhesive wear. If this does not appear to be the cause of the wear, then improved material combinations should be considered. When there is no lubrication, harder surfaces are required, and ceramics and cermets or their coatings are normally used. In the case of nonmetals, it is acceptable to use identical material pairs. For low wear, the hardness of the mating members should be high

and should be comparable with each other. The hardness of the mating members should be comparable in an unlubricated contact in order to distribute wear unless one of the members can be sacrificed.

There is a general tendency for wear rate to increase as the load increases with a critical point beyond which an increase in load leads to seizure rather than to an increase in wear rate.

Wear rate can change considerably with change in speed, but there is no general relationship between speed and wear rate. An increase in speed can lead to an increase or a decrease in wear, depending on the effect on the temperatures of the surfaces. In general an increase in temperature tends to produce an increase in wear rate, because with increasing temperature the materials involved become softer. The transient or non-equilibrium wear sometimes decreases with an increase in temperature.

In two-body abrasive wear, the roughness of the harder surface has a major influence on the wear rate. In adhesive wear, initial roughness may lead to severe damage or may gradually be reduced to an equilibrium 'run-in' level. There is also evidence that surfaces which are initially very smooth can become roughened in service until they reach a similar equilibrium 'run-in' roughness.

1.4 Literature Review

1.4.1 Introduction

A literature search for the present study has been carried out with an emphasis on depicting the subject from its early days to the present stage of knowledge. The literature search was done under the following headlines.

1.4.2 Sputtering

Application of the sputtering process to the deposition of thin films has been known and practiced since the first observations of Grove [1] as reported in 1852.

A literature search shows that Sir J.J. Thomson [2] used the word 'spluttering' but that I. Langmuir and K.H. Kingdon eliminated the 'l' in their publications in the years 1920 to 1923. An early interpretation of sputtering was that localized heating in the vicinity of an ion impact was sufficient to cause target material to be released through evaporation. Such a theory would predict that the ejection of material could be described by Knudsen's cosine law.

In 1960, a group of researchers postulated a simple model. They assumed that only the first collision made by an impinging ion contributes to sputtering. They postulated that subsequent collisions occur too deep within the target to lead to sputtering events. The sputtering yield was assumed to be proportional to the energy transferred in the first collision and to vary inversely with a quantity which they called the mean free path. This was actually a parameter introduced so as to include the energy dependence of the average distance that an ion would travel before making its first collision and resulted in a sputtering yield which varied slightly less than linearly with impinging ion energy - which generally agrees with yield data in this range. This theory gave a qualitative interpretation of the dependence of the sputtering yield of a single crystal on the direction of impingement relative to crystallographic axes [16,21]. The model has been criticized by some as being insufficient [22].

The concept of sputtering efficiency defined as the fraction of bombarding ion energy leaving the target via sputtering and back-scattering, was first introduced by Sigmund [28]. His calculation surprisingly indicated that efficiency equal to 0.024 for self-sputtering, independent of ion energy and target material, for the elastic-collision range above 1 keV. In 1968, Whener et al [44] quickly became convinced that the process of sputtering could be greatly enhanced by the appropriate application of magnetic fields. This feeling grew stronger and led to the formation of Telic Corporation and the development of one of the major forms of magnetron sputter cathodes.

Reactive magnetron sputtering is a complex process. It involves a variety of ionized and molecular species which react with the target,

the substrate and the chamber walls. A number of researchers, Abe and Yamashina [35], Elthouky et al [38], Steenbeck et al [45], Lemperière and Poitenvin [50], Berg et al [62] have treated these mechanisms by mathematical modelling, the most comprehensive of which is the work of Berg et al. Their focus is mainly on the study of N_2 flow rate dependences of the deposition rate and they could consistently explain the often found hysteresis with respect to increasing and decreasing flow rate of N_2 .

Jankowski and Schrawyer [73] used reactive d.c. magnetron sputtering process to deposit molybdenum oxide thin films with controlled composition and crystalline structure. Their approach emphasizes the target power-molybdenum concentration scaling relationship. Rudnik et al [78] have investigated the reactive sputtering of MoN_x films utilizing feedback control technology. Maoujoud et al [83] investigated the influence of the discharge power, the gas pressure and the substrate temperature on MoN_x films deposited using reactive sputtering. Jankowski and Schrawyer [81] also investigated the range of deposition conditions needed to reproduce stable crystalline Mo_2O_3 films. Perry et al [84] used the PVD method of reactive cathodic arc evaporation for deposition because this method is known for the high degree of ionization of the metal species produced during the evaporation process. However this is not a sputtering process.

1.4.3 Wear

The first attempt to relate wear to the mechanical properties of materials was made by Tonn [3] in 1937, who proposed an empirical formula for abrasive wear. Burwell and Strang [6], Archard [7], and Archard and Hirst [8] developed an adhesion theory of wear, and proposed a theoretical equation. They considered that microvolumes of material are removed during wear. Archard [7], on the assumption that the wear particles are hemispheres of radius equal to the radius of a contact point, showed that

$$W = (k/3)(N/H_b),$$

where k is the probability of removing a wear particle from the contact point, N is the load and H_b is the brinell hardness of material. The value of k changes over the range 10^{-2} to 10^{-7} . This equation is relevant for plastic contacts which implies that wear rate is proportional to real area of contact in plastic contacts and may not be applicable to cases involving elastic contacts, e.g. magnetic storage devices [72]. When sliding involves a lubricant, an additional multiplier $\alpha < 1$ is introduced into this equation, this being the ratio of the area of metal contact to the total area. Rabinowicz [24] established a connection between α and the coefficient of friction of lubricated and unlubricated contacts and overall coefficient of friction. Rowe [20] allowed for the increase in dimensions of an individual contact point in the presence of tangential stresses and lubricant desorption processes.

The Archard [7] equation, which employs only hardness as a material property, has been extended by Hornbogen [34]. He proposed a model to explain increasing relative wear rates with decreasing toughness of metallic materials. This model is based on a comparison of the strain that occurs during asperity interactions with the critical strain at which crack growth is initiated. If the applied strain is smaller than the critical strain, the wear rate is independent of toughness and Archard's law is followed. Applied strain larger than the critical strain of the material leads to an increased probability of crack growth and therefore to a higher wear.

The next important stage in the development of wear theory was the emergence of the fatigue theory for the wear of solids. The first paper on this theory was published by Kragelsky [9]. Further papers were published soon afterwards giving a somewhat wider view of the theory, i.e. papers by Kragelsky [9,18], a paper by Kragelsky et al [27]. This theory, which is discussed in detail below, incorporates the concept of an individual frictional bond deformed by the bulk of the rubbing bodies, and the stress distribution in this volume as a function of the load, friction, and the geometrical profile of the microasperities is considered. The type of stress distribution determines the way in which the frictional bonds are distributed. The main concept of this theory is that destruction of sliding surfaces requires repeated sliding

effects, the number of which can be expressed quantitatively as a function of the stress distribution.

The most important mechanisms predicted by this theory were tested on various classes of materials by different authors. This theory has been used as the basis for engineering methods of calculating the wear of various machine elements and mechanisms.

The fatigue theory of wear has been widely accepted amongst various scientists in different countries, and a paper by Rozeanu [13] is an example of an important contribution to the field. Endo et al [15,19,30] provide important evidence for the fatigue nature of wear, and a number of specialists, which includes Polzer [26] have been working on this aspect of wear.

Bayer et al [14] developed a method for calculating the wear of various machine contacts on the basis of an engineering model of the process devised by the authors and based on the concept of the fatigue nature of wear. The authors consider that the life of a machine contact is inversely proportional to $N^{1/3}$, i.e. they use the connection between the actual stress and the number of loading cycles resulting in damage to the material, which is the most important relation in the fatigue theory of wear. These authors consider that the tangential stresses at the contact, which are expressed in fractions of the yield point in shear, are responsible for damage.

Yoshimoto and Tsukizoe [10] published an important study in which wear was associated with the thickness of the oxide films formed on a metal surface. According to these authors the oxide film is ruptured at the real contact point, the thickness of the oxide films depending on the time interval between two successive contacts, the time interval depending on the density of the contact points. Accordingly, the first part of this study was concerned with calculation of the contact parameters of rough bodies. The calculated results were in good agreement with experiment.

Khrushchov [33] has studied the influence of material properties on abrasive wear and has shown that in the case of pure metals and

nonmetallic hard materials, a direct proportionality exists between the relative wear resistance and hardness. Moreover, he has also shown that heat treatment of structural steels, normal hardening and tempering, improves their abrasive wear resistance. Rabinowicz [17] derived an expression for abrasive wear by assuming that the asperities of the harder surface are conical. Zum Gahr [44] proposed a model for abrasive wear in which he considered the detailed processes of microcutting, microploughing and microcracking of ductile metals. This model includes other microstructural properties of the material worn beside the flow pressure or hardness. It has been observed that the following factors influence abrasive wear mechanisms: the magnitude of the work hardening, the ductility, the homogeneity of the strain distribution, the crystal anisotropy and the mechanical instability.

1.5 Objective of the Present Study

1. Development of the test rig as a group research project and then its commissioning and standardization using TiN film deposition.
2. Characterization of the films obtained from the present study and the deposition by external supplier.
3. Study of the effect of deposition parameters on film properties, and comparison with existing works and other coatings.
4. Optimization of deposition process by systematic variation of the process parameters.
5. Comparative wear study of different coatings with the variation of substrate materials.

Chapter 2

Experimental Equipment

2.1 Introduction

Test rigs were developed to facilitate deposition of thin films and also for carrying out wear tests. The test rig developed to carry out the deposition of films is shown in Figs.2.1(a)&2.1(b). It consists of mainly - a deposition chamber, a substrate table assembly and the associated control devices. The rig was designed, manufactured, assembled and commissioned at Dublin City University (D.C.U.); only the deposition chamber was fabricated by an external contractor (Vacweld, North Walsham, England). The deposition chamber is equipped with Cooling arrangement, Compressor, Pumping stack, Pirani gauge, 'Reactaflo' reactive sputtering controller, Monochromator, Magnetron power supply, Magnetron shutter, Vacscan gas analyzer, Substrate preheating arrangement, Substrate biasing arrangement, Argon and Reactive gas incorporation line. Detailed drawings of the chamber can be in Appendix A.

To characterize the deposited films, the following equipment has been used: Interferometer, Profilometer, Microhardness tester and Scratch tester.

The test rig developed to carry out the wear test is shown in Fig.2.2(a). A schematic diagram of the wear test rig is shown in Fig.2.2(b). The rig was designed, constructed and commissioned at D.C.U. The following units constitute the wear test rig: Substrate table, Wear tools, Sliding mechanism and Revolution counter. A close up of the wear tool in contact with the specimen is shown in Fig.2.2(c). A worn specimen obtained from wear test is shown in Fig.2.2(d). Ti_xC coated and TiN coated unworn specimens are shown in Fig.2.2(e).

2.2 Equipment for Deposition

2.2.1 Deposition Chamber

The deposition chamber is a double walled high vacuum chamber, made of non-magnetic AISI 304 stainless steel. The basic geometry is a vertical axis cylinder with a top plate and a bottom plate. The top plate has 1 magnetron port, 8 rotatable shutter ports and 4 plasma emission spectrometer ports. Bottom plate has 2 pressure gauge flanges (KF16, KF25), 1 thermocouple feedthrough flange (KF25), 1 substrate

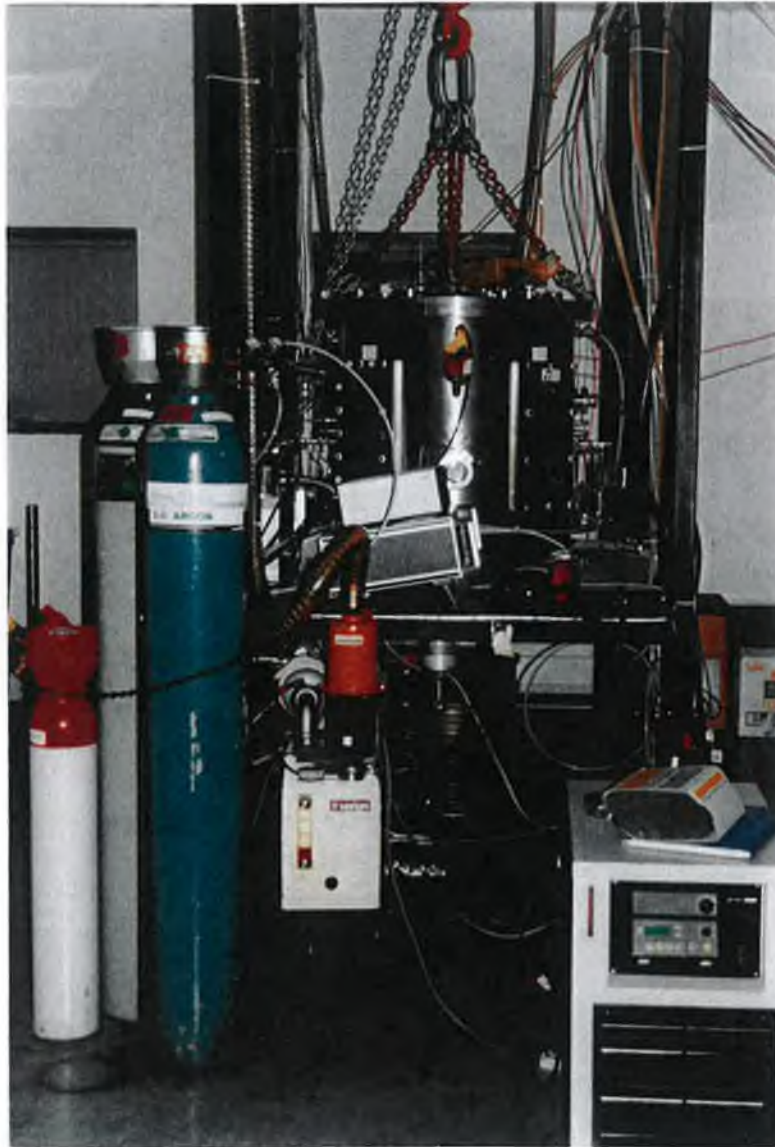


Fig.2.1(a) Magnetron sputtering system.

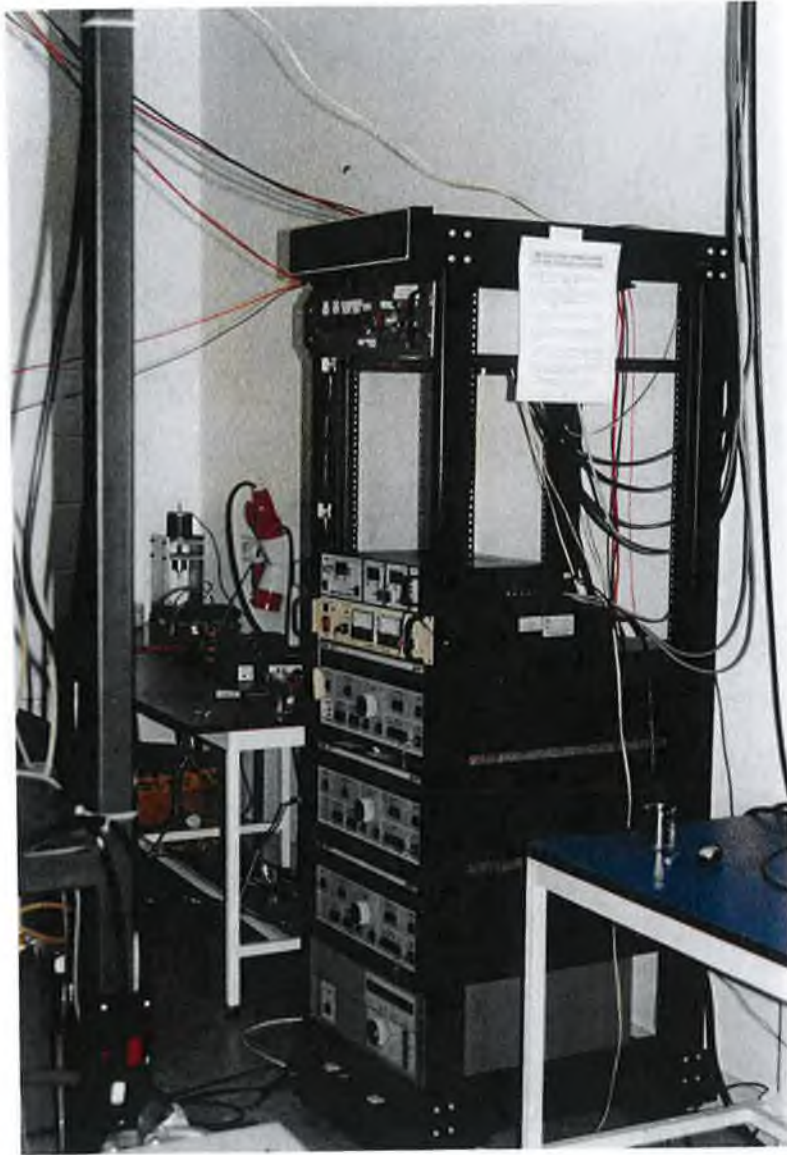


Fig.2.1(b) Magnetron sputtering system.

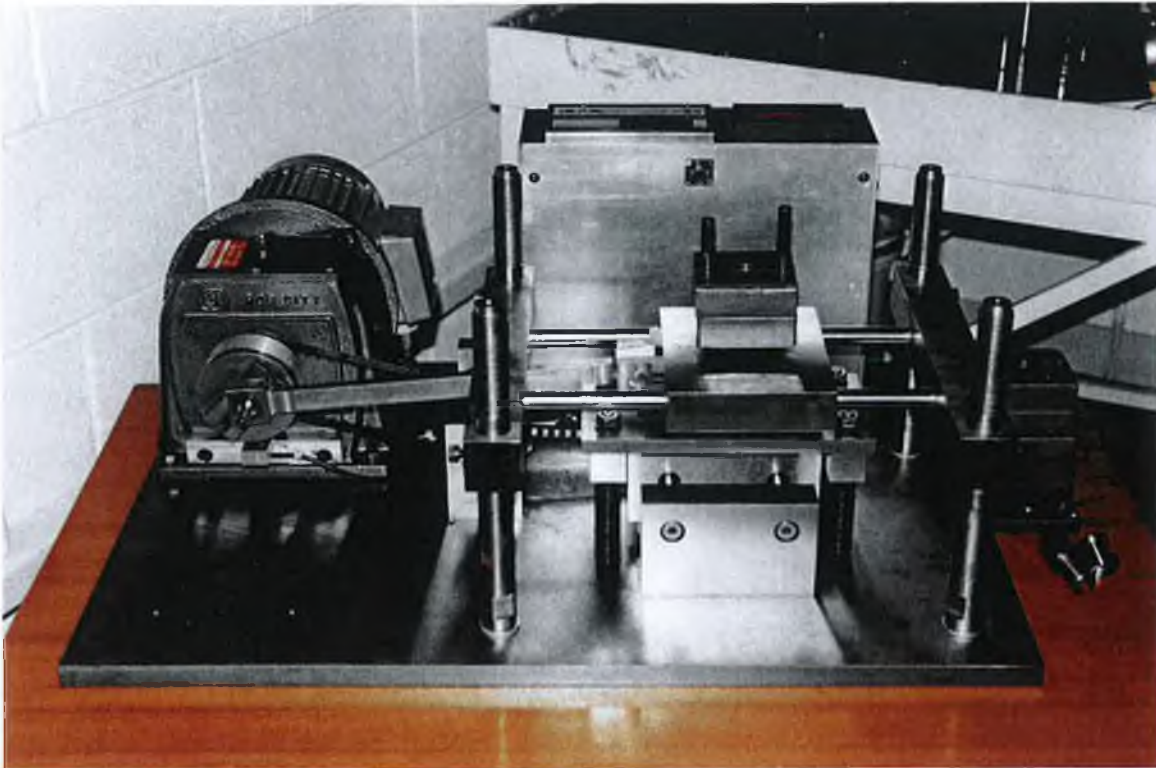
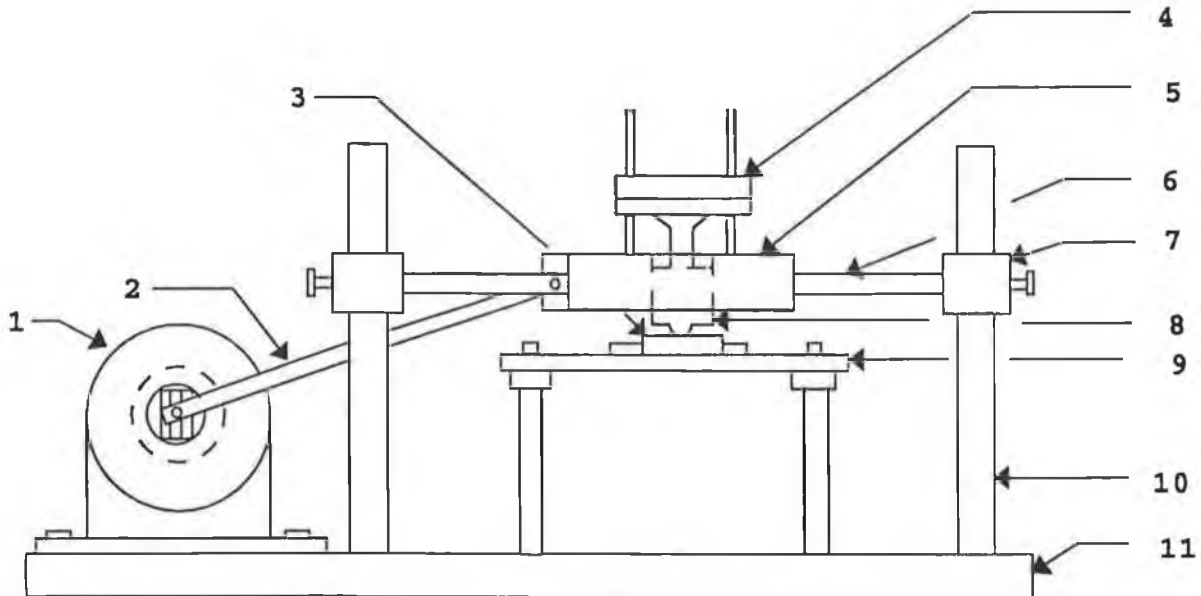


Fig.2.2(a) Wear test rig.



- | | |
|-------------------|----------------------|
| 1. Motor | 7. Rectangular bar |
| 2. Connecting arm | 8. Wear tool |
| 3. Substrate | 9. Substrate table |
| 4. Load | 10. Ball screw shaft |
| 5. Platform | 11. Base plate |
| 6. Guiding rod | |

Fig.2.2(b) Schematic diagram of wear test rig.

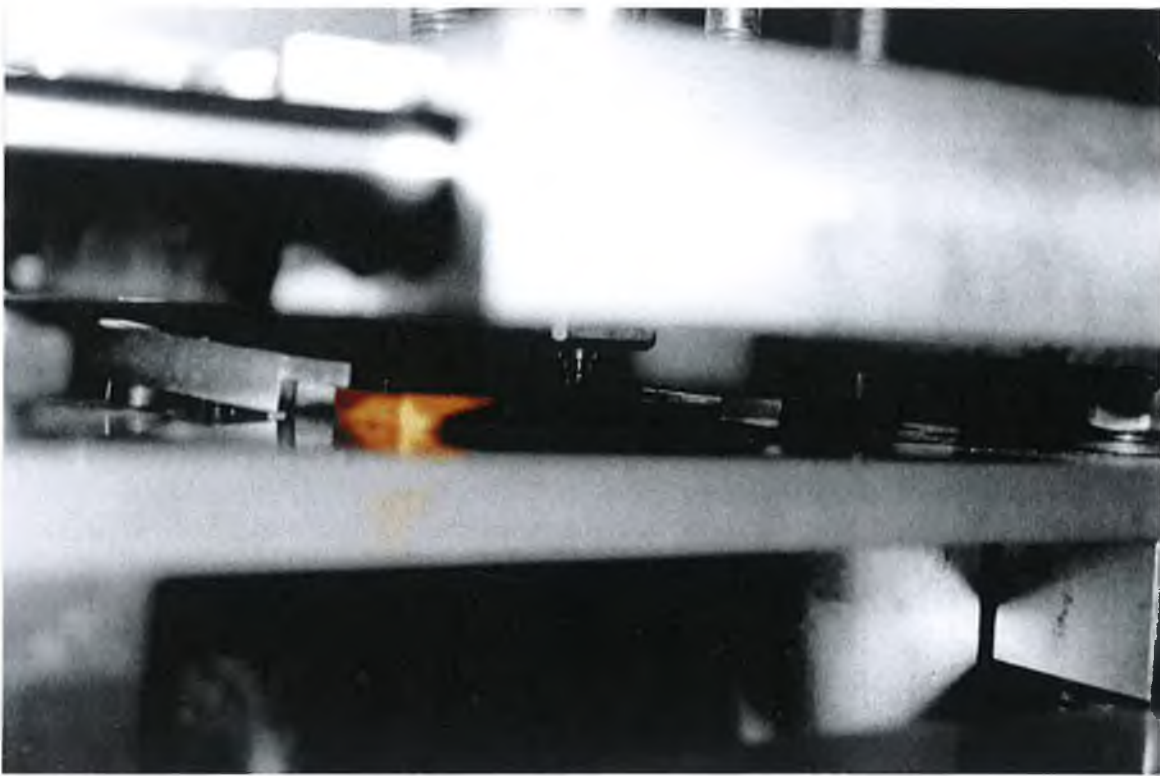


Fig.2.2(c) Close up of the wear tool and specimen.

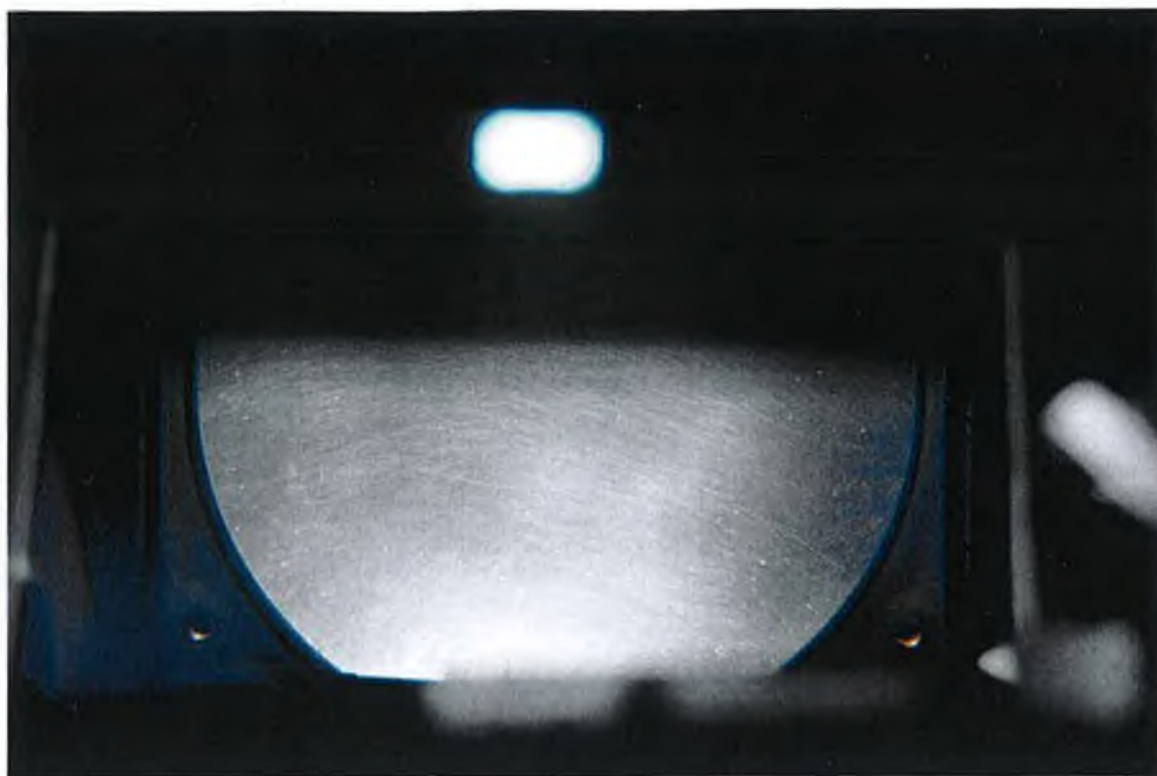


Fig.2.2(d) A worn specimen.



Fig.2.2(e) Unworn specimens.

table port, 1 high vacuum port, 1 backing line port, 8 rotatable shutter ports and 2 swagelok water inlet/outlet ports for water cooling of the substrate table. There are 4 magnetron ports on the cylindrical walls, along with 2 viewports (KF40, KF50), 1 optical pyrometer port (KF25), 2 rotatable magnetron shutter ports (for the top magnetron) and 1 plasma emission spectrometer port. A small sample can be coated using only one or two magnetrons.

The flanges were all o-ring sealed, using either Viton^R or Nitrile elastomers. KF clamping arrangements were employed to expedite the reconfiguring of the apparatus when necessary. The chamber was made double walled to enable the circulation of cooling water. Detailed drawings of the chamber can be found in Appendix A. All peripheral Blanking plates, Magnetron shutters, Wilson seals etc. were designed and fabricated at D.C.U.

The deposition chamber could be raised by means of a 2-ton pulley. A frame incorporated a linear side rail in order to place the chamber on a resting area while maintenance and sample loading was undertaken. The frame was constructed of box section steel which supported the chamber, the lifting device and the peripheral equipment.

2.2.2 Magnetrons

Magnetrons are a class of cold cathode discharge devices which are generally used in a diode mode. The plasma is initiated between the cathode and the anode at pressures in the mtorr range by the application of a high voltage, which can be either d.c. or r.f. The magnetrons used in the present study are planar magnetrons supplied by D.G. Teer Coating Services Ltd., Hartlebury, England and its housing material is Aluminum. On a backing plate the target of dimensions 13.97cm x 33.66cm x 1cm is mechanically secured. The permanent magnets are placed directly behind the cathode. The directly cooled magnetrons with titanium targets are constructed from either ferrite magnets or neodymium-iron-boron magnets. The indirectly cooled magnetron with a molybdenum target contains ferrite magnets. The maximum transverse component of the magnetic field in front of the target is about 300 G. The recommended minimum threshold flux density for a magnetron

discharge is about 200 G. The magnetron source is operated in argon at a typical pressure of $\approx 3.0 \times 10^{-3}$ mbar, maximum cathode potential of about 400 V, maximum current density of 26.6 mA/cm² and maximum power density of 10.6 W/cm².

The individual magnetrons were not only unbalanced but the magnetrons themselves were in a closed field array. For instance in the case of four magnetrons, a closed field arrangement is ensured where the magnetic field lines from the edges of one magnetron closed with the edge of the adjacent magnetron as shown in Fig.2.3(a). This effectively confines the plasma to the middle of the chamber where the substrate is placed. In practice, only two magnetrons, both ferrite magnet type, were utilized to achieve this closed field. Only one was energized during deposition and the other one served as a dummy to confine the plasma between the two magnetrons as shown in Fig.2.3(b).

The magnetrons receive power from magnetron drive MDX 5K as shown in Fig.2.1(b). This drive is an efficient advanced high-frequency switch mode power supply for use in plasma environments. Each MDX is equipped with a built in impedance-matching transformer. The MDX can be used as a power, current or voltage source, depending on the method of output regulation selected. There are 3 magnetron drives in the system, each has a maximum output power of 5 kW and a maximum current of 12.5 A at output ripple frequency of 50 kHz.

2.2.3 Cooling System

The cooling arrangement for the test rig is as shown in Fig.2.4, where water supply consists of a Lauda UKT 1000 cooler and a laboratory water supply line. The supplied water returns to the respective sources i.e. the cooler and the basin of the supply line. Operating and ambient temperature ranges of the cooler are -25°C to 40°C and 0°C to 40°C respectively. In the water supply line, there is provision such that the diffusion pump is switched off automatically if the water supply fails.

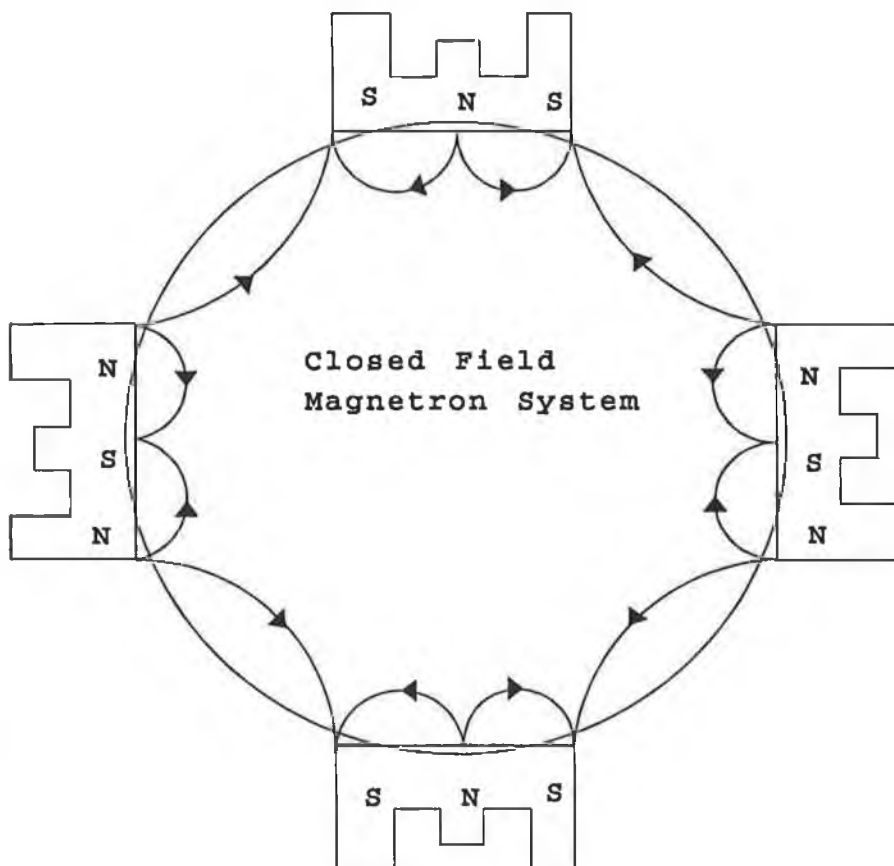


Fig.2.3(a) Four magnetrons closed field system [85].

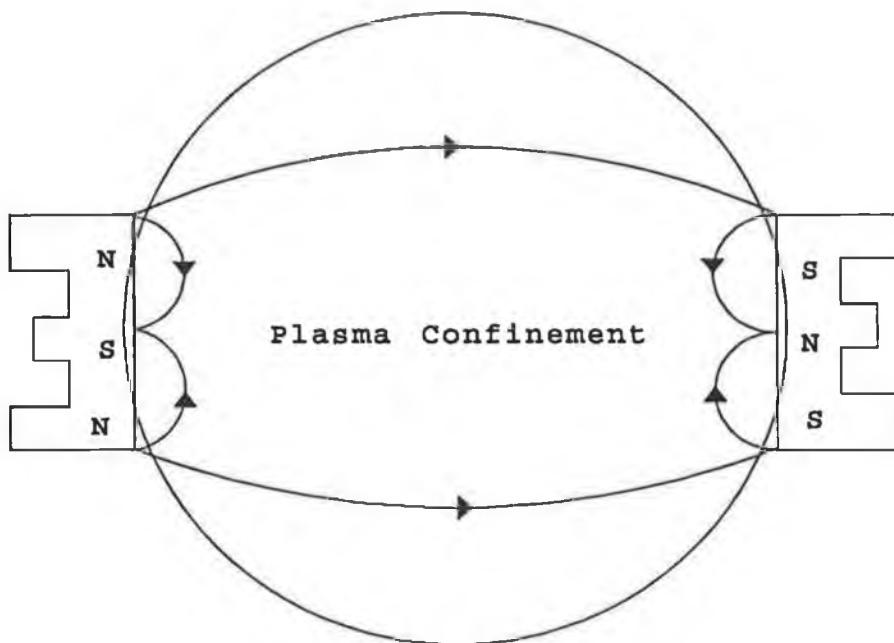


Fig.2.3(b) Two magnetrons closed field system [85].

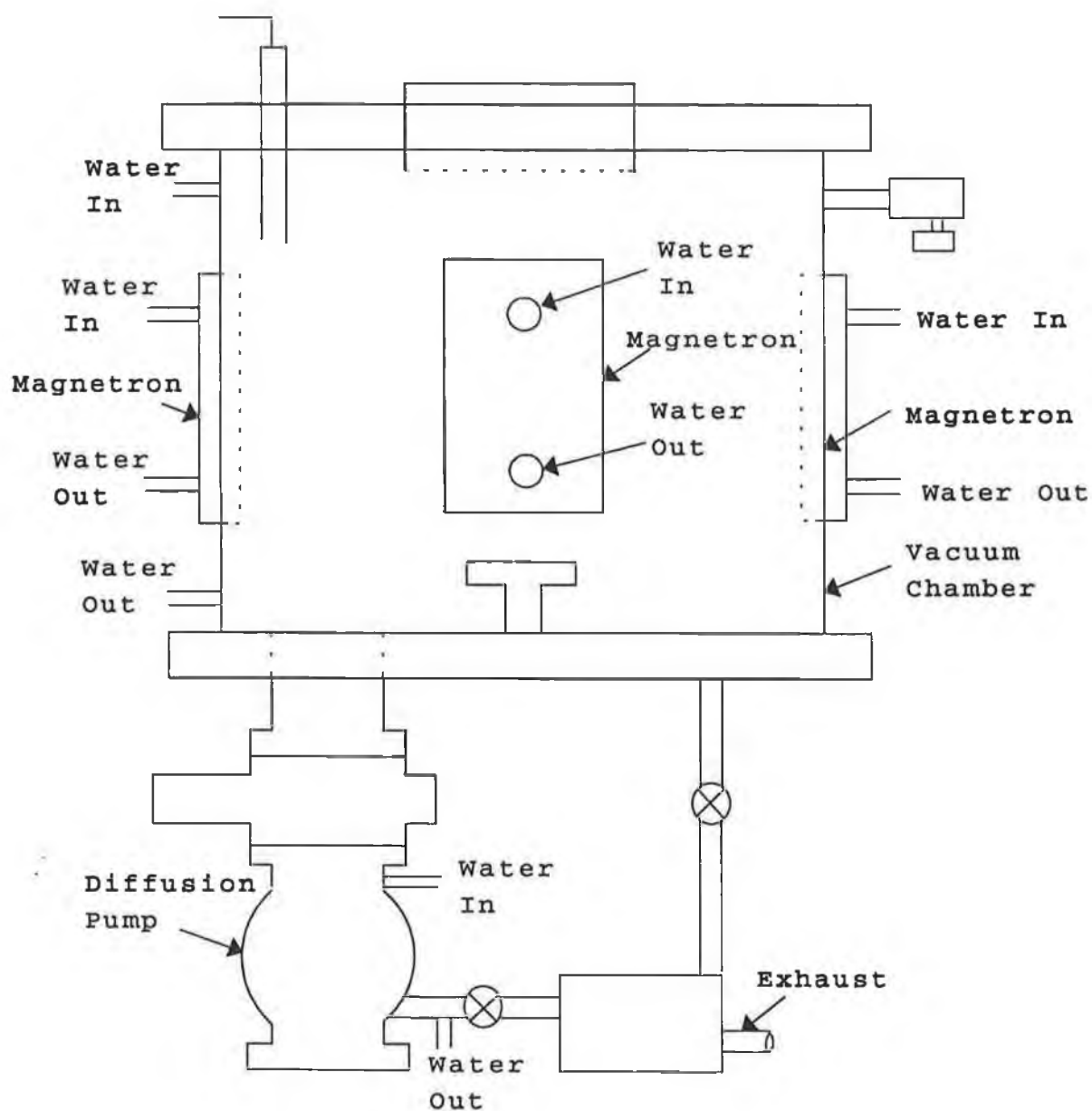


Fig.2.4 Cooling water circuit of the deposition system [85].

2.2.4 Pumping Stack

The compressor has a test pressure of 16.5 bar and discharge pressure of 11.0 bar. Its capacity is 10 litres and working temperature range is -10°C to $+100^{\circ}\text{C}$. Compressed gas from the compressor is introduced into the deposition chamber. The pumping stack consists of a diffusion pump, a roughing pump, a high vacuum valve, a roughing valve and a backing change over valve. The Varian VHS-6 diffusion pump is a water cooled oil diffusion pump with optimum operating range from 10^{-3} to 10^{-9} torr. The heat up time or cool down time of the diffusion pump is 10 minutes. The Varian SD-700 roughing pump is an oil-sealed vane pump equipped with an appropriate motor and is capable of handling neutral or only slightly corrosive gases. The ultimate vacuum the roughing pump can create is 10^{-4} mbar.

The Pirani-penning 1005 vacuum gauge is a microprocessor based instrument for vacuum measurement and process control. The instrument has a large easy to read liquid crystal display. It records low pressure on the principle that at a low pressure, the thermal conductivity of any gas varies with pressure. The interior of the gauge head is open to the vacuum system and contains a filament that is heated by current from control circuits. The filament forms one arm of a Wheatstone bridge and the bridge voltage is a function of pressure.

2.2.5 Gas Supply System

A 'Megatech Ltd reactaflo' reactive sputtering controller controls the plasma based reactive sputter deposition process. This involves a plasma, a source of depositing material, and admission of argon and reactive gases into the vacuum chamber. The controller for N_2 gas is 0-100 sccm full scale calibrated with dry N_2 and the controller for Ar gas is 0-142 sccm full scale calibrated with N_2 . The sputtered material passes through the plasma where it is excited and emits light at characteristic wavelengths. The emission intensity is proportional to the density of the excited species. The reactaflo unit monitors this plasma emission and uses it as a control signal for the reactive gas supply. This signal is received by an optical fibre probe connected to a monochromator (EP 200Mm). The received signal is converted to a

voltage and is recorded by a voltmeter (Kaise Electronic Works, Ltd; Model: SK-5000G) which has 10 different ranges in between 0 to 1000 V (d.c.). In order to maintain stoichiometric control, the optical emission intensity of the excited target species was observed and monitored as shown in Fig.2.5. The main advantage of using an optical emission spectrometer is that it allows for the rapid compensation in fluctuations of the plasma composition. If the monochromator is tuned to a metal emission line then this line will fall as the reactive gas is admitted (normal control sense). In either case the emission line signal is a unique function of the reactive gas pressure. The reactaflo unit dynamically controls the reactive gas flow to keep the chosen emission line constant. This eliminates the pressure instability and allows operation across the whole range of target conditions.

2.2.6 Substrate Biasing

Biasing of the substrate holder is achieved by use of a Wilson seal with a copper rod. The Wilson seal was adapted such that a PTFE sleeve fitted around the copper rod was in contact with the steel of the seal to prevent grounding. The power supply unit (Glassman High Voltage, Inc; Series EW, Model: PS/EW01 R600-220) for biasing the substrate has working ranges of 0-1000 V(d.c.) and 0-600 mA(d.c.).

2.2.7 Substrate Preheating

The preheating arrangement is made of tungsten wire of 0.38 mm diameter to heat the substrate by means of radiant heating. The tungsten is supported on a ceramic and steel frame. Both the heater and the substrate holder are electrically isolated from the earthed substrate table by means of ceramic tiles. The temperature achieved by this method of radiant heating is greater than 400°C. The power supply connection to the arrangement is made through a feedthrough at the bottom plate of the chamber. The power supply is manufactured by Sorensen, DCR 60-30B. There is a thermocouple feedthrough at the bottom plate of the chamber with which a thermocouple (K type, Chromel-Alumel combination wire) and a millivoltmeter (Keithley Instruments, Inc, Model: 169 DMM) are attached. To measure the temperature of the substrate, the thermocouple is placed on the sample.

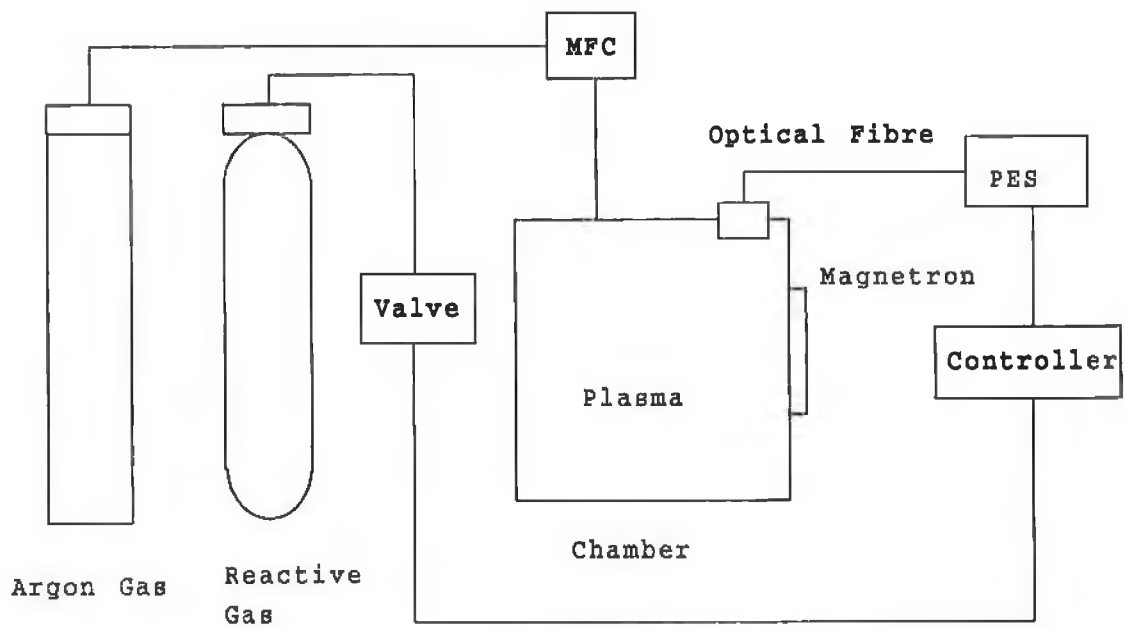


Fig.2.5 Optical emission feedback loop[85].

2.2.8 Residual Gas Analyzer

Leak checking is often necessary when working with vacuum systems. The leak check and residual gas analysis are done using a Vacscan gas analyzer. During the residual gas analysis, it was required to be differentially pumped which necessitated the use of a Varian V60 turbomolecular pump and a Varian SD-40 rotary backing pump. The turbomolecular pump can evacuate the chamber from the atmosphere to the 10^{-9} mbar range when backed by a two-stage mechanical pump. The Vacscan has a number of different applications. The different modes offer different advantages. In residual gas analysis mode, the peak intensity information is presented in a histogram format. This mode is used for taking a general overview of the vacuum system. If it is not known what is going on in the vacuum system then this mode could be used to see which species are dominating.

2.2.9 Substrate Table Assembly

The substrate table shown in Fig.A.5 in Appendix A is made of non-magnetic 304 stainless steel mounted through the center port in the bottom plate of the vacuum chamber. The diameter and the thickness of the substrate table are 30 cm and 1 cm respectively. The total height of the substrate table assembly is 110 cm. The spiral cooling coil beneath the earth shield constitutes the water cooling in the substrate table assembly. The substrate table is designed to facilitate the exposure of the substrate towards the magnetron. It is provided with two types of motion, rotating about the vertical axis and reciprocating along the vertical axis. Moreover, there is provision at the periphery of the substrate table for the substrate to rotate about its own axis or to rotate on its own axis as well as to rotate along with the substrate table as shown in Figs.A.6 & A.7 in Appendix A. Whatever the type of motion provided to the substrate, the purpose is to ensure uniformity of coatings.

There are two stepping motors (Parker Digiplan Ltd., S Series Drive, Models: S57-102 and S83-93), one is giving rotating motion and other one is giving reciprocating motion to the substrate table. The motors are connected to the computer (IBM PC Computer) by compumotors

(Parker Hannifin Corporation, S57-102 and S83-93) and compumotor adaptor (PC23 Adaptor, Parker). The compumotors get power from the laboratory power supply line through a step down transformer (S6 drive or S8 drive power rating).

2.3 Equipment for Characterization

2.3.1 Interferometer

An interferometer is an arrangement in which commercial microscopes utilize two-beam or multiple-beam techniques for measuring coating thickness. The Tolansky [4] technique is generally used in measuring coating thickness with multiple-beam.

The wedge or step technique is generally used for thickness measurements of opaque coatings. A step is made in the coating by masking a portion of the substrate during deposition or by removing part of the coating from the substrate. The interference fringes are formed between an optical flat and the surface of the coated specimen using a white light that can be observed with the microscope as shown in Fig.2.6. If there is a slight angle between the two surfaces of the optical flat and the specimen, the fringe pattern will appear as alternating parallel light and dark bands that are perpendicular to the step on the coatings. Two adjacent fringes are separated by half the light wavelength (λ). The step in the coated specimen surface will displace the fringe pattern as shown in Fig.2.6(a), and this displacement is a measure of the difference in the level of the surface of the specimen. The coating thickness is measured as the displacement of the fringe pattern at the step area and this coating thickness is given by

$$t = d/s \times \lambda/2$$

where d is the displacement of the fringe pattern at step area, s is the distance between the two adjacent fringes and λ is the wavelength of light.

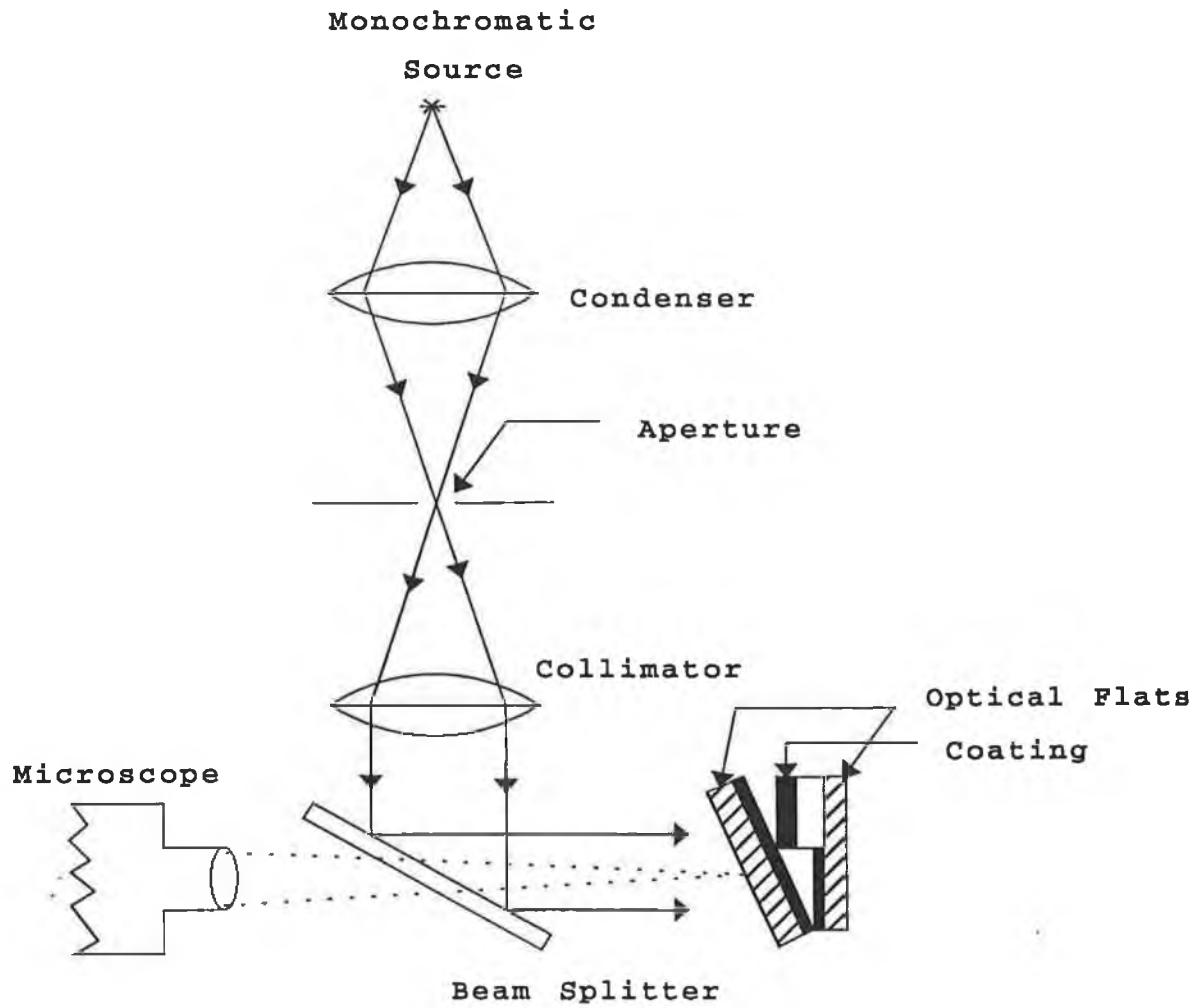


Fig.2.6 Schematic diagram of Mirau interferometer[76].

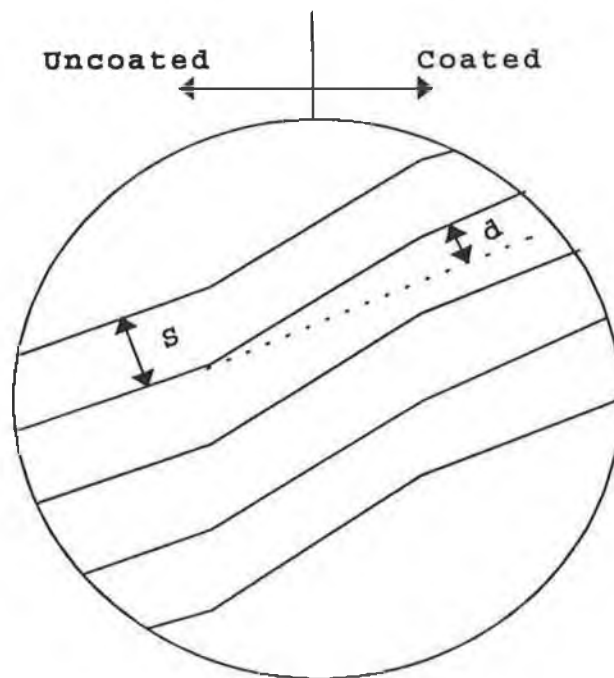


Fig.2.6(a) Interference pattern.

The sharpness of the fringes (resulting in greater accuracy in the measurement) increases markedly if interference occurs between many beams (multiple-beam interference), and this can be accomplished if the reflectivity of the two samples at interfaces is very high. While the displacement of the fringes of a double-beam instrument can be estimated to about one-tenth of the fringe spacing, the fringes of a multiple-beam instrument are much more sharply defined, and their displacement can be estimated to perhaps one-hundredth of the fringe spacing (≈ 3 nm).

2.3.2 Microhardness Tester

Microhardness measurements allow the indentation to be shallow and of small volume so as to measure the hardness of brittle materials or thin materials or coatings. The microhardness tester used in measuring the hardness of the films permits Vickers and Knoop hardness measurements [5]. For both measurements highly polished diamond pyramidal indenters are used. The Vickers indenter is a diamond in the form of a square pyramid with face angles of 136° (corresponding to edge angles of 148.1°) as shown in Fig.2.7(a), and relatively low loads varying between 1 and 120 kg are used. The Knoop indenter is a rhombic-based pyramidal diamond with longitudinal edge angles of 172.5° and 130° as shown in Fig.2.7(b). In general, the loads used in the Knoop tester vary from about 0.2 to 4 kg. Smaller loads as low as 1 to 25 g may also be used in both the testers when a microhardness examination is needed. In making the Vickers or Knoop hardness measurements, the lengths of the diagonals of the indentation are measured using a medium-power compound microscope after the load is removed. If d is the mean value of a diagonal in millimeters and W is the imposed load in kilograms, Vickers hardness number H_v , is given by

$$H_v = 1.8544W/d^2$$

If b is the long diagonal in millimeters, the Knoop hardness number H_k , is given by

$$H_k = 14.229W/b^2.$$

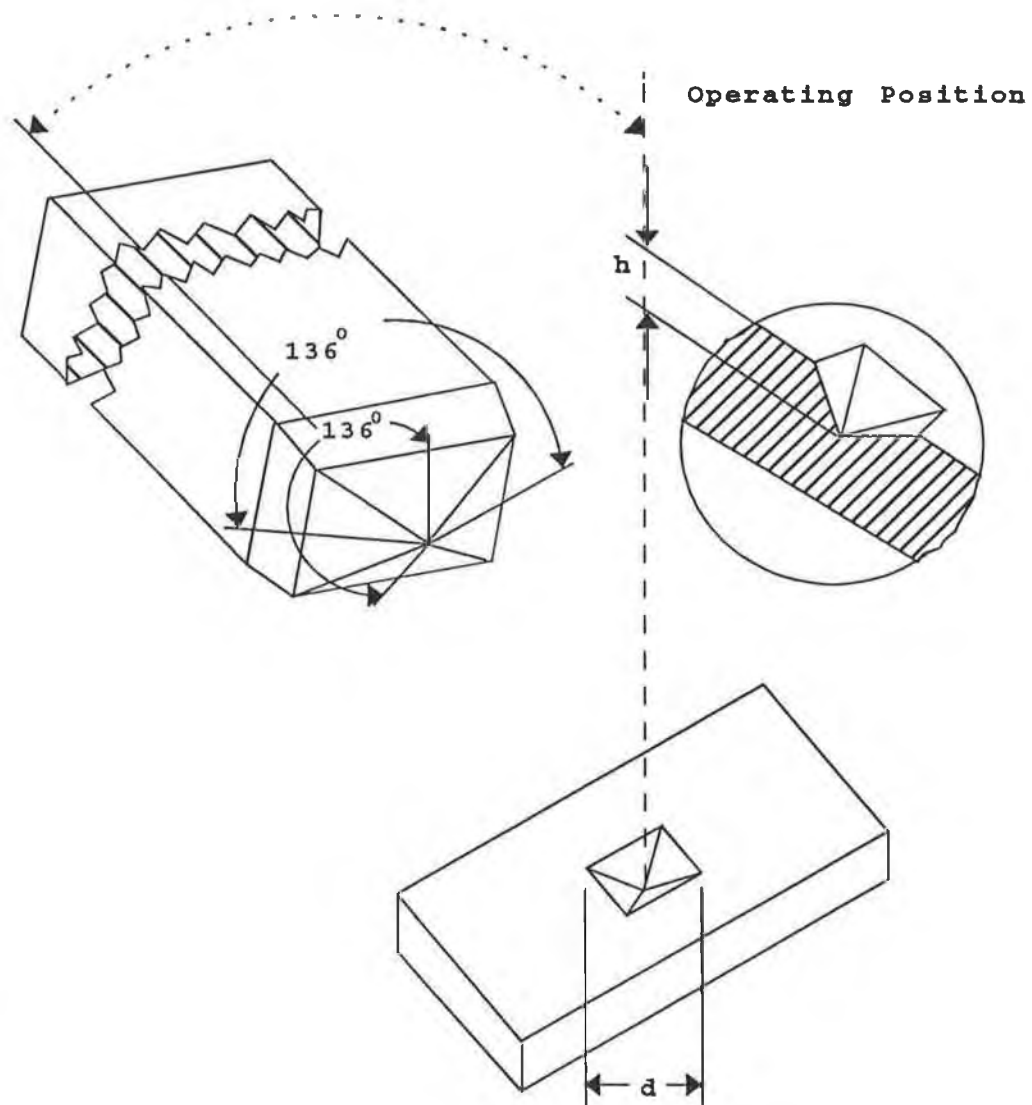


Fig.2.7(a) Geometry and indentation with a Vickers indenter [76].

Operating Position

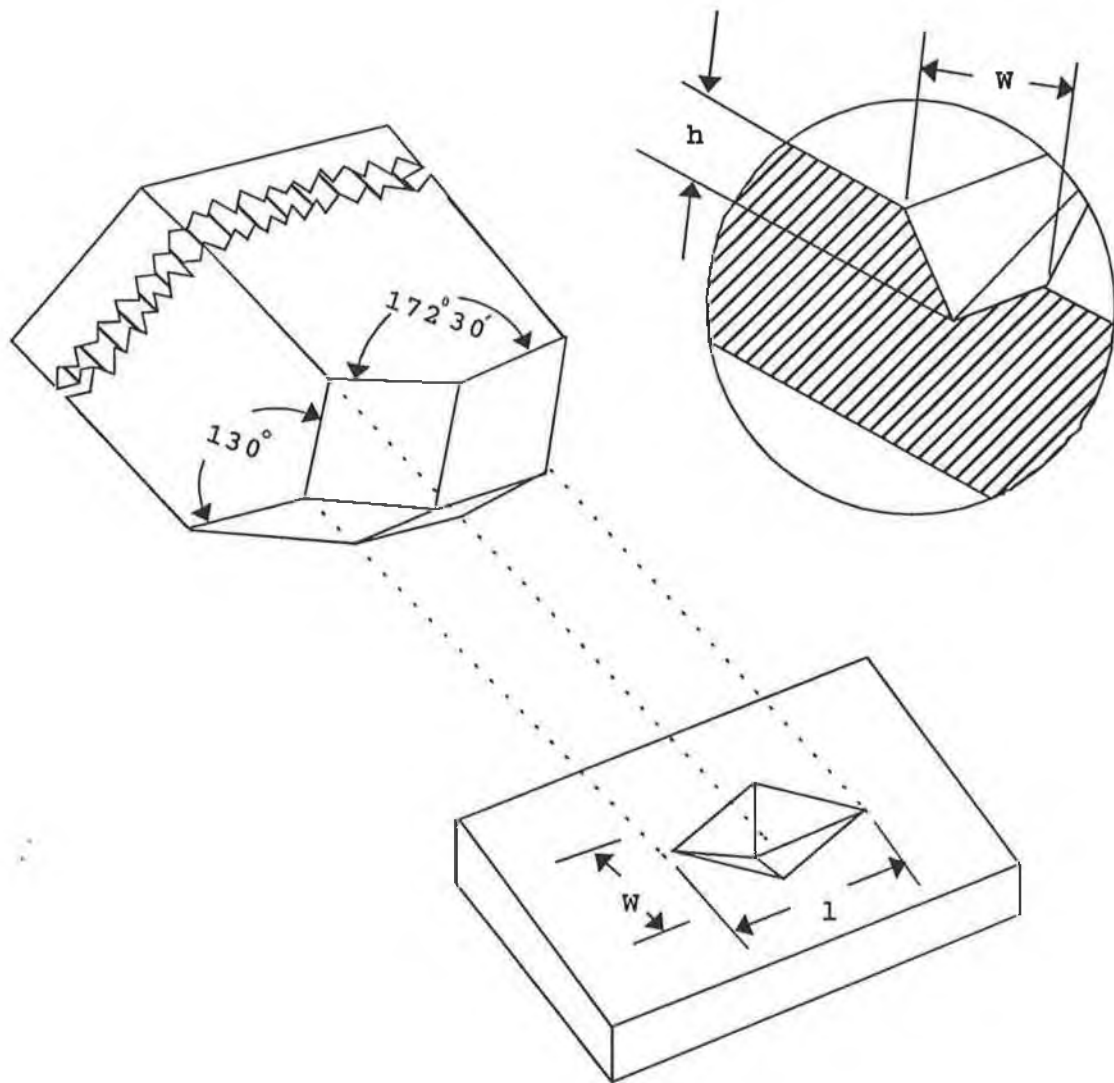


Fig.2.7(b) Geometry and indentation with a Knoop indenter[76].

The advantages of the Knoop indenter over the Vickers indenter in microhardness testing lie in the fact that a longer diagonal is obtained for a given depth of indentation or a given volume of material deformed. It can be shown that for the same measured diagonal length, the depth and area of the Knoop indentation are only about 15% of those of the Vickers indentation. The Knoop indenter is thus advantageous when shallow specimens or thin, hard layers must be tested. The Knoop indenter is also desirable for brittle materials such as glass or diamond, in which the tendency for fracture is related to the area of stressed material.

2.3.3 Scratch Tester

A scratch tester has a smoothly rounded chrome-steel stylus with a tungsten carbide or Rockwell C diamond tip (in the form of a 120° cone with a hemispherical tip of 0.2 mm radius). The Vickers microhardness tester was used as scratch tester by mounting a stylus with diamond tip. This stylus is drawn across the coating surface, and a vertical load is applied to the point and is increased in step until the coating is completely removed. The minimum or critical load at which the coating flakes (adhesive failure) or chips (cohesive failure) is used as a measure of adhesion. To avoid damage to the diamond, measurement of unknown substances should be started with the smallest force.

Adhesion is measured on the basis of critical load values. An accurate determination of critical load sometimes is difficult. Several techniques, such as 1) microscopic observation (optical or scanning electron microscope) during the test, 2) chemical analysis of the bottom of the scratch channel (with electron microprobes) and 3) acoustic emission, are used to obtain the critical load. Microscopic observation has been used in determining the critical load by the scratch tester.

2.4 Equipment for Wear Generation

2.4.1 Substrate Table

The substrate table shown in Fig.2.2(b) is made of D2 tool steel (heat treated) mounted on the base plate (D2 tool steel). There are 2 clamps (D2 tool steel, heat treated) for holding the sample in position against a fixed locating face.

2.4.2 Wear Tools

Two types of wear tools were fabricated for the present wear test rig. One was point contact as shown in Fig.2.2(c) and other one was line contact. Both the tools (i.e. stylus) are made of tungsten carbide. The stylus is placed in the tool holder. The tool holder is a high carbon steel block. The line contact stylus is fixed by two screws at two of the four vertical planes of the tool holder block and the point contact stylus is fixed by a groove screw. On the top of each tool holder block, a screw is placed on which a wear load rests. In the case of the point contact stylus, the screw on the top of the tool holder block also tightens the groove screw.

2.4.3 Sliding Mechanism

The sliding mechanism provides sliding motion to the tool as shown in Fig.2.2(b). One end of the connecting arm (mild steel) is hinged to the platform (mild steel). The other end of the connecting arm is attached to the motor shaft (0.75 kW, Hanning Elektro Werke) with an offset from the centre of the shaft as shown in Fig.2.8(a), where r is the crank arm length and L is the connecting arm length. The offset distance yields a crank effect to the sliding mechanism. The end of the connecting arm which is connected to the motor output shaft can be adjusted to vary the sliding length as shown in Fig.2.8(b). The maximum sliding length which can be obtained is 60 mm. As the motor shaft rotates, crank and connecting arm translates rotary motion into reciprocating motion, and the platform starts sliding. The rotational speed of the output shaft of the motor is 106 rpm. The platform is guided to slide on two fixed horizontal rods (hardened steel). To

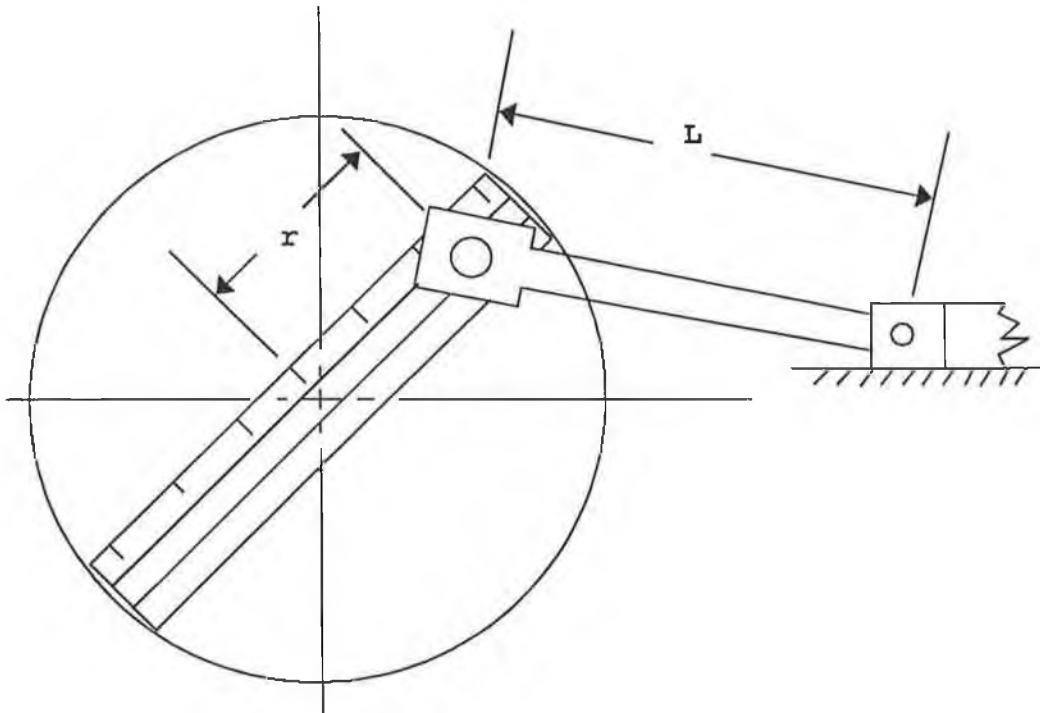


Fig.2.8(a) Transformation of rotational motion into reciprocating motion by crank and connecting arm.

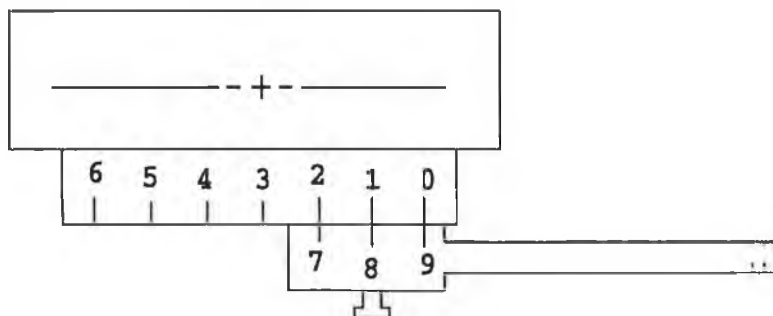


Fig.2.8(b) Adjustment of sliding length.

facilitate sliding, the guiding rods are provided with linear bearings. As the tool holder is placed through the square hole in the platform, the stylus comes in contact with the sample surface. As the tool slides over the sample surface, the wear is produced. The sample size can vary but must be longer than the stroke of the tool which reciprocates on the surface under test. The sample is offset from the centre of the tool holder block in order to produce wear at two different positions of the sample surface. The sample position is reversed to produce wear on the second track. The wear load rests on the screw and is guided by two rods as shown in Fig.2.2(b). The loads are made of lead. Maximum wear load can be applied is 10 kg where the base load is 1 kg including the load of the tool holder. This maximum wear load is constituted of one 1 kg and six 1½ kg blocks of lead.

2.4.4 Revolution Counter

The revolution counter (RS 260-937, RS Components Limited) records the number of revolutions of the motor at output shaft where a revolution is constituted of a forward stroke and a return stroke in the sliding motion.

2.5 Equipment for Wear Measurement

A profilometer was used in wear measurement. It is also known as a stylus instrument. It amplifies and records the vertical motions of a stylus displaced at a constant velocity by the surface to be measured. The instrument consists of the following components: a pickup, driven by a transverse unit (gear box) that draws the stylus over the surface at a constant speed, roughly 3 mm/min; an electronic amplifier to boost the signal from the stylus to a useful level; and a chart recorder and a meter for recording the amplified signal as shown in Fig.2.9. The transducers used in most stylus instruments for sensing vertical motion are linear variable differential transformers.

The electrical signal from the pickup represents the relative movement between the stylus and the pickup body. For this signal to be truly representative of the surface profile, the pickup body must traverse a path parallel to the general shape of the surface without

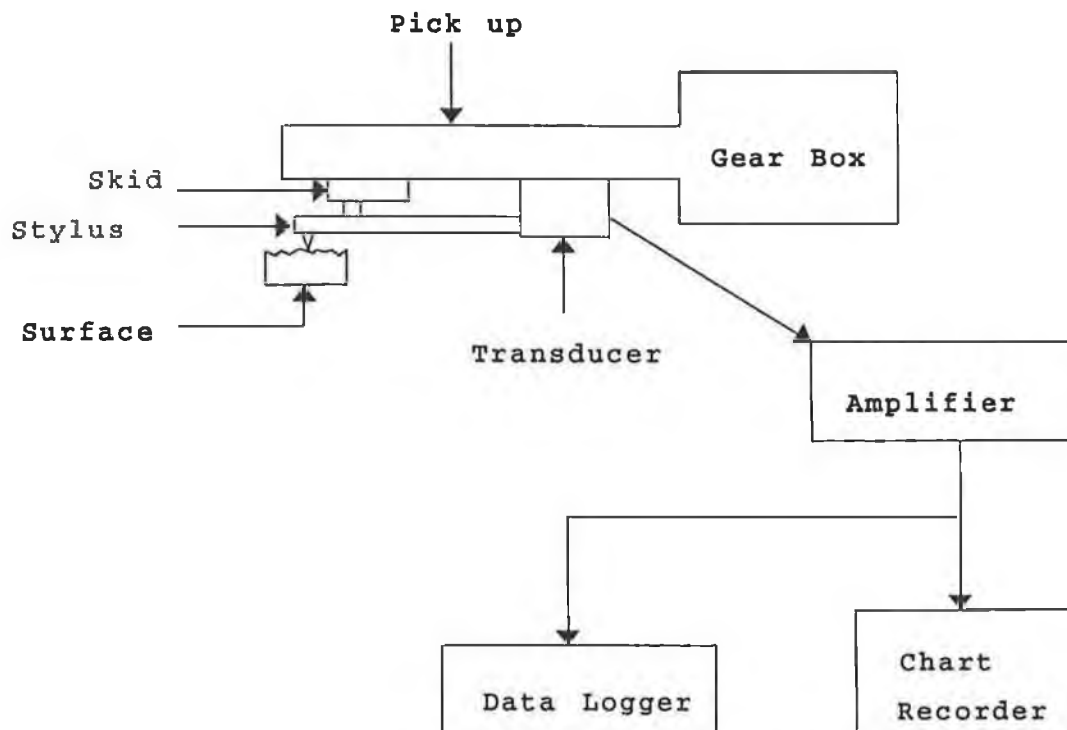


Fig.2.9 Schematic diagram of a typical stylus instrument [76].

vertical movement due to surface irregularities. This is achieved by supporting the pickup body on the surface being measured by means of skid or datum that has a large radius (≈ 50 mm) in comparison with the texture spacing. The skid provides a datum only if the crests are close enough together. If the crests are widely spaced, the measurements are made without the skid, and the traverse shaft provides a straight reference datum. Diamond styli are universally used. In many instruments they are cones of 90° included angle with a tip radius of 4 to 12 μm [48]. The stylus of the profilometer used in the present study is a cone of tip radius 5 μm .

A profilometer gives two types of reading, one by the roughness tester or data logger as a digital display and other one by the chart recorder as a graphical representation. The roughness tester (Surftest 402, Series 178, Mitutoyo Corporation) displays the value of surface roughness which can be displayed as any one of the following: R_a , R_q , R_z and R_{max} . The chart recorder (Mini Recorder for Surftest 402, Series 178, Mitutoyo Corporation) is a thermosensitive type recorder which provides profile curve and roughness curve of the surface texture at profile mode and roughness mode respectively. The recording chart is a section paper of 0.1"x0.2", one division of which is equal to 0.1" vertically and 0.2" horizontally. For correct reading of roughness and profile curves, gain adjustment is needed for the recorder prior to measurement. After adjusting the recording pen position, horizontal magnification, vertical magnification and heat control switches, gain is adjusted with the standard specimen by turning the gain adjustment screw.

The chart recorder has the following features. The horizontal magnification can be varied from 2 to 100. The vertical magnification factors for R_a and R_q can be varied from 80 to 2,000 for a range of 50 μm , 400 to 10,000 for a range of 10 μm and 2,000 to 50,000 for a range of 2 μm and for R_z and R_{max} can be varied from 80 to 2,000 for a range of 250 μm , 400 to 10,000 for a range of 50 μm and 2,000 to 50,000 for a range of 10 μm .

Chapter 3

Experimental Procedure

3.1 Introduction

In order to commission the vacuum deposition system, the commissioning tests were undertaken by depositing titanium and titanium nitride films onto glass substrates. After commissioning, deposition of molybdenum nitride films was done. The process parameters applicable to the present sputtering apparatus for growing hard, adherent and wear resistant films are gas flow ratio, bias voltage, substrate preheating, deposition time, deposition pressure, deposition power, target to substrate distance and surface conditioning of the substrate. Knowledge of the relationship between desired properties of the films and process parameters is a guideline for systematic variation of the process parameters.

3.2 Deposition of Films

3.2.1 Commissioning with Ti Film Deposition

The tests with Ti film deposition were undertaken to investigate the effects of variation in pressure, magnetron power and target to substrate distance on the deposition rate. It was necessary to standardize some operating conditions in the vacuum chamber to conduct these experiments. Thus, it was decided from literature that the following were in the range of normal operating conditions. Base pressure is 5×10^{-5} mbar (to ensure a clean vacuum environment), operating pressure is 10^{-3} mbar (argon back-filled to this pressure), magnetron power is 1.8 kW and target to substrate distance is 6 cm. These last three magnitudes relate to the normal operating condition for the variables involved in Ti film deposition.

Experiments were conducted to measure deposition rate which was evaluated by measuring the thickness of the films and expressing the thickness per hour. The results of successive tests are graphed in Figs.3.1(a), 3.1(b) & 3.1(c). In Fig.3.1(b) deposition rate vs. power is depicted as deposition rate vs. magnetron current due to the fact that the operating characteristics of both directly cooled and indirectly cooled magnetrons follow the empirical current-voltage relationship

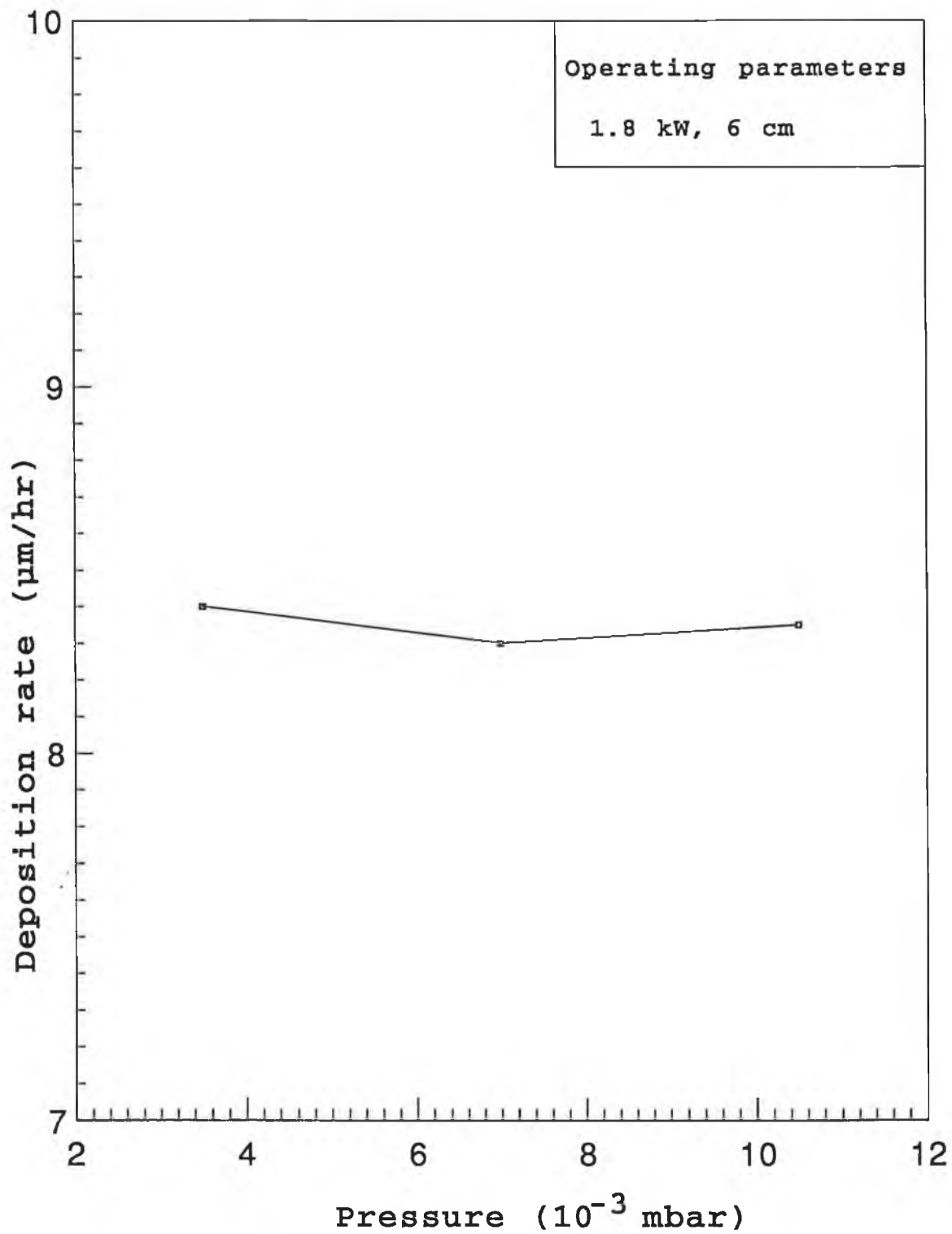


Fig.3.1(a) Deposition rate vs. pressure for titanium [85].

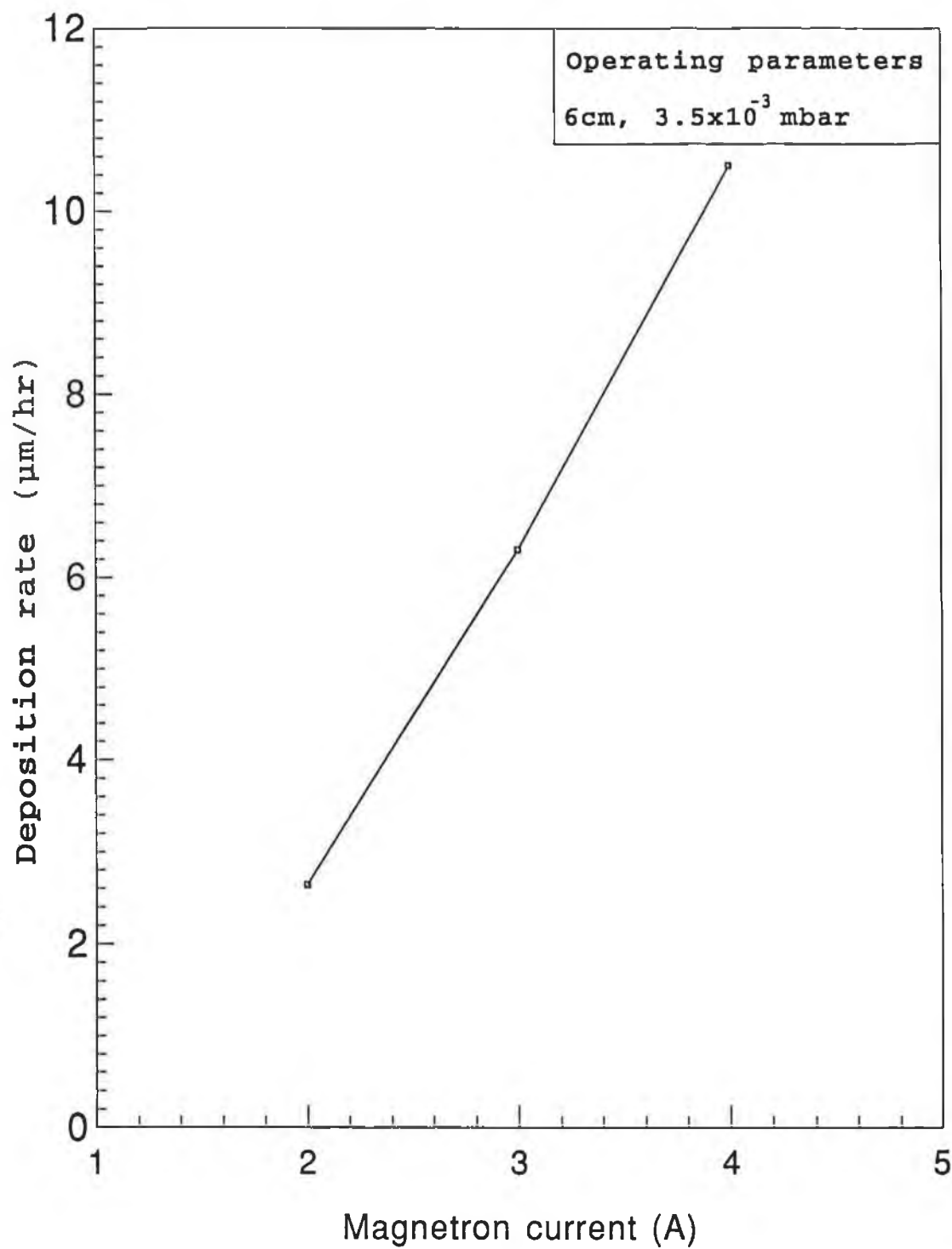


Fig.3.1(b) Deposition rate vs. magnetron current for titanium [85].

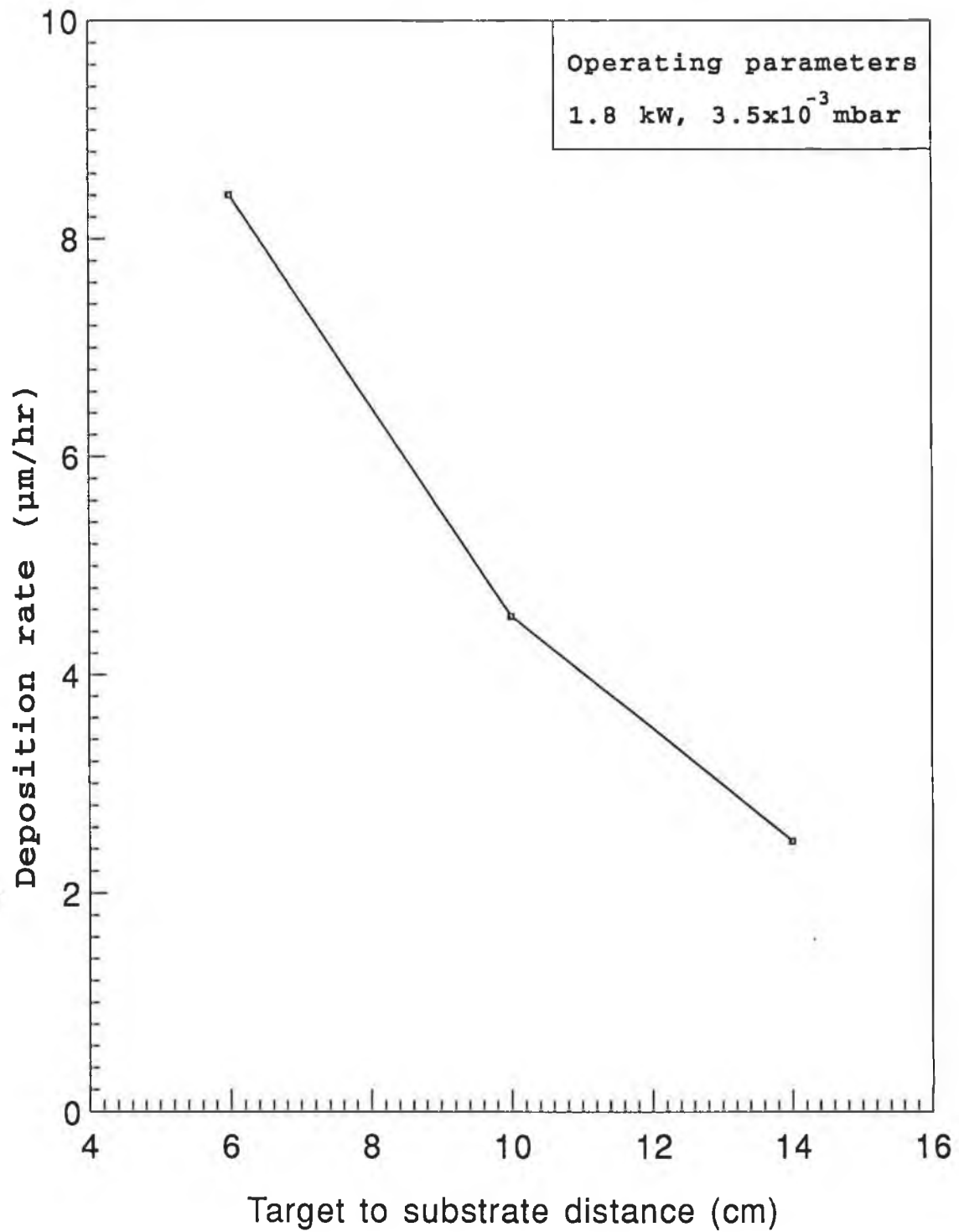


Fig.3.1(c) Deposition rate vs. target to substrate distance for titanium [85].

$$I = kV^n$$

where I is the cathode current, k is a constant, V is the cathode voltage and n is an exponent which reflects the electron trapping efficiency of the plasma.

Using these tests to determine the influence of d_{ts} , power and pressure on the deposition rate of Ti films onto glass substrates, an equation describing the relationship of the parameters was developed by the author of the report in reference [85]. The equation describing the thickness of each film, as dictated by any one of the three parameters was first ascertained. Then the three equations were combined and the constants were determined. The equations are as follows:

- i) $t = k_1 P$, where k_1 is a constant and P is power;
- ii) $t = k_2 / d_{ts}^2$, where k_2 is a constant; and
- iii) $t = k_3 p$, where k_3 is a constant and p is pressure.

However, the above inverse square relationship may not be appropriate since only 3 nearly colinear points have been used. The deposition rate was found to be unaffected by system pressure in the region of 10^{-3} mbar. So this parameter was ignored. Combining these equations the following single equation is obtained,

$$t = A. (P/d_{ts}^2)$$

where A is a constant equal to $4.125 \text{ nm.cm}^2/\text{kW}$. This was found to predict accurately the deposition rate of Ti films onto glass.

In addition to these preliminary tests on the deposition of Ti films, other tests which gave boundary parameters for operation were carried out by the author in reference [85]. It was found, for example, that the minimum voltage for ignition of the plasma in the 10^{-3} mbar pressure range was about 380 V and did not vary much with pressure variations from 3.5×10^{-3} mbar to 5.8×10^{-3} mbar. The range of pressures within which the magnetron shutters worked i.e. maintained a plasma between the target and the shutters was 4×10^{-3} mbar to 8×10^{-4} mbar. Floating potential of the plasma itself is about 10 V at magnetron powers of between 1 kW to 2 kW and operating pressure between

10^{-2} mbar to 7.8×10^{-3} mbar. The ion current varied between 390 mA at 1 kW and 7.8×10^{-3} mbar to 774 mA at 2 kW and 10^{-2} mbar.

3.2.2 Commissioning Tests with TiN Film Deposition

The commissioning tests with TiN film deposition were conducted on glass slides of dimensions 76mmx 26mm x 1mm. All samples were degreased in an ultrasonic bath of 1,1,1 trichloroethane and air dried.

TiN films was deposited by reactive magnetron sputtering, without the use of the optical emission spectrometer and reactaflo feedback loop, experiments yielded the following results:

1. Nitrogen was found to be evenly distributed throughout the chamber but Ti was concentrated near the magnetron target. Hence, the sample placed near the target (small d_{ts}) were Ti rich, while those at greater distances from the target (greater d_{ts}) were nitrogen rich. Therefore, although for a given distance any one composition could be attained, this result was not readily reproducible.
2. It was found that samples exposed to excessive nitrogen levels produced over stoichiometric films. This is especially true at large d_{ts} . However, stoichiometric coatings could be obtained by balancing nitrogen partial pressures and target to substrate distances.
3. Samples placed in the center of the table were found to be over stoichiometric or nitrogen rich due to the fact that Ti flux did not penetrate into the chamber from any one target to any great level. Also, deposition rates at large d_{ts} were quite low.
4. Deposition rates were found to decrease as the level of nitrogen in the chamber increased which indicated that target poisoning had occurred.

Thus it was found that in order to produce stoichiometric films at a

satisfactory deposition rate, the samples had to be placed close to the target face.

In the deposition of MoN_x films by reactive magnetron sputtering using an optical emission spectrometer and reactaflo feedback loop, the characteristic wavelength (λ) for Mo has been determined as 376 nm. Imai et al [68] have used $\lambda = 380$ nm for Mo in their investigation.

3.2.3 Deposition of MoN_x Films

Deposition of MoN_x films was done on substrates of steel flats (50mm x 20mm x 0.6mm), cleaned with a wash in 1,1,1 trichloroethane and dried in air. All the necessary power supply points (shown in Fig.3.2) to the deposition system were switched on. To warm up the diffusion pump, the cooling water supply, air compressor and roughing pump were switched on sequentially. When the pressure on gauge 2 (shown in Fig.3.3) is less than 0.3 mbar, the backing valve and then the diffusion pump were switched on. The system was left in this condition for at least 15 minutes to allow the diffusion pump to heat up before operation.

The substrate was placed at a desired position on the substrate holder and the chamber was closed up. To pump down the chamber, ensuring the chamber was sealed and the diffusion pump was warmed up, the backing valve was closed and the roughing valve was opened. When the pressure on gauge 1 is less than 0.3 mbar, the roughing valve was closed and the backing valve was opened. Then the gate valve was opened and the chamber was evacuated to the base pressure of 5×10^{-5} mbar where the pressure was monitored on gauge 1 and gauge 3.

The argon gas bottle and then the argon gas inlet valve were opened. On the reactaflo system, the main gas flow was switched on and the cooling water to the magnetron was switched on. Prior to the film growth, both the substrate and the target were sputter cleaned at working pressure. The working pressure was set by varying the flow of the Ar gas into the system using the setpoint potentiometer. Sputter cleaning was done for 30 minutes at -1000 V substrate bias voltage and 0.2 A magnetron current. These values were selected based on advise

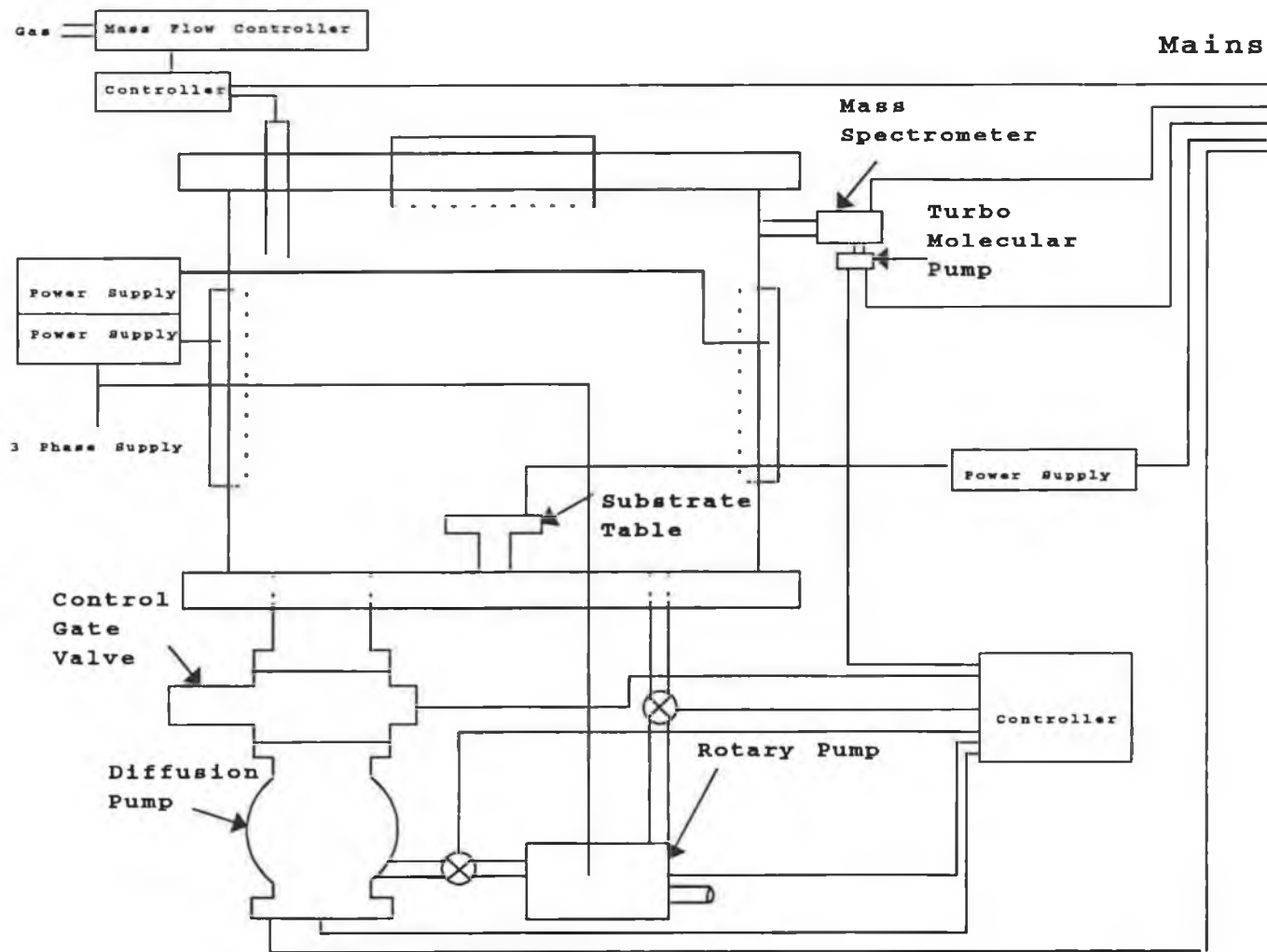


Fig.3.2 Electrical circuit of the deposition system[85].

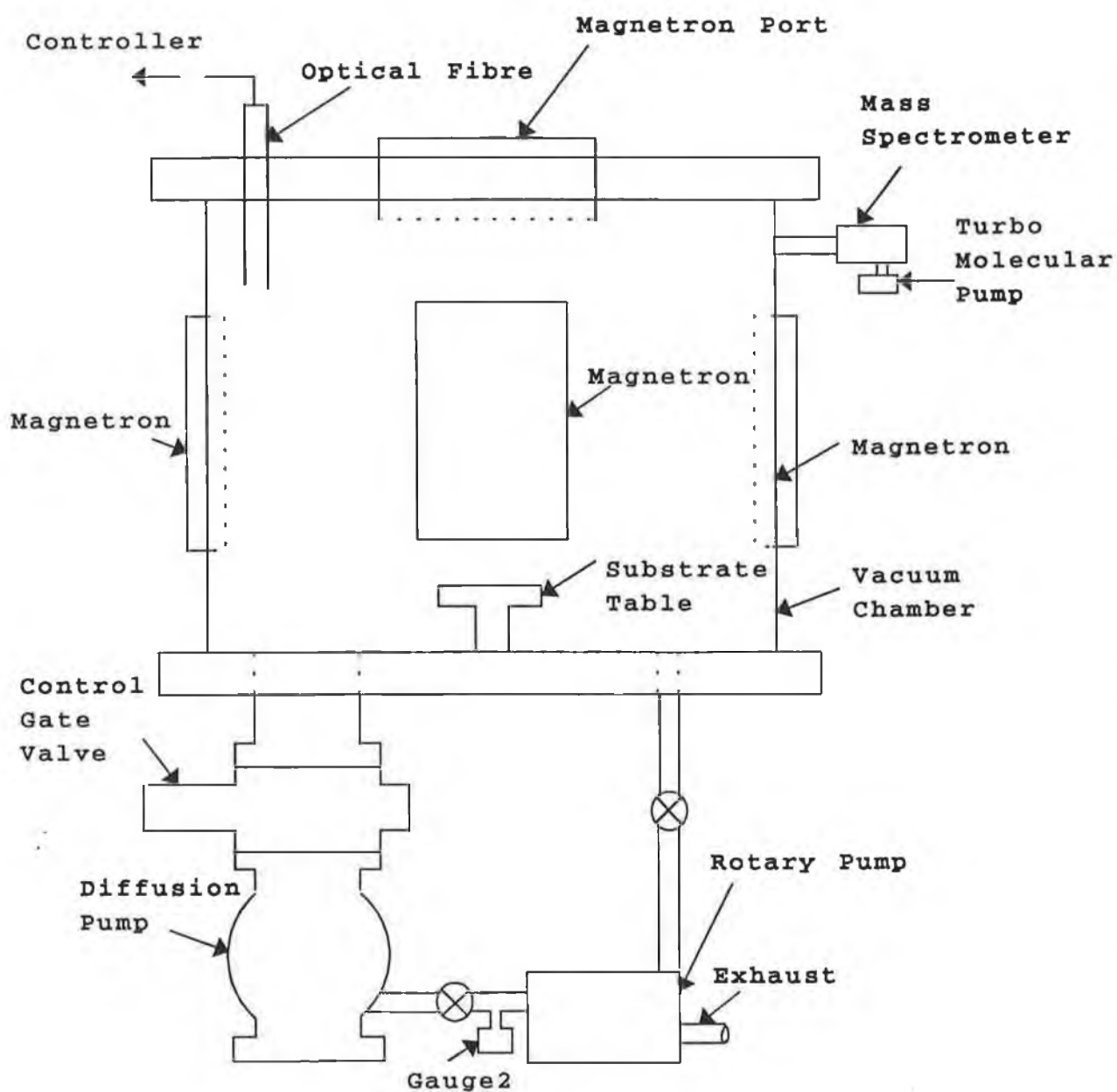


Fig.3.3 Schematic of the deposition system[85].

received from the supervisor. Then the desired bias voltage and magnetron current was set by gradually decreasing the bias voltage and increasing the magnetron current in 20 minutes. The film was deposited for a desired time. When the required deposition time had elapsed, the magnetron power supply was switched off. The Ar inlet valve and the high vacuum valve were closed. The substrate was allowed to cool for 30 minutes before venting the chamber to the atmosphere.

To shut off the system, ensuring the air admittance valve was closed, the backing valve was closed and then the roughing valve was opened. When the pressure on gauge 1 was less than 0.3 mbar, the roughing valve was closed and then the backing valve was opened. The diffusion pump was turned off and the system was left in this condition for at least 15 minutes to allow the diffusion pump to cool down. Then the backing valve, the roughing pump, the air compressor, the water supply and the power supply points to the deposition system were switched off sequentially.

In total, a deposition sequence would require at least 15 minutes of warm up of the diffusion pump, about 45 minutes to pump down, about 50 minutes of presputtering, about 30 minutes deposition time and about 30 minutes cooling which results in a deposition cycle time of about 3 hours.

To grow films with substrate bias, the necessary electrical connections were made after placing the substrate on the substrate holder which were always done for sputter cleaning. A desired negative bias was applied to the substrate after setting the working pressure. The temperature of the substrate during the deposition process was measured by the thermocouple as mentioned in Section 2.2.7. The measured temperature reached a steady state value in a short time after initiating the deposition.

To grow films with substrate preheating, the required electrical connections were made after placing the substrate on the substrate holder. A desired temperature was generated by supplying power to the tungsten wire. After the preheating temperature reached a steady state value, the heating was maintained for about 15 minutes. The temperature of the substrate was measured by the thermocouple as mentioned above.

The temperature was enhanced by the energetic impinging flux of ions. In this case the substrate was allowed to cool for an hour before venting the chamber to the atmosphere.

To grow films with reactive sputtering, the Ar gas bottle and the reactive gas bottle were opened simultaneously. After setting the working pressure, in addition to the steps in nonreactive sputtering (presputtering), the reactaflo 'Auto' was turned on. The system was brought under control by choosing a setpoint and varying the gain. When the required deposition time had elapsed, the reactaflo 'Auto' was switched off.

3.3 Deposition of Ti_xC and TiN Films by External Supplier

Ti_xC and TiN coatings were deposited on various substrates by D.G. Teer Coating Services Ltd., Hartlebury, England. Ti_xC films were produced with a low percentage of titanium ($x=0.05$). The substrates were D2 tool steel (51mm x 26mm x 5mm), D3 tool steel (56mm x 29mm x 5mm), Vanadis 4 (56mm x 29mm x 5mm) and Vanadis 10 (51mm x 26mm x 5mm) cut off from the respective material bar. The substrates were prepared by sequentially milling, stress relieving, heat treating and grinding.

3.4 Characterization of Films

In order to make exhaustive use of a coating, its full characterization is essential. With this in mind, the films obtained from the deposition of MoN_x were characterized in terms of their thickness, hardness and adhesion. Also the specimens coated by external supplier under standard conditions were characterized in terms of their hardness and adhesion.

3.4.1 Thickness

Thickness is undoubtedly the coating characteristic most often measured and specified quantitatively. Optical, mechanical, electrical, magnetic, electromagnetic, radiation and miscellaneous techniques are used for coating thickness measurements. The coating thickness was

measured by Mirau interferometer. A step was made in the coating by masking a portion of the substrate during deposition. The interference fringes were formed between an optical flat and the surface of the coated specimen using a white light ($\lambda = 550 \text{ nm}$) that was observed with an interference microscope (Nikon, Optiphot). The fringe pattern is shown in Fig.2.6(b). There is no fixed limit to how thick a coating may be measured, but the method is best suited to coatings of less than about $2 \mu\text{m}$ thick. The thickness was calculated by using the formula mentioned in Section 2.3.1.

3.4.2 Hardness

Hardness is defined as the resistance of a material to deformation and is usually measured by indenting a diamond stylus of known shape under load into the specimen and measuring the size of the resulting deformation. Common practice among workers in the coating field is to ensure that only the hardness of the coatings is measured i.e. there is no contribution to the measured hardness from the substrate.

Indentation microhardness measurements are a well known and reliable test method frequently applied to coatings. The reproducibility is good but when the ratio D/t i.e. indentation depth to film thickness exceeds a critical value, the measured hardness H is influenced by the substrate material and no longer a characteristic of the coating. The critical D/t ratio varies between approximately 0.07 and 0.2. The most unfavorable case is that of a hard coating on a softer substrate and in most cases a value of 0.1 is adopted. To overcome the problem of thin films on soft substrate, i.e. $0.1 < D/t < 1$, a correction factor is suggested [49]. With this correction factor the hardness of the films is given by

$$H_f = H_s + [D^2 (H_c - H_s)] / (2DCt - C^2t^2)$$

where H_f is the hardness of the films in kg/mm^2 , H_s is the hardness of the substrate in kg/mm^2 , D is the indentation depth in mm, d is the diagonal in mm, H_c is the hardness of the composite in kg/mm^2 , t is the film thickness in mm and C is $\text{Sin}^2 22^\circ$ for plastically strained films or $2 \text{ Sin}^2 11^\circ$ for hard, brittle films on soft substrates.

In this study, the hardness was measured in Vickers hardness tester (Leitz Miniload 2 Microhardness Tester).

3.4.3 Adhesion

Adhesion describes the sticking together of two materials. Adhesive strength, in a practical sense, is the stress required to remove a coating from a substrate. The value of the adhesive strength can lie somewhere between the adhesion due to Van der Waals forces at one extreme and the cohesive strength of either component at the other extreme, i.e. typically between the limits of about 1 MPa and 3 GPa.

Many techniques have been developed to measure the coating adhesion. The scratch method is one of these. Scratching the surface with a finger nail or a knife is probably one of the oldest methods for determining the adhesion of paints and other coatings. In the modern version of this method, a scratch tester is used. To determine the adhesive strength in the present study a scratch tester was used. Scratches were made with increasing load until the edges of the scratch became jagged. The critical load was determined from the first appearance of the jagged edge scratch.

3.5 Generation of Wear

The sample was clamped onto the substrate table at the desired position. The connecting arm was adjusted for desired sliding distance. After setting the tool on the sample surface, the desired wear load was applied. As the motor is switched on, the tool starts sliding. The revolution counter records the number of tool reciprocations to which the sample was subjected to produce wear. After the desired number of revolutions the motor was switched off, the dead load was withdrawn and the tool was taken out. The connecting arm was disengaged from the motor shaft and the sample was declamped.

In the progressive wear study, the first step of wear (fraction of a micron depth) was produced under a given load and very low number of cycles. The sample was taken for wear measurement. To make wear in the second step, the sample was placed at the same position of the

preceding step of wear and further wear was made under the same load and for the same or different number of cycles as in the preceding step of wear. The sample was taken for wear measurement and the process was repeated until desired wear depth was attained.

3.6 Measurement of Wear

Wear is generated on the surface layer of a solid by the action of another body or medium. The generation of wear for the present study is stated in Section 3.4. Common wear measurements are weight loss, volume loss or displacement scar width or depth, or other geometric measures and indirect measurements such as time required to wear through a coating or load required to cause severe wear or a change in surface finish. Scanning electron microscopy (SEM) of worn surfaces is commonly used to measure microscopic wear. A stylus or noncontact optical profiler and Vickers or Knoop microhardness indentation techniques are easy to use and are commonly used to measure depth of wear with a resolution of up to a fraction of a nanometer [72].

There is a comprehensive description of a profilometer in Section 2.5. The one used for measuring wear depth has a resolution of up to 0.05 μm for a range of 10 μm . To record the profile curve from which wear depth can be measured, the specimen surface must be properly levelled. The higher the vertical magnification, the higher the importance of precise levelling. When the stylus traverses across the wear track, profile of the wear track as well as the specimen surface is recorded on the chart. The wear depth is given by

$$d = [(n \times 2.5 \times 1000) / \text{Vertical magnification}] \mu\text{m}$$

and the wear width is given by

$$w = [(n \times 5 \times 1000) / \text{Horizontal magnification}] \mu\text{m}$$

where n is the number of divisions vertically and horizontally for the wear depth and wear width respectively.

Chapter 4

Results and Discussions

4.1 Introduction

Molybdenum nitride films have been produced with argon and nitrogen plasma by using reactive magnetron sputtering. To study the effect of substrate bias, deposition pressure and magnetron current on thickness, hardness and adhesion of the films, depositions have been done on steel flats.

The deposition of titanium nitride and titanium carbide films have been done under the coating company's standard conditions. To study the wear behaviour, the depositions were done on substrates of D2 tool steel, D3 tool steel, Vanadis 4 and Vanadis 10 for a range of film thicknesses (3-5 μm).

4.2 Deposited MoN_x Films

The effect of substrate bias, deposition pressure and magnetron current on thickness, hardness and adhesion of films has been studied. The results obtained from the measurements of various characteristics of the produced films are presented in Figs.4.1 to 4.6. Each of the experimental points in Figs.4.1 to 4.6, is a result of only one test. For this reason reproducibility of any of the experimental point is not known. From microscopic observation, it was seen that flakes of coatings were all over the coated surface of the samples which was a clear indication of poor adhesion. The results of the tests are presented in Figs.4.7 to 4.12 for comparison with the existing works of others and other types of coatings. Discussion of the results was carried out with regard to observed agreements and discrepancies in the comparisons.

4.2.1 Effect of Substrate Bias

Experiments have been performed to study the effect of the bias voltage, U_b on the desired characteristics by depositing films on 3 substrates at 3 different bias voltages, where deposition pressure, $P_d = 2.0 \times 10^{-3}$ mbar and magnetron current, $I_m = 3.5$ A in each of the depositions.

4.2.1.1 Deposition Rate

The results of deposition rate of the present study as a function of bias voltage are shown in Fig.4.1. The reproducibility of the results is unknown. With this limitation it can be said that the deposition rate bears an inverse relation with the bias voltage. Deposition rate of MoN_x films of the present study and TiN [80] films are presented in Fig.4.7 for comparison. Deposition rate of MoN_x films from the works of others could not be presented for comparison due to unavailability of results. From the figure it is observed that the deposition rate of MoN_x films is similar to that for TiN films.

4.2.1.2 Hardness

The results of hardness of the present study as a function of bias voltage are shown in Fig.4.2. Hardness is found to bear a square relation with the bias voltage. Hardness attained a peak when bias voltage was near to the saturation current point. This saturation voltage was determined as being about -40 V. Hardness of MoN_x films from present depositions and other studies, and hardness of TiN [82] films are presented in Fig.4.8 for comparison. The results of the present study have shown the same trend of results as those of Rudnik et al [78] though their deposition conditions were different. Unlike MoN_x films, hardness of TiN films increased with increasing bias voltage.

4.2.2 Effect of Deposition Pressure

Experiments have been performed to investigate the effect of deposition pressure on the desired characteristics by depositing films on 3 substrates at 3 different deposition pressures, where $U_b = -30$ V and $I_m = 3.5$ A in each of the depositions.

4.2.2.1 Deposition Rate

The results of deposition rate, in the present study, as a function of deposition pressure are shown in Fig.4.3. A maximum deposition rate

is found to occur at 2.4×10^{-3} mbar which is because of a suitable deposition pressure for maximum plasma formation. This plasma is consisted of target particles, Ar and N_2 gases. Deposition rate of MoN_x films from present study and SiN [66] films (results of TiN films are not available) are presented in Fig.4.9 for comparison. Deposition rate of MoN_x films from the works of others could not be presented for comparison due to unavailability of the results. Deposition rate of MoN_x films is in good agreement with that of SiN films qualitatively but differs quantitatively, the deposition powers were being considerably different. The deposition powers were 2 kW for MoN_x films and 1 kW for SiN films.

4.2.2.2 Hardness

The results for hardness as a function of deposition pressure are shown in Fig.4.4. A minimum or lower hardness at a suitable pressure for maximum deposition rate is not revealing any well known fact. It can be stated with the limitation of unknown reproducibility that hardness follows an inverse relation with the deposition pressure. Hardness of MoN_x films from present study and TiN [82] films are presented in Fig.4.10 for comparison. Hardness of MoN_x films from the works of others could not be presented for comparison due to unavailability of results. It is observed that with increasing deposition pressure, hardness of MoN_x films decreases smoothly whereas that of TiN films decreases haphazardly.

4.2.3 Effect of Magnetron Current

Experiments have been done to investigate the effect of the magnetron current on the desired characteristics by depositing films on 3 substrates at 3 different magnetron currents, where $U_s = -30$ V and $P_d = 2.0 \times 10^{-3}$ mbar in each of the depositions.

4.2.3.1 Deposition Rate

The results for deposition rate as a function of magnetron current are shown in Fig.4.5. With the limitation of unknown reproducibility of the results, it can be said that deposition rate obeys linear

relation with the magnetron current. The deposition rate of films from present study, other studies and results available for TiN [79] are presented in Fig.4.11 as functions of deposition power. This is because the results of other studies and TiN films are available as functions of deposition power rather than magnetron current. The results of the present study are in agreement with those studied by Maoujoud et al [83]. Deposition rate of MoN_x films from the present study and others works are in good agreement with that of TiN [79] films.

4.2.3.2 Hardness

The results of hardness as a function of magnetron current are shown in Fig.4.6. With the limitation of unknown reproducibility of the results, it can be stated that hardness follows a square relation with the magnetron current. Hardness of MoN_x films from present study, other studies and hardness of TiN [82] films are presented as functions of deposition power in Fig.4.12. This is because results of other studies on MoN_x and TiN films are available as functions of deposition power rather than magnetron current. Hardness of MoN_x films from present study and as studied by Rudnik et al [78] are in good agreement. But the hardness of TiN [82] films did not increase with increasing power. This is in contrast to MoN_x films.

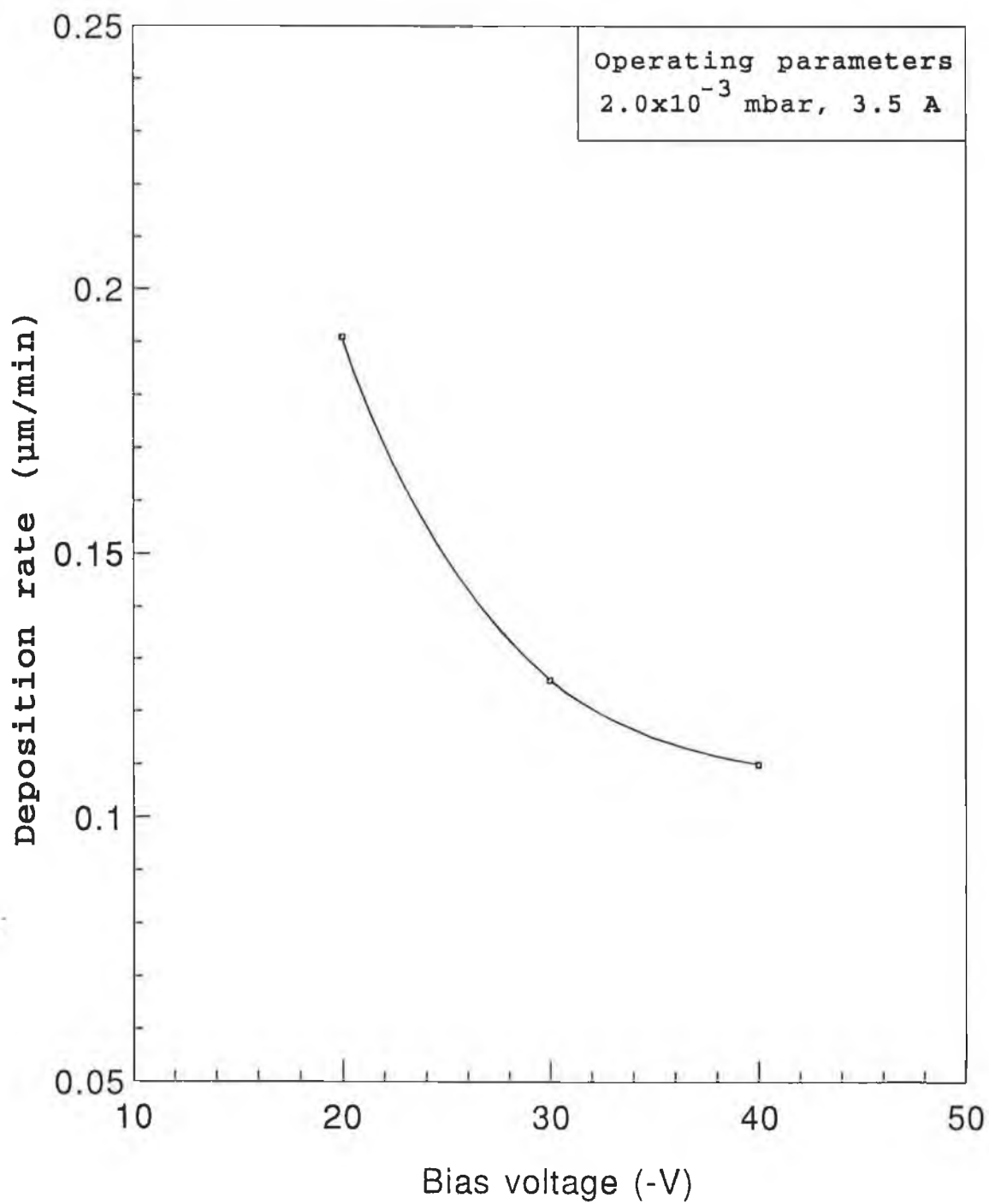


Fig.4.1 Deposition rate of MoN_x films as a function of bias voltage.

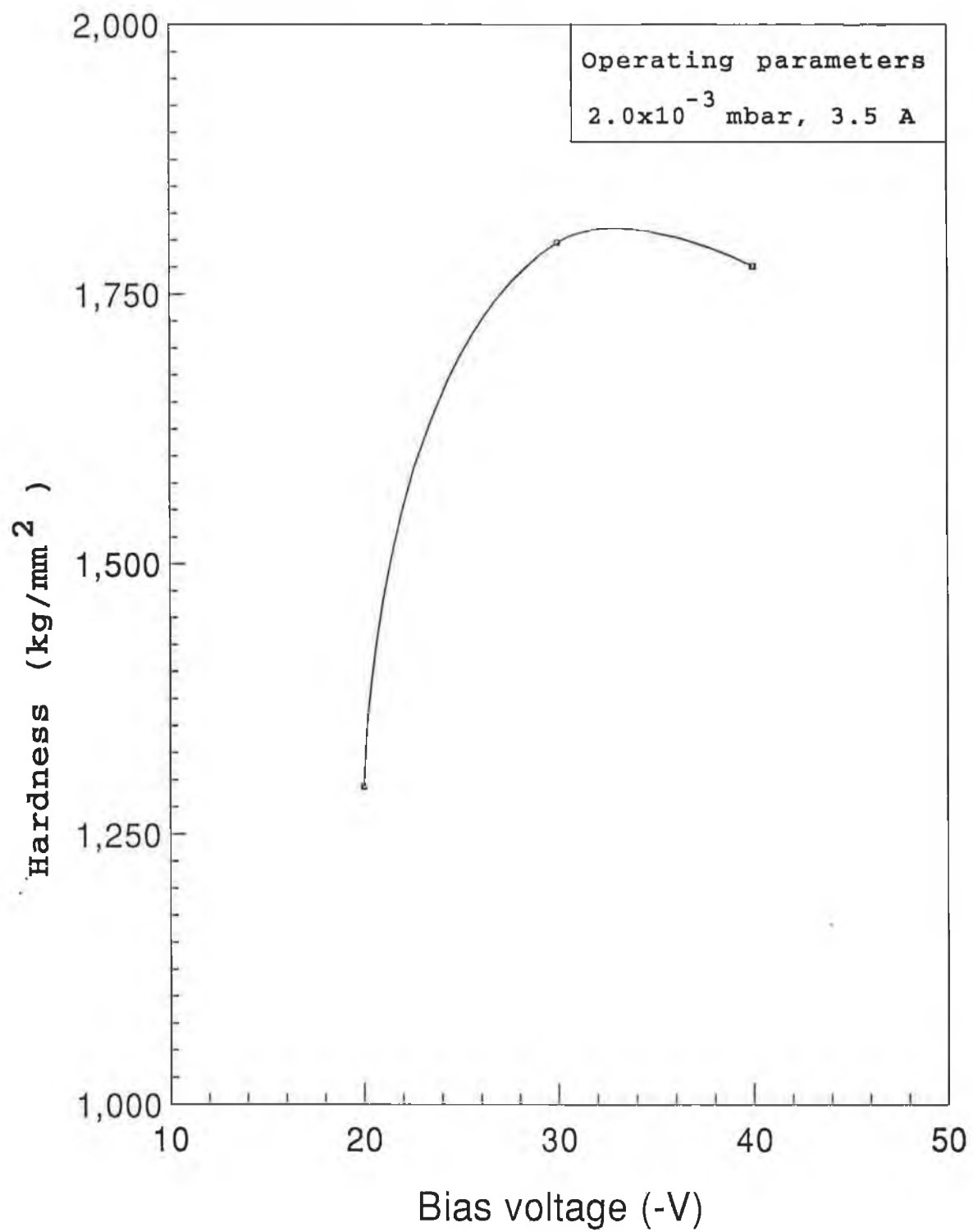


Fig.4.2 Hardness of MoN_x films as a function of bias voltage.

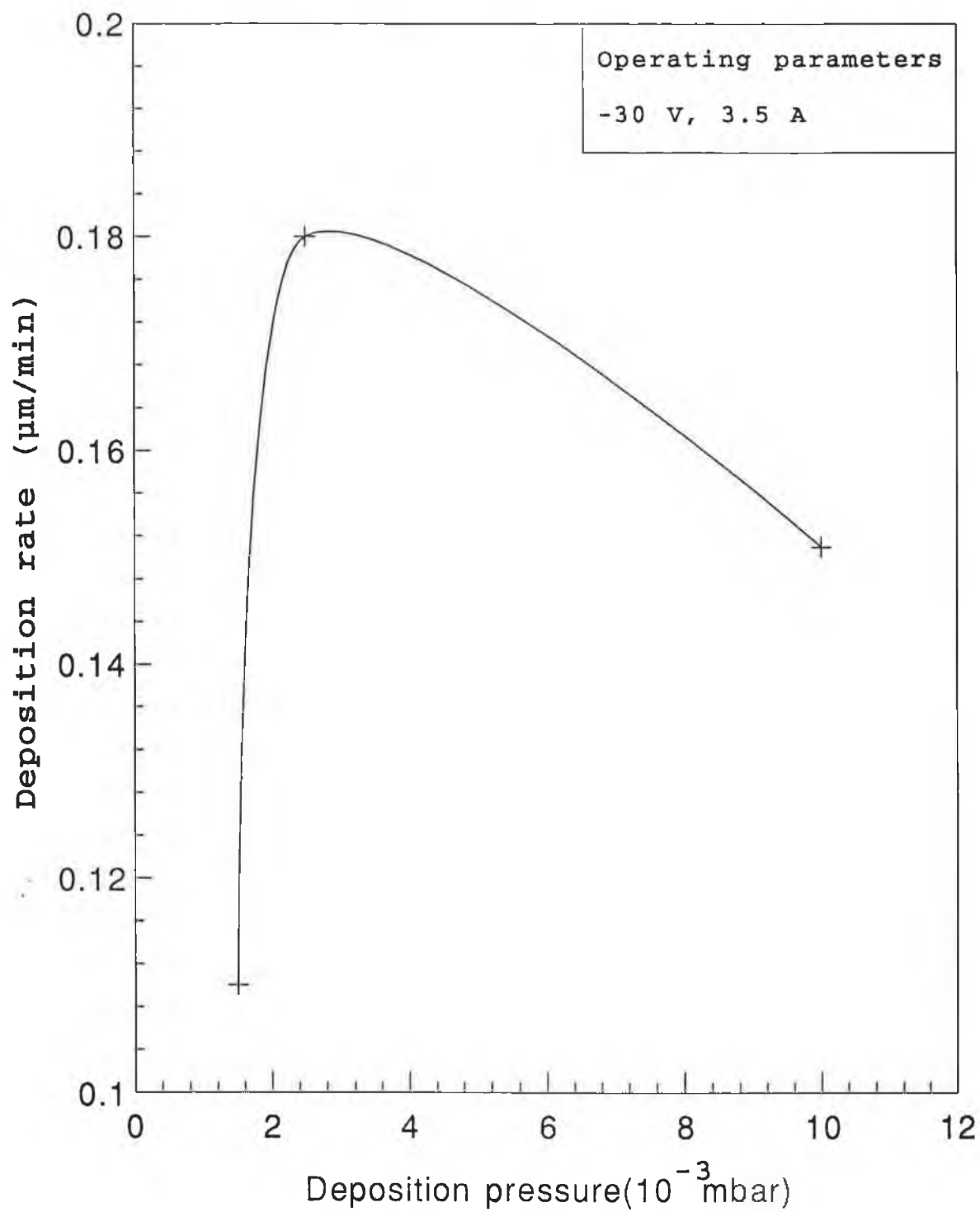


Fig.4.3 Deposition rate of MoN_x films as a function of deposition pressure.

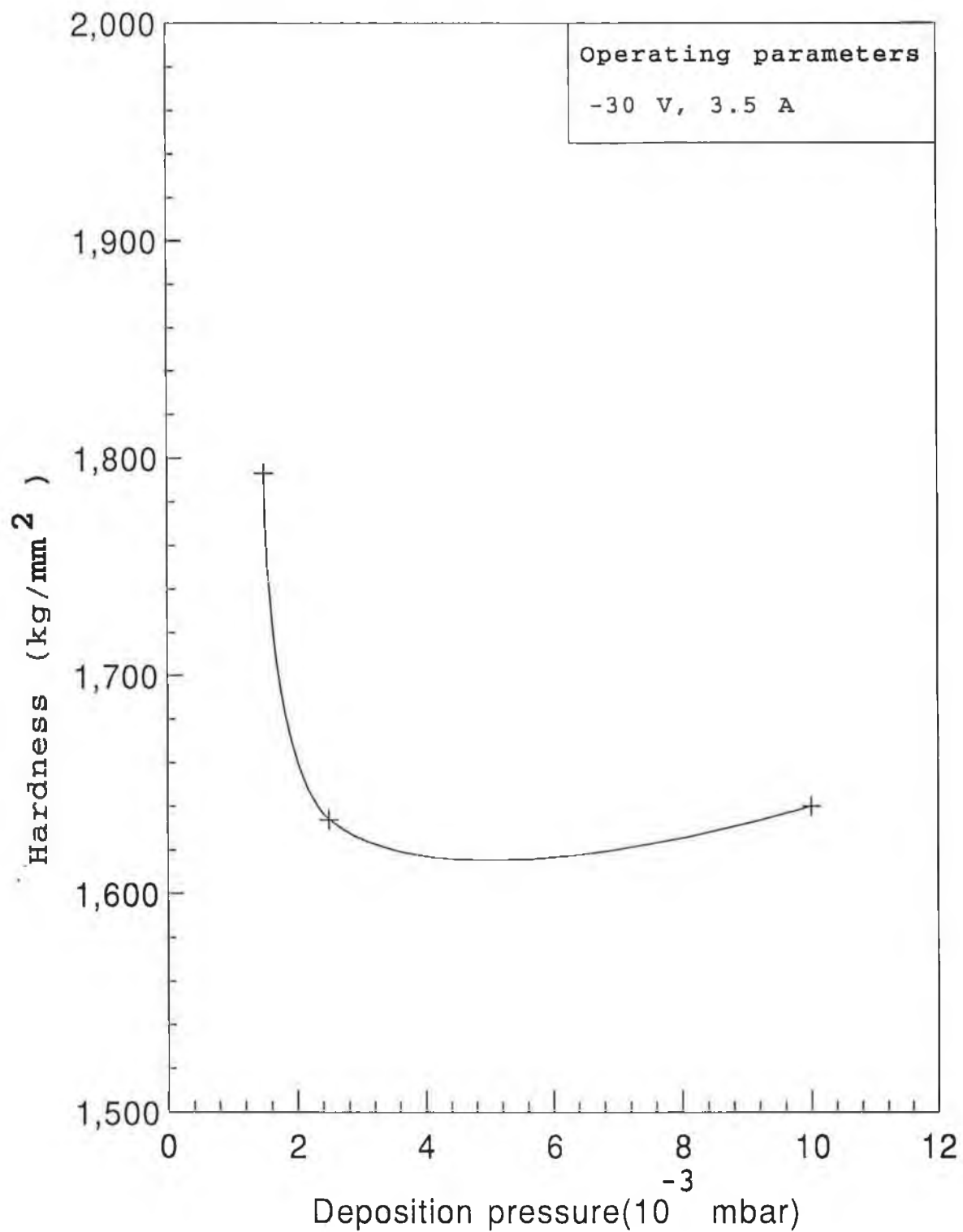


Fig.4.4 Hardness of MoN_x films as a function of deposition pressure.

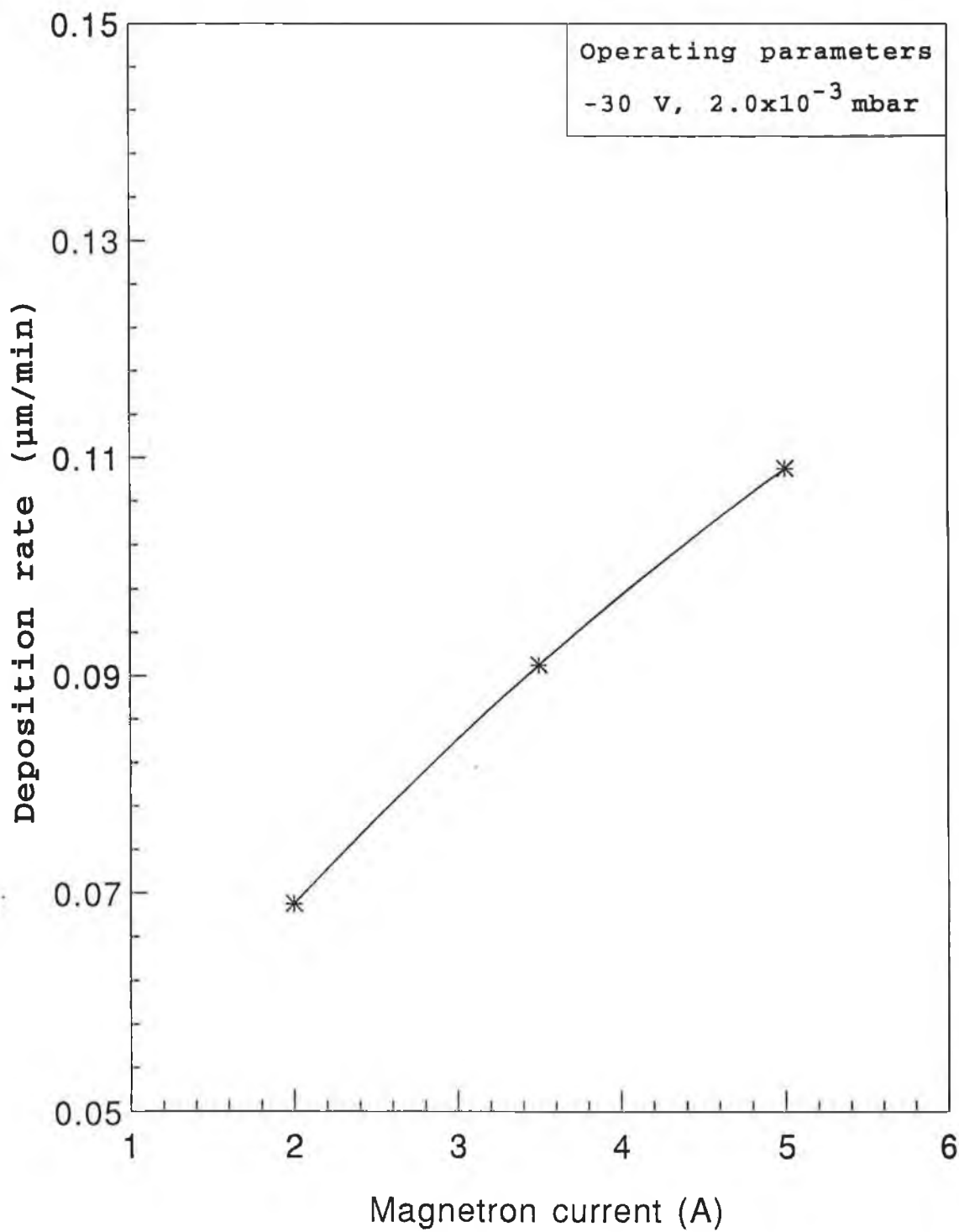


Fig.4.5 Deposition rate of MoN_x films as a function of magnetron current.

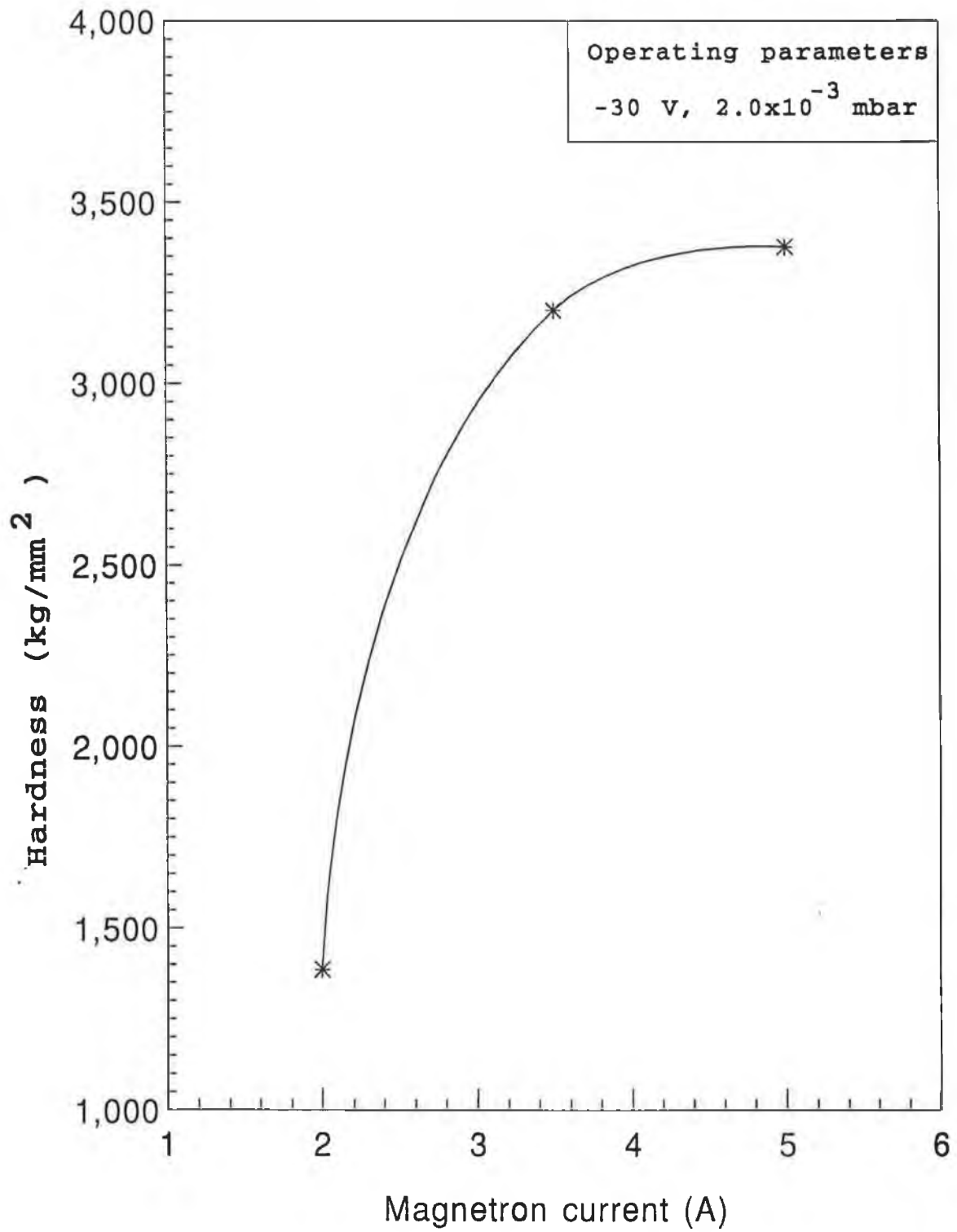


Fig.4.6 Hardness of MoN_x films as a function of magnetron current.

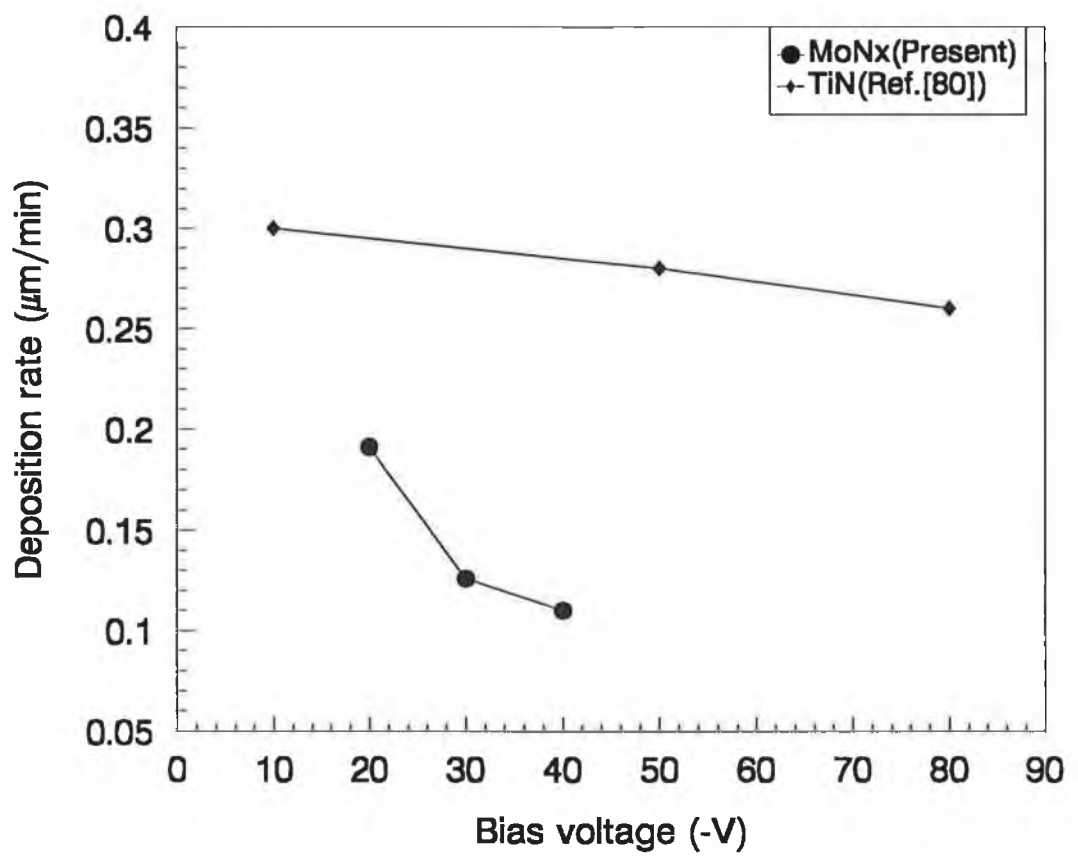


Fig.4.7 Deposition rate as a function of bias voltage.

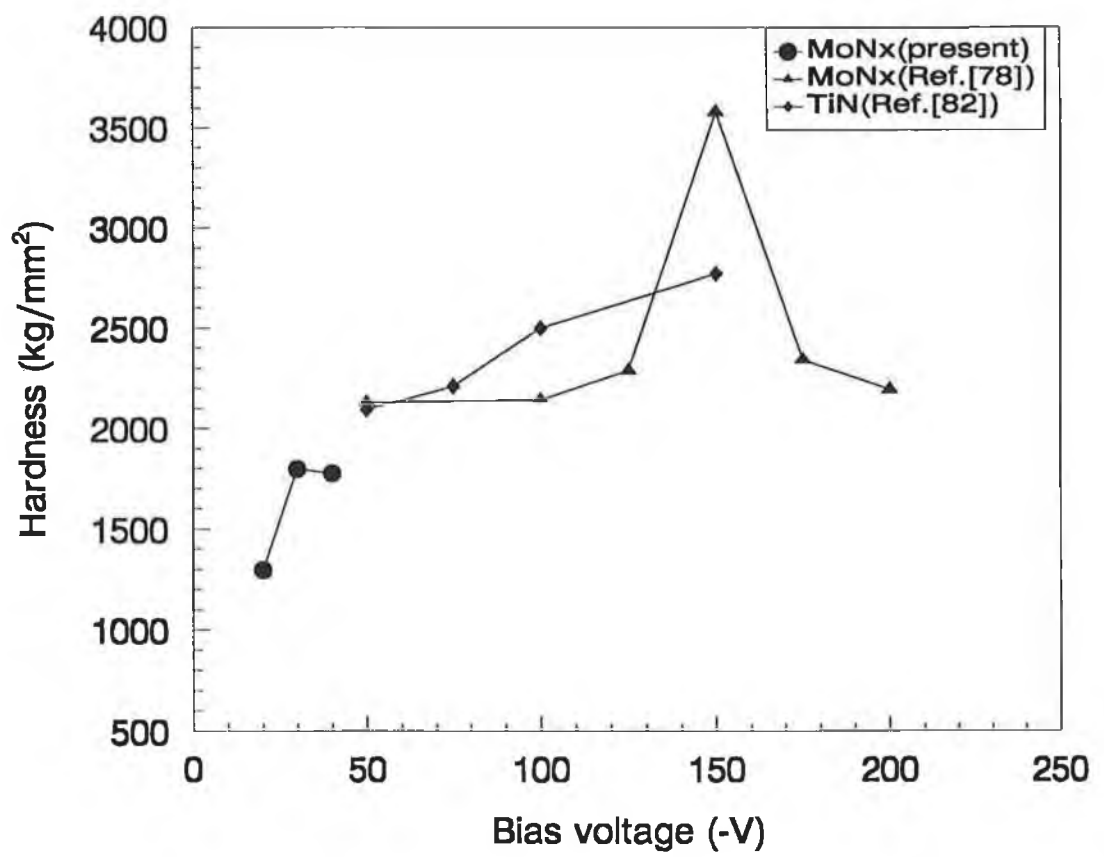


Fig.4.8 Hardness as a function of bias voltage.

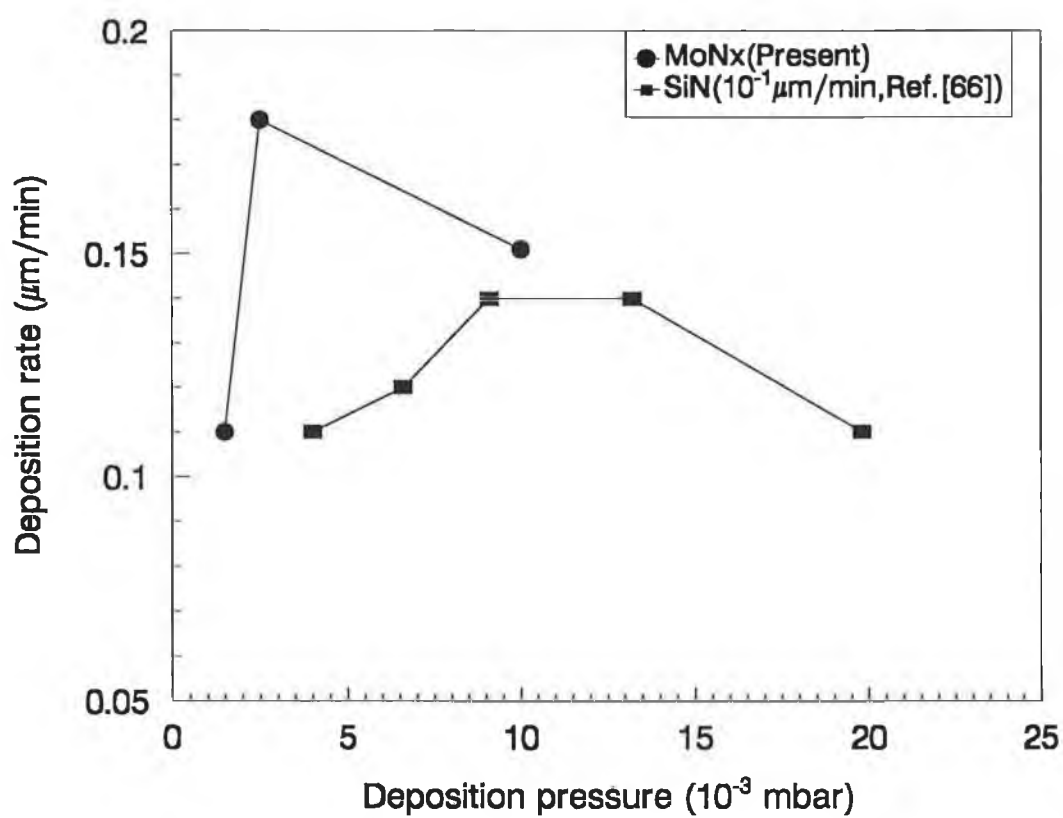


Fig.4.9 Deposition rate as a function of deposition pressure.

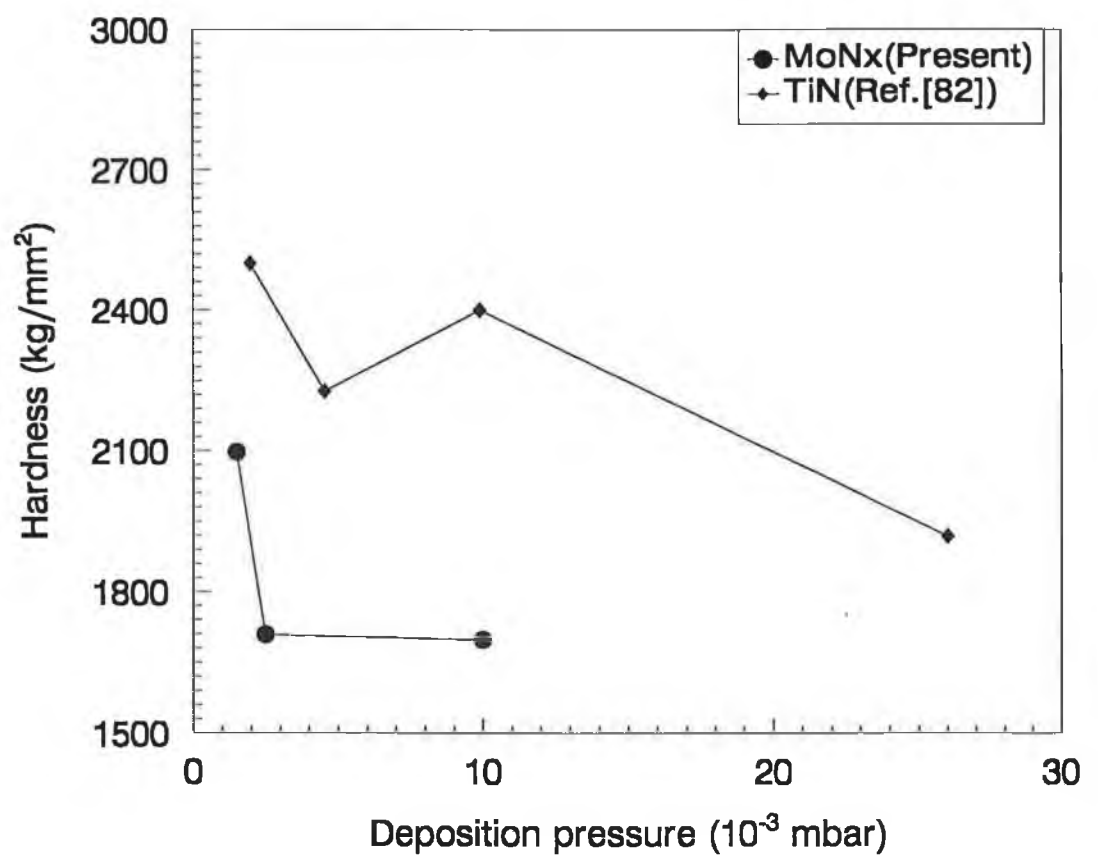


Fig.4.10 Hardness as a function of deposition pressure.

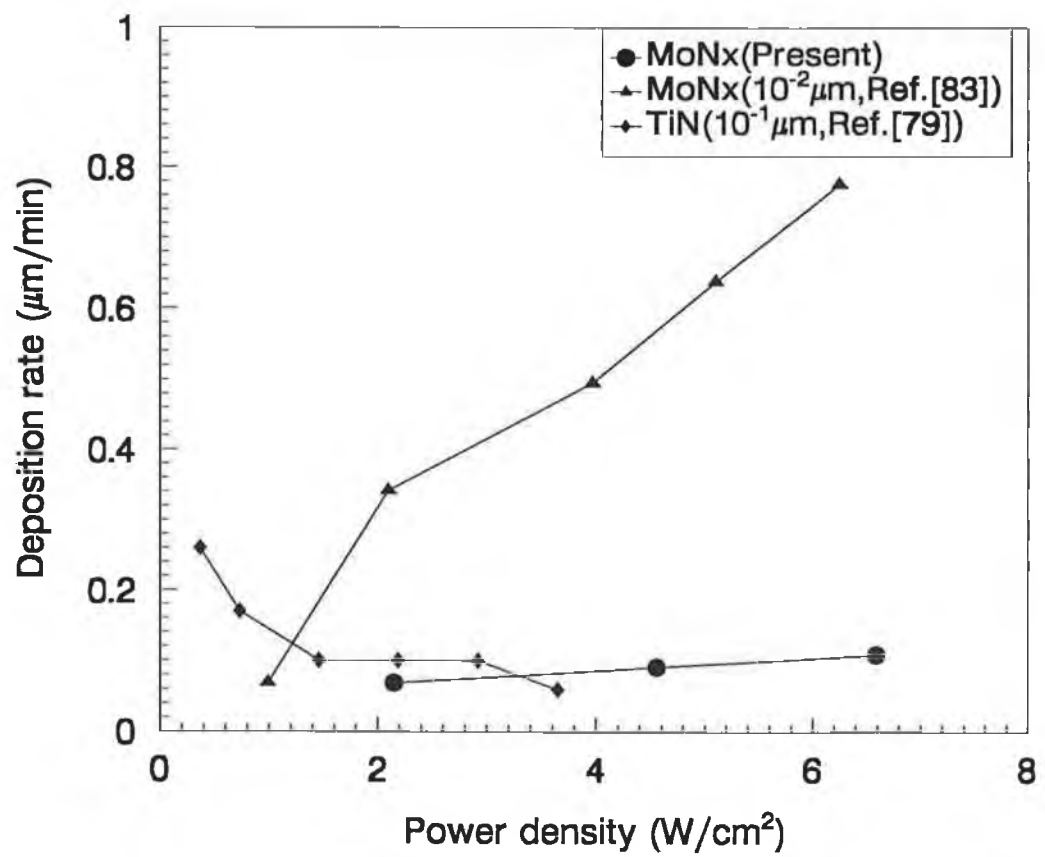


Fig.4.11 Deposition rate as a function of power density.

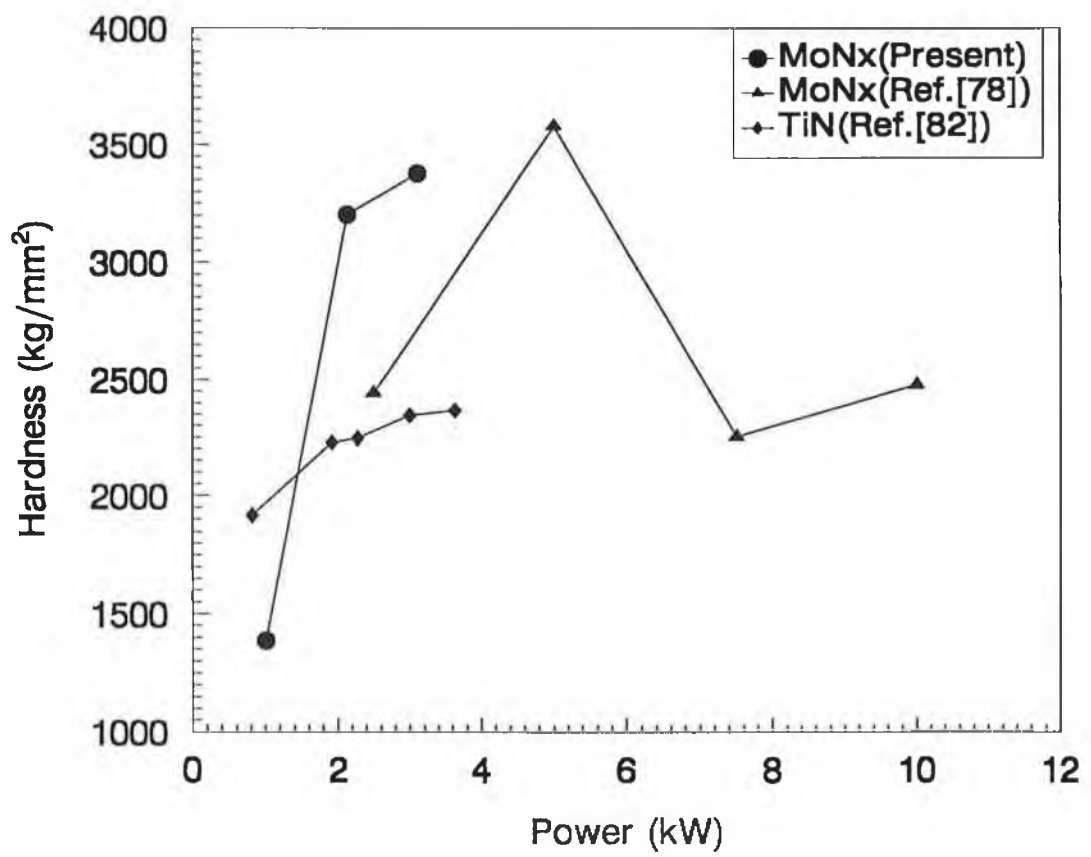


Fig.4.12 Hardness as a function of deposition power.

4.3 Wear Tests on Specimens Coated by External Supplier

Wear measurements were made at two different wear tracks on each of the coated and uncoated specimens of four different aforementioned materials. Wear was generated on all the specimens with the round contact wear tool of 1.5 mm tip radius under the same condition until equilibrium load situation occurred. At each step of the progressive wear, wear depth was measured by a profilometer as mentioned in Section 3.5. The profiles across the wear track of coated and uncoated specimens are presented in this chapter. The results were used to study the following: 1) effect of number of cycles on wear resistance, 2) improvement of wear resistance of the coated surface over uncoated surface, 3) comparative wear of different coatings and 4) effect of substrate materials on wear.

Hardness of coated and uncoated specimens and also adhesion of coated specimens was measured as mentioned in Sections 3.4.2 and 3.4.3 respectively. The results were utilized to study the effect of hardness and adhesion of different coatings on wear.

4.3.1 Profiles Across the Wear Track

Wear profiles across the wear track of Ti_xC coated and uncoated specimens of D2 tool steel, D3 tool steel, Vanadis 4 and Vanadis 10 are shown in Figs.4.13 to 4.20. All the wear profiles shown are from the first wear track generated under the same load (5.5 kg) and sliding distance (20 mm) unless stated otherwise. Horizontal magnification was 5 for all the profiles shown. In the caption of the figure VM represents vertical magnification. In Fig.4.17 the 4th profile is after 75,000 cycles where the sample had been subjected to 70,000 cycles with 5.5 kg and 5,000 cycles with 7 kg. In the same figure the 5th profile is after 85,000 cycles where the sample had been subjected to 70,000 cycles with 5.5 kg, 10,000 cycles with 7 kg and 5,000 cycles with 10 kg.

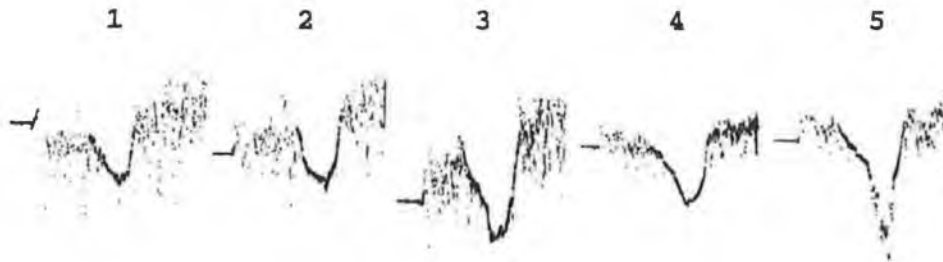


Fig.4.13 Profiles across the wear track of Ti_xC coated D2 specimen with increasing number of cycles: 1) 10000 cycles, VM 4000; 2) 15000 cycles, VM 4000; 3) 25000 cycles, VM 4000; 4) 35000 cycles, VM 2000 and 5) 45000 cycles, VM 2000.

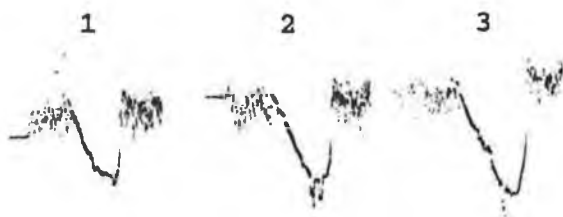


Fig.4.14 Profiles across the wear track of uncoated D2 specimen with increasing number of cycles: 1) 10000 cycles, VM 2000; 2) 15000 cycles, VM 2000; and 3) 25000 cycles, VM 2000.

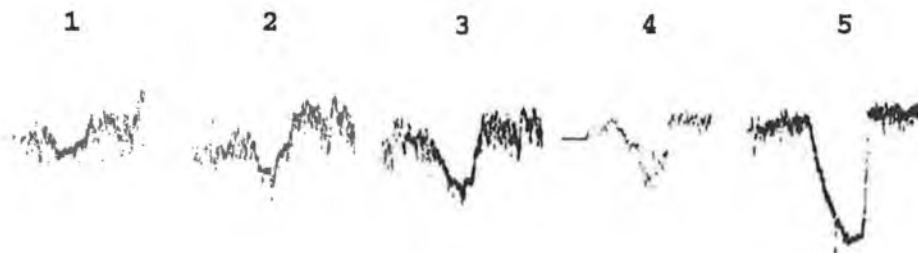


Fig.4.15 Profiles across the wear track of Ti_xC coated D3 specimen with increasing number of cycles: 1) 2000 cycles, VM 4000; 2) 3000 cycles, VM 4000; 3) 5000 cycles, VM 4000; 4) 10000 cycles, VM 2000 and 5) 15000 cycles, VM 2000.

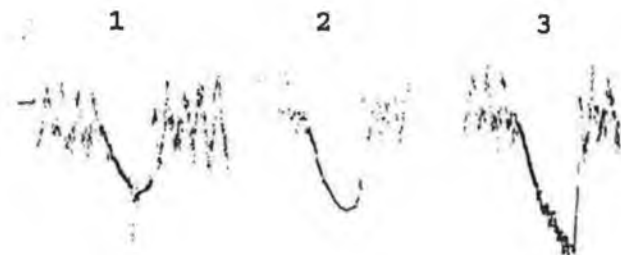


Fig.4.16 Profiles across the wear track of uncoated D3 specimen with increasing number of cycles: 1) 2000 cycles, VM 2000; 2) 7000 cycles, VM 2000; and 3) 10000 cycles, VM 2000.

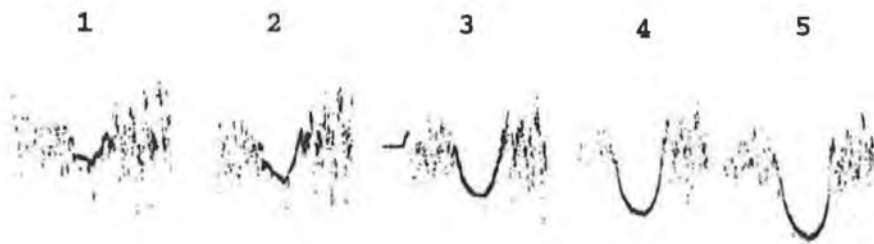


Fig.4.17 Profiles across the wear track of Ti₂C coated V4 specimen with increasing number of cycles: 1) 15000 cycles, VM 4000; 2) 30000 cycles, VM 4000; 3) 50000 cycles, VM 4000; 4) 75000 cycles, VM 4000 and 5) 85000 cycles, VM 4000.

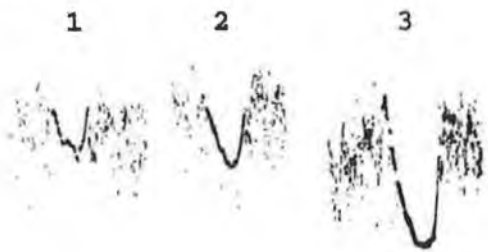


Fig.4.18 Profiles across the wear track of uncoated V4 specimen with increasing number of cycles: 1) 7000 cycles, VM 4000; 2) 15000 cycles, VM 4000; and 3) 30000 cycles, VM 4000.

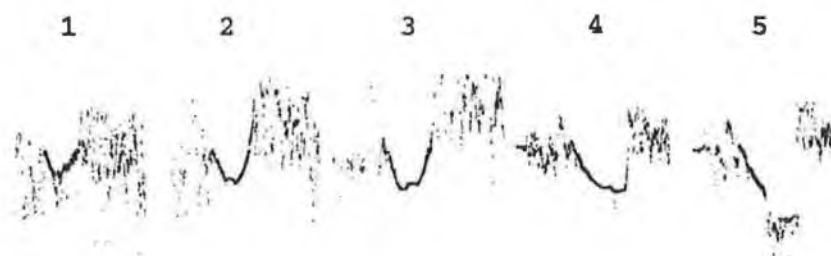


Fig.4.19 Profiles across the wear track of Ti_xC coated V10 specimen with increasing number of cycles: 1) 3000 cycles, VM 4000; 2) 15000 cycles, VM 4000; 3) 30000 cycles, VM 4000; 4) 60000 cycles, VM 2000 and 5) 70000 cycles, VM 2000.

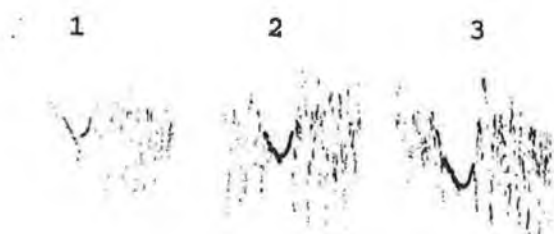


Fig.4.20 Profiles across the wear track of uncoated V10 specimen with increasing number of cycles: 1) 15000 cycles, VM 4000; 2) 25000 cycles, VM 4000; and 3) 40000 cycles, VM 4000.

4.3.2 Effect of Number of Cycles on Wear

Wear depth of both the wear tracks on each of the test specimens is shown as a function of number of cycles in Figs.4.21 to 4.32. The solid lines in the figures illustrate the trend through experimental points. In the generation of wear, material was removed continuously with increasing number of cycles until an equilibrium load condition occurred. In the present study such an equilibrium load condition occurred in the case of coated specimens before the coating was broken. At this stage the load was increased to 10 kg and the specimen was subjected to extreme wear for a range of a few kilo cycles to 35 kilo cycles in order to break the coating. In the case of uncoated specimen wear depth increases with increasing number of cycles, initiating with the non-equilibrium stage and continuing with steady state conditions. The coating imparts increased wear resistance to the surface. In Figs.4.22, 4.25, 4.28 and 4.31 it can be observed that the base material wears out more slowly than the coated surface or nearly at the same rate as the coated surface. The exception is in Fig.4.25 on the second wear track where the base material wears out faster than the coated surface.

Average wear depth of two tracks on each of the specimens are shown in Figs.4.33 to 4.44. In Figs.4.36 and 4.37 it can be observed that the average wear rate of coated surfaces is the same as for the base material. It can also be observed that in Figs.4.33, 4.34, 4.40, 4.42 and 4.43 the coating was broken under a wear load of 5.5 kg about 33,000 cycles, 3,000 cycles, 9,000 cycles, 56,000 cycles and 6,000 cycles respectively.

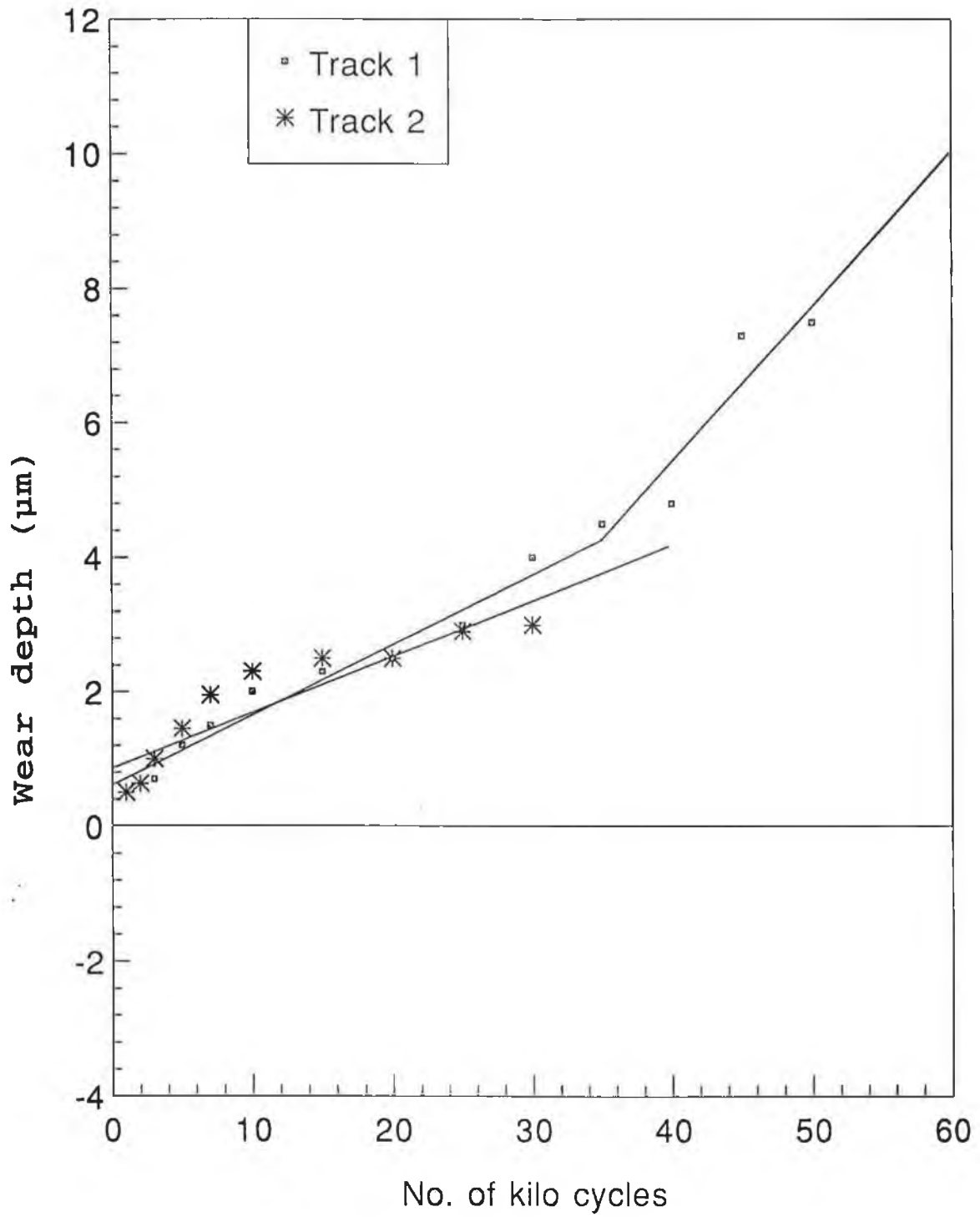


Fig.4.21 Wear depth of Ti_xC coated D2 specimen.

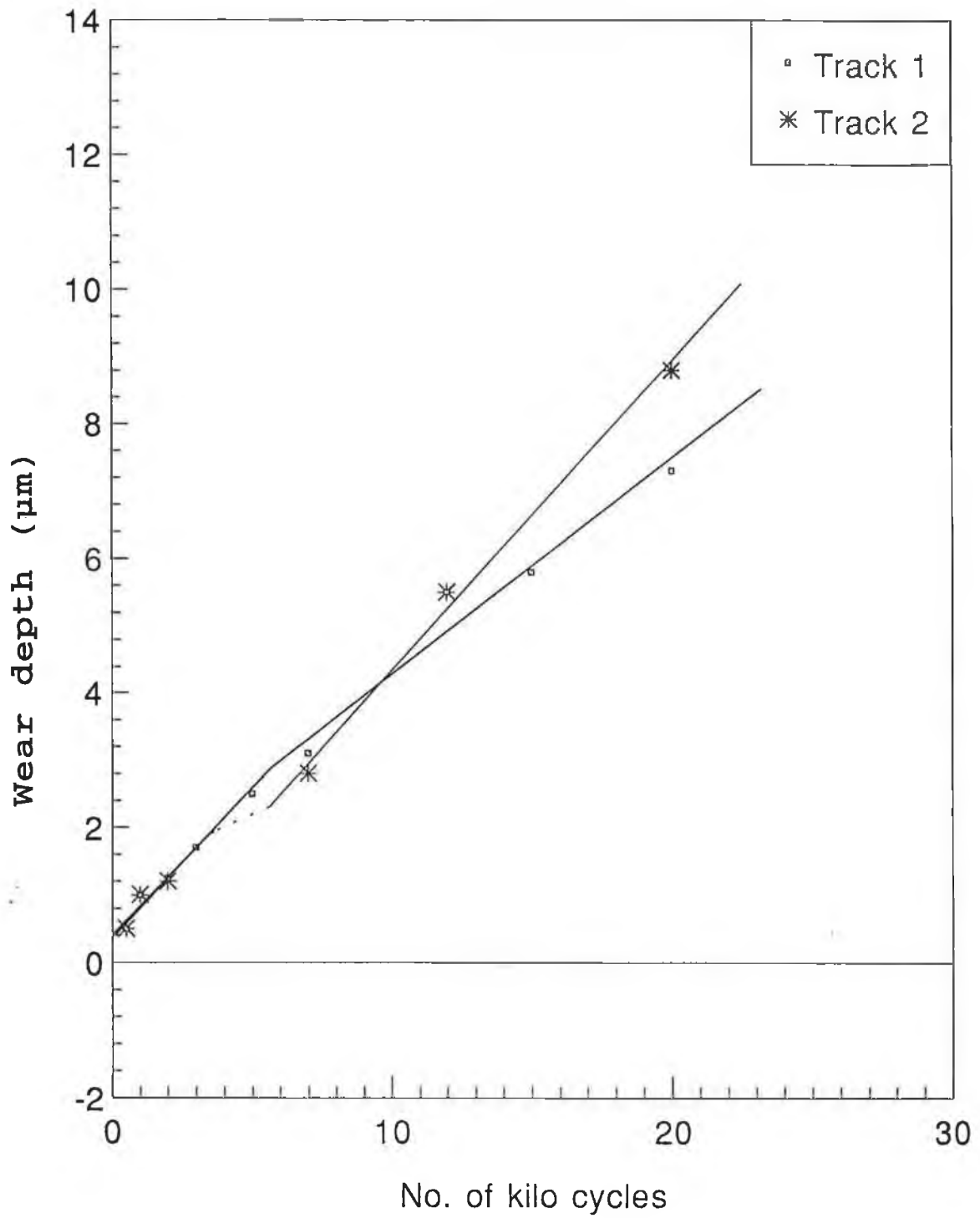


Fig.4.22 Wear depth of TiN coated D2 specimen.

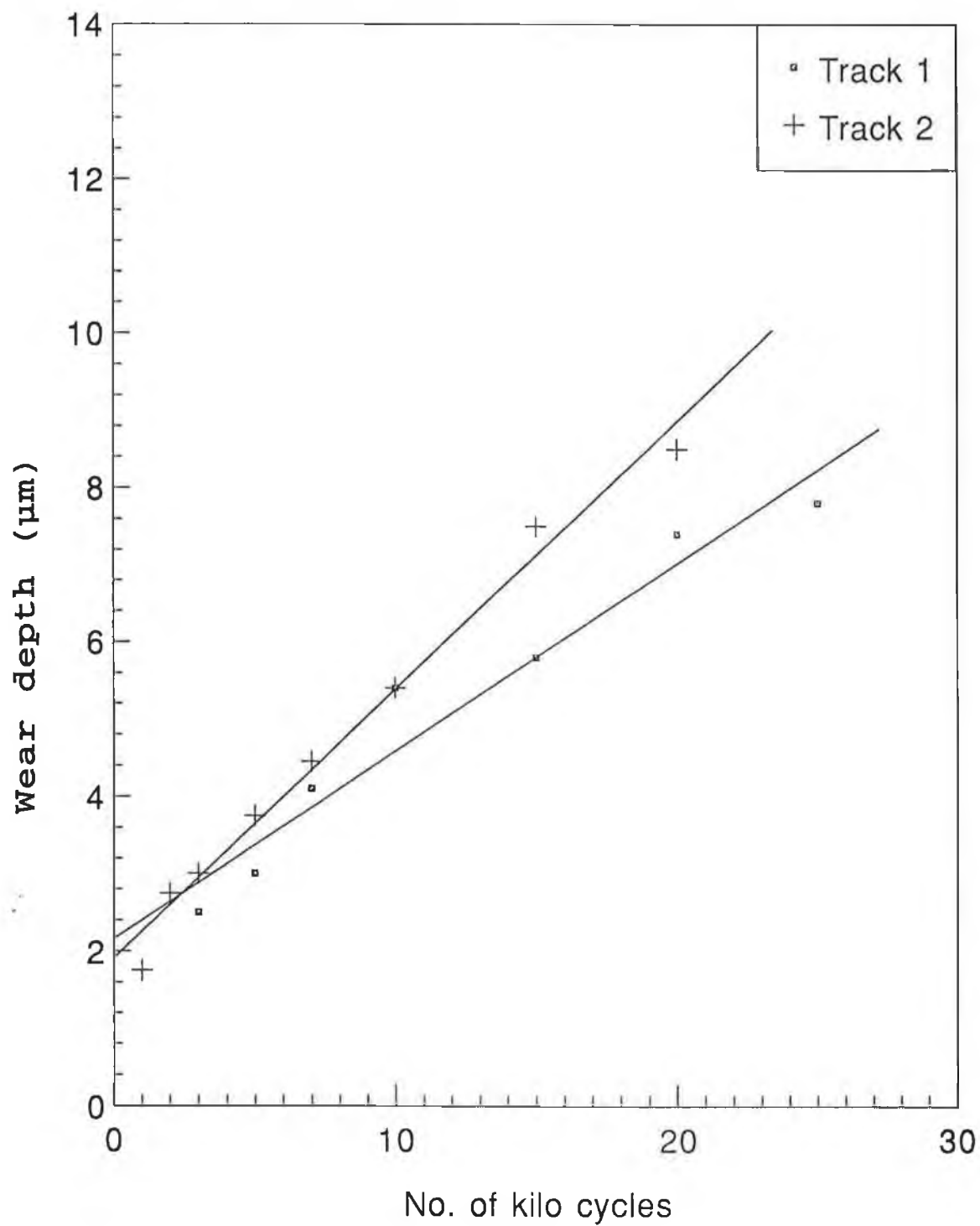


Fig.4.23 Wear depth of Uncoated D2 specimen.

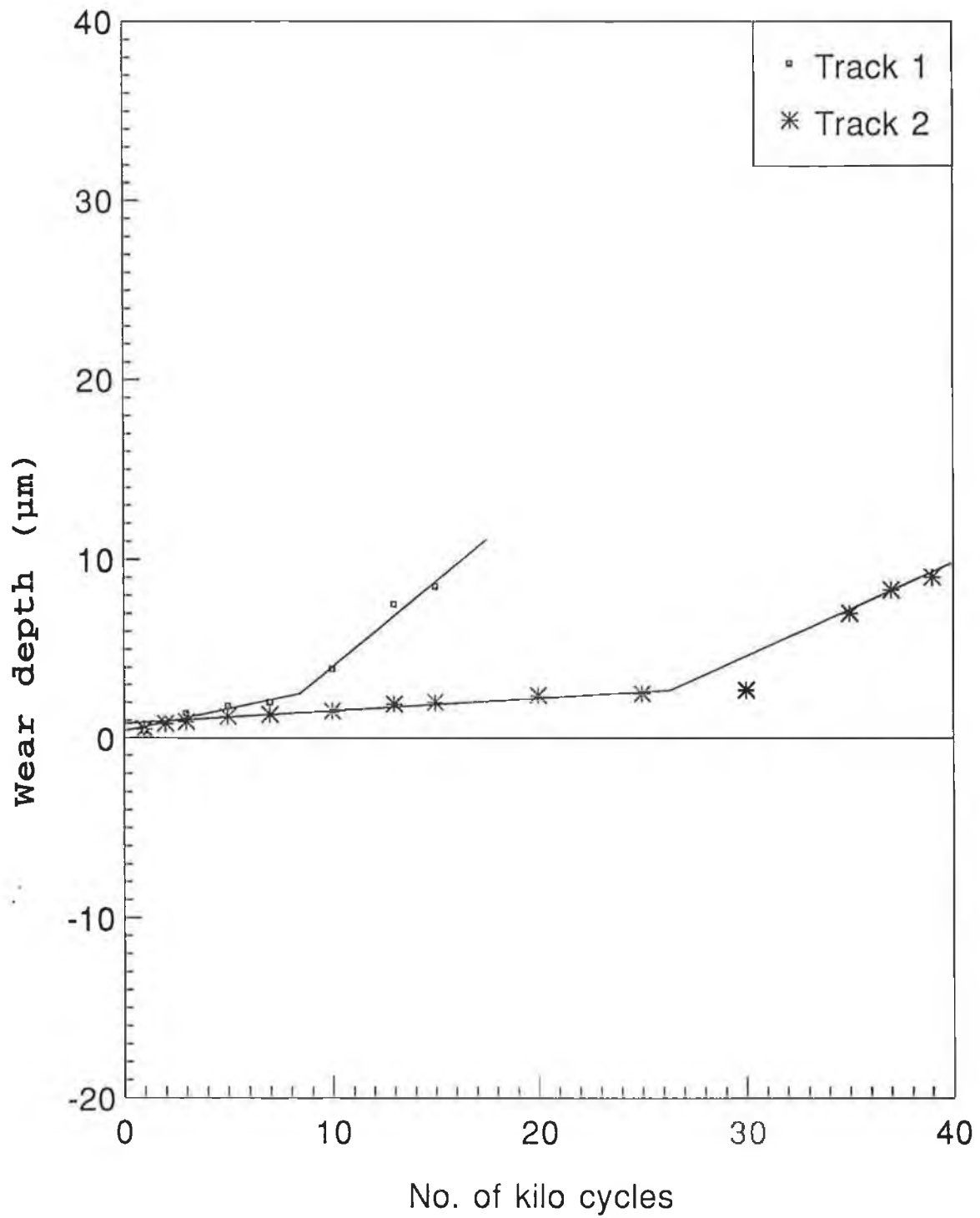


Fig.4.24 Wear depth of Ti_xC coated D3 specimen.

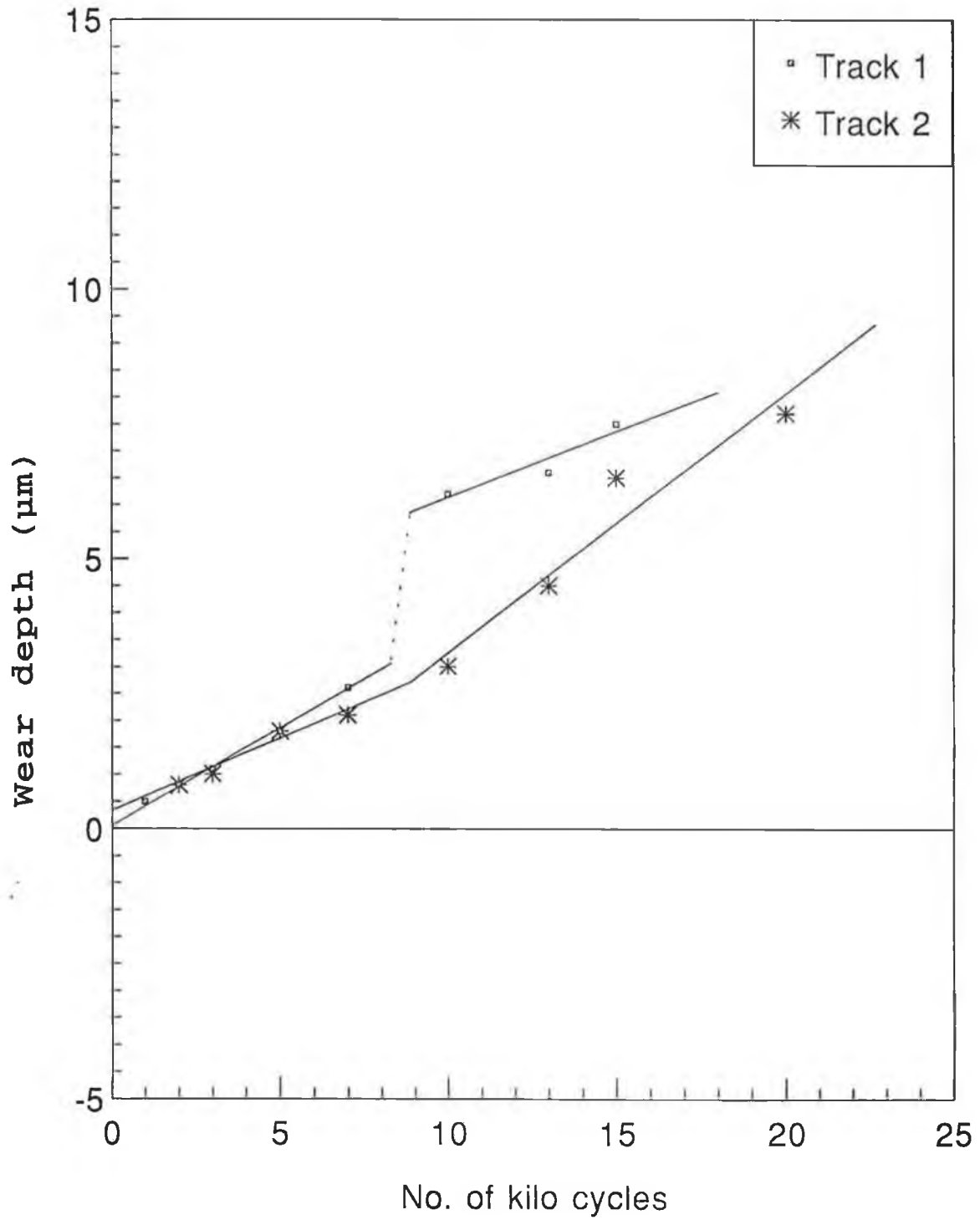


Fig.4.25 Wear depth of TiN coated D3 specimen.

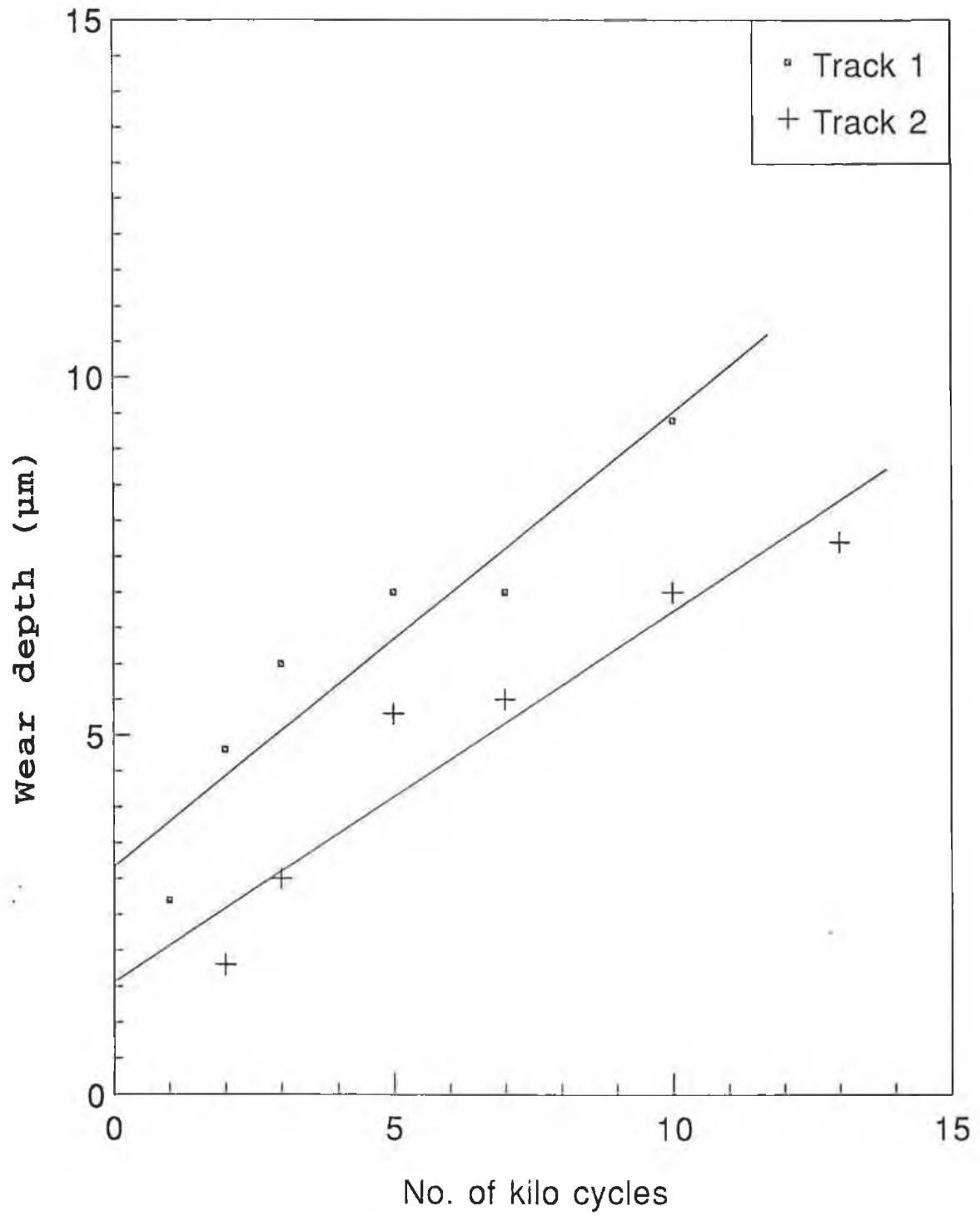


Fig.4.26 Wear depth of Uncoated D3 specimen.

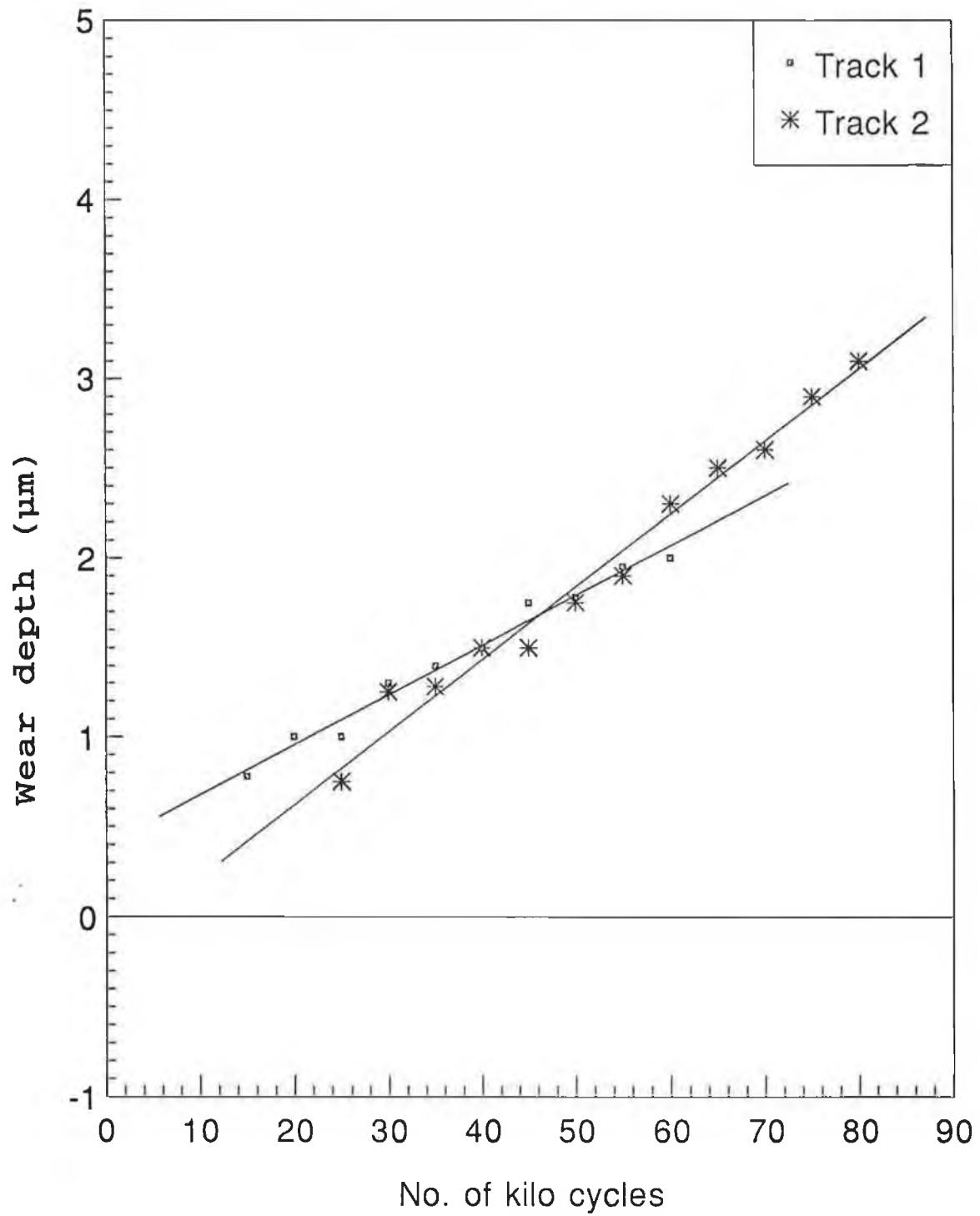


Fig.4.27 Wear depth of Ti_xC coated V4 specimen.

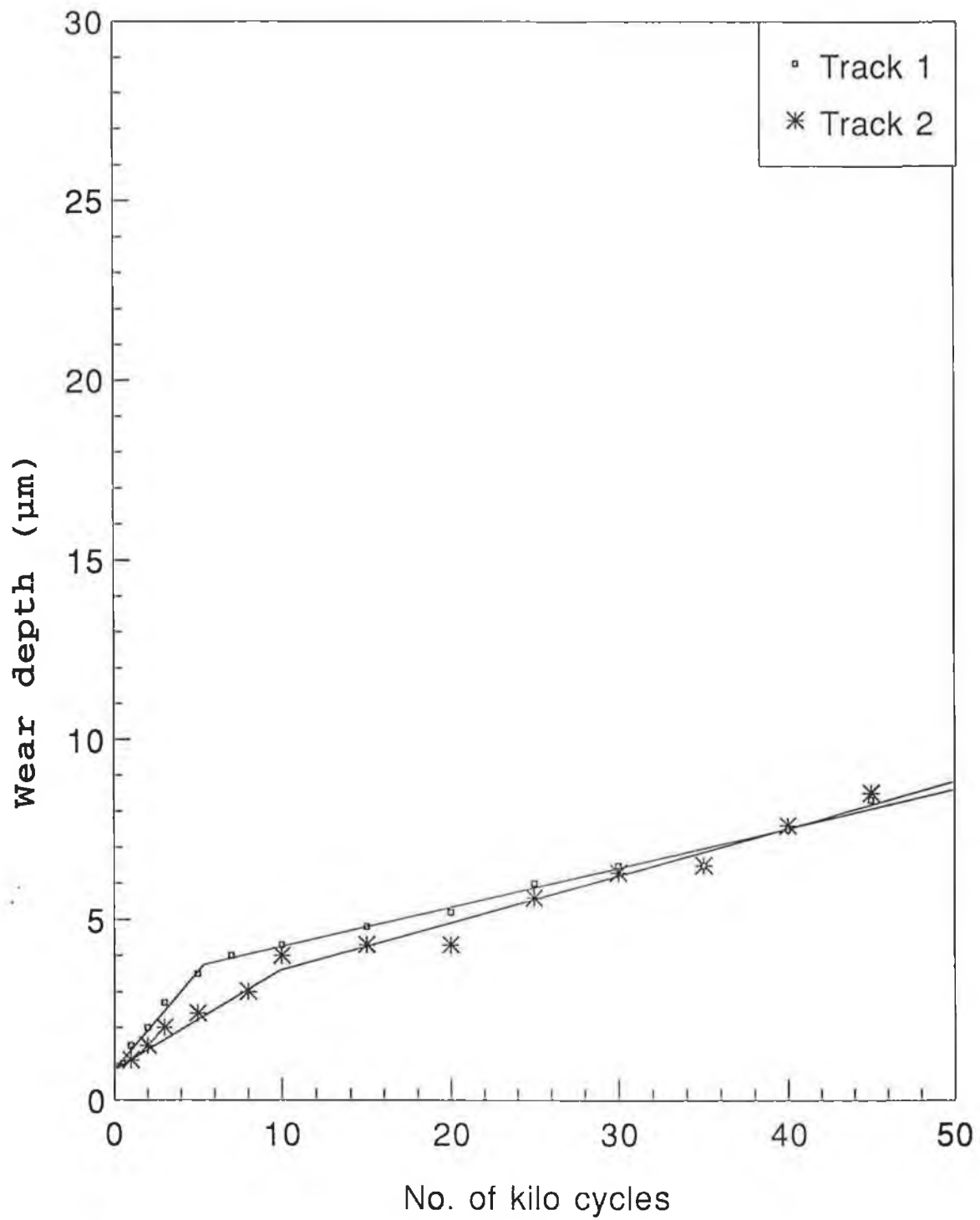


Fig.4.28 Wear depth of TiN coated V4 specimen.

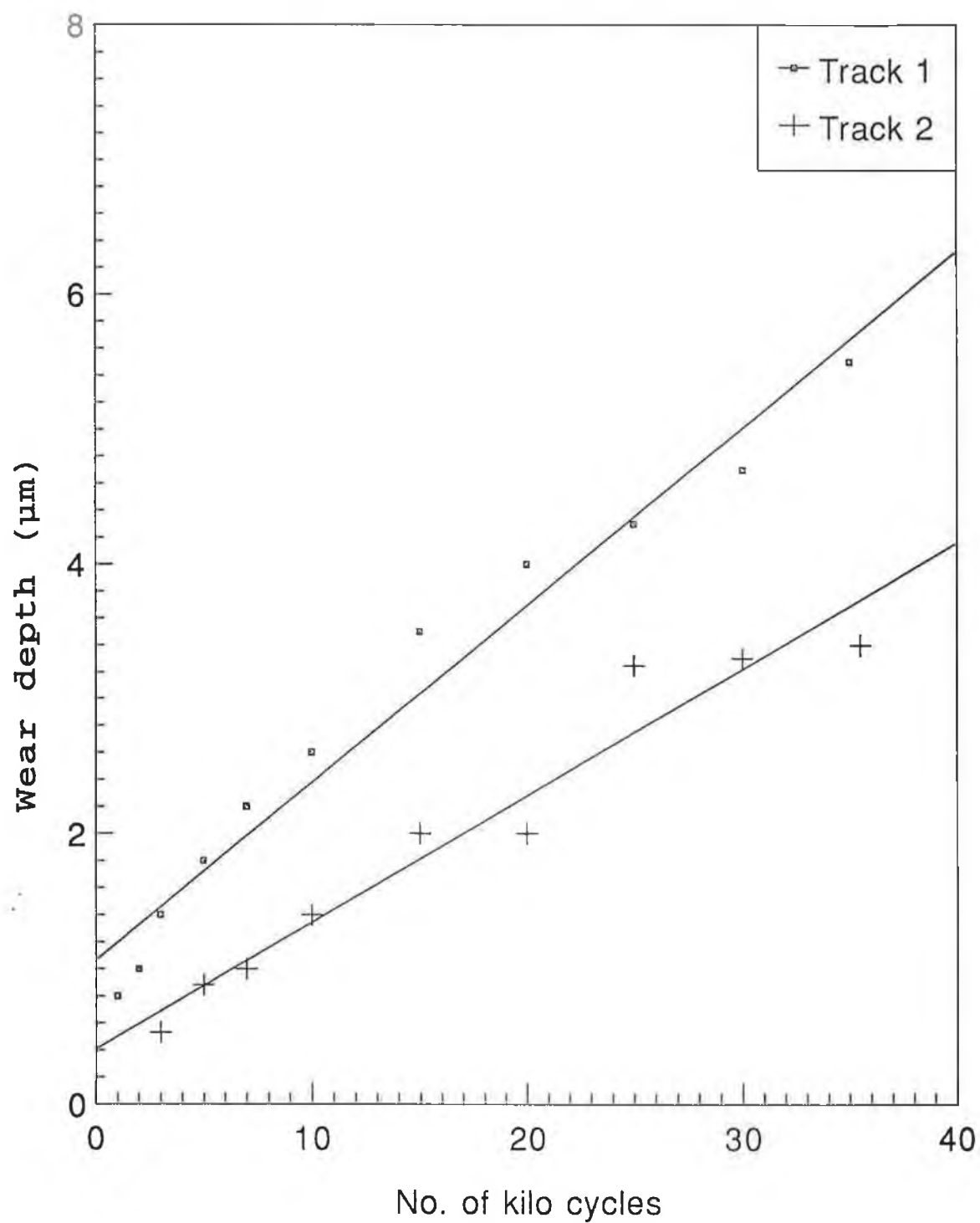


Fig.4.29 Wear depth of Uncoated V4 specimen.

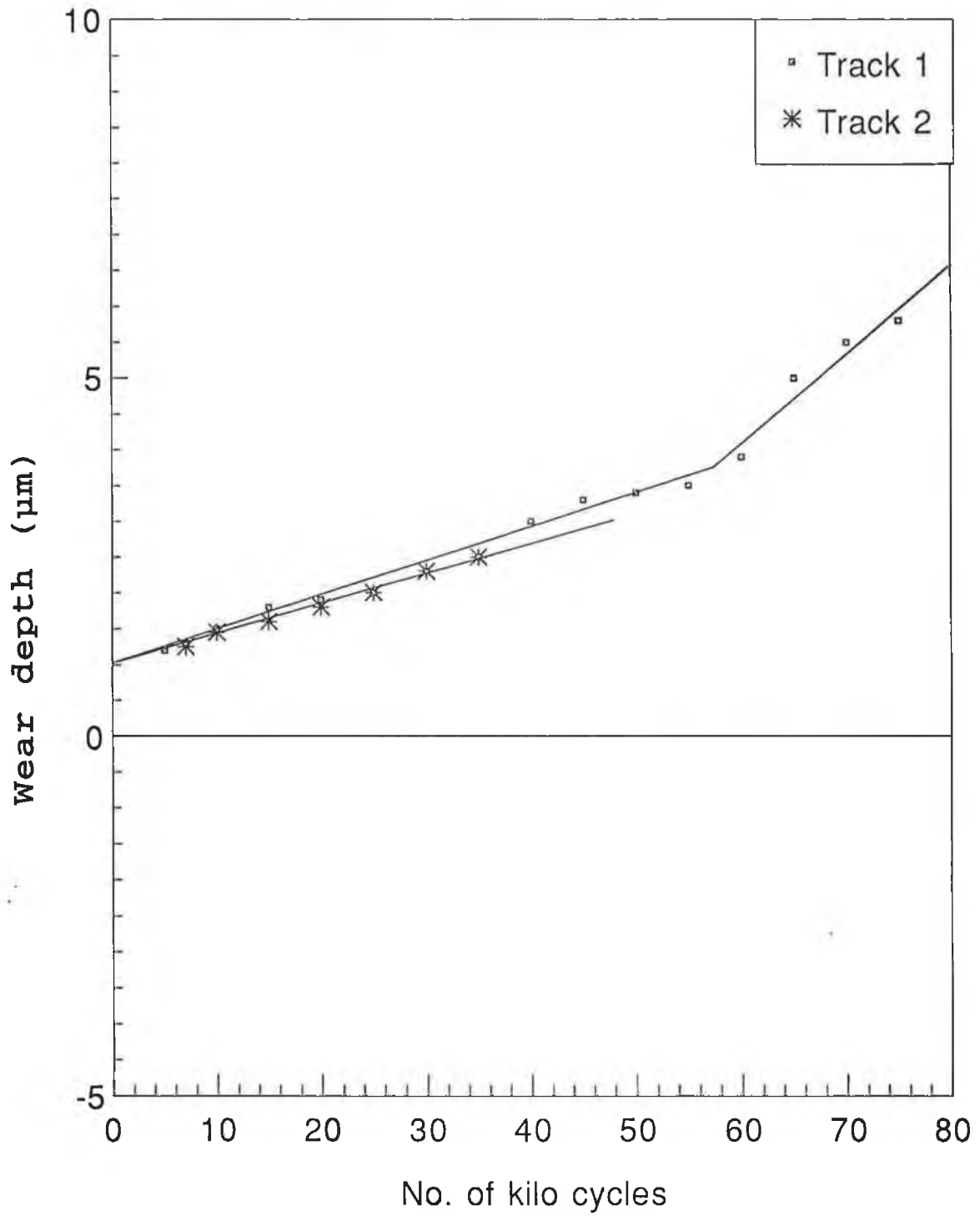


Fig.4.30 Wear depth of Ti_xC coated V10 specimen.

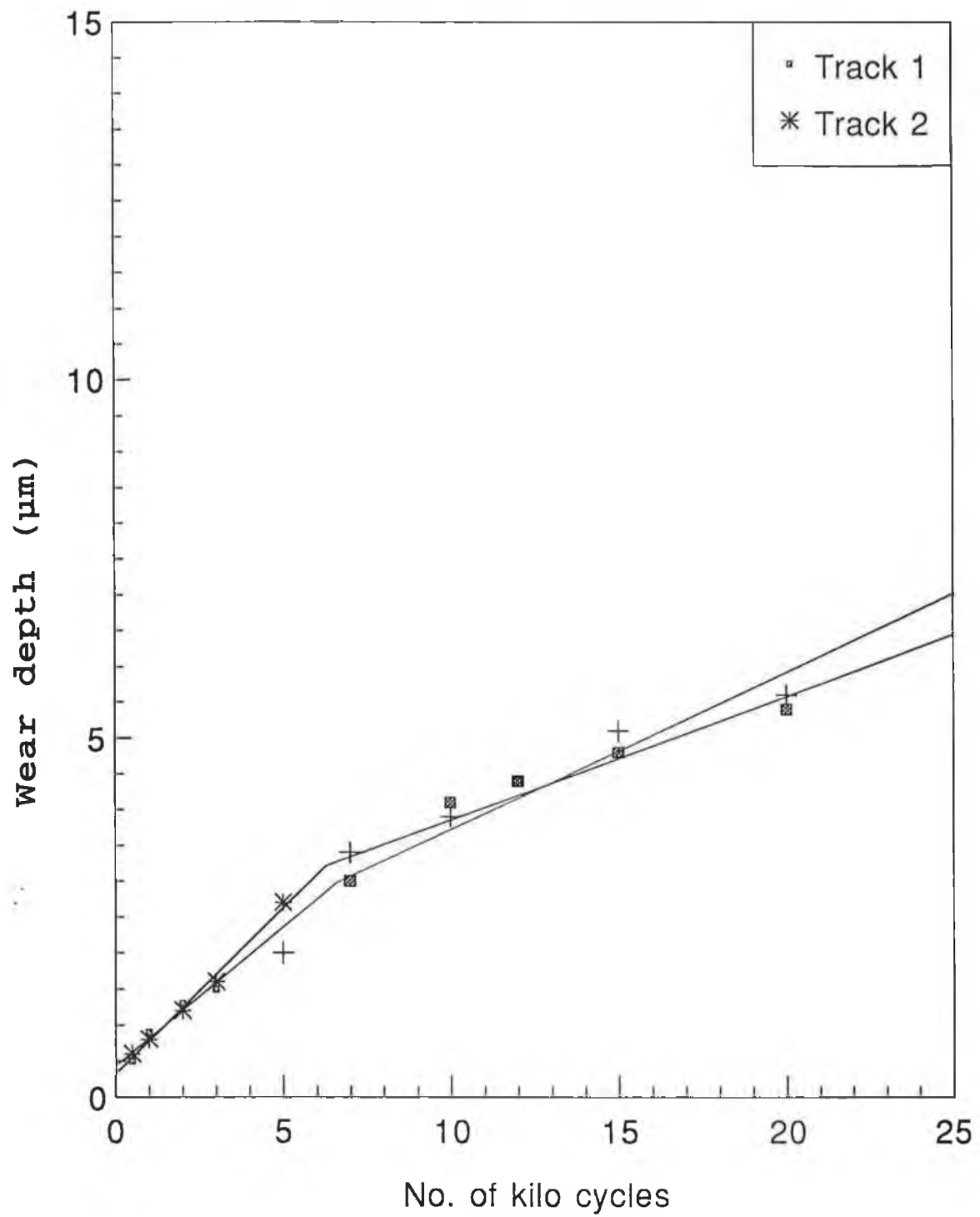


Fig.4.31 Wear depth of TiN coated V10 specimen.

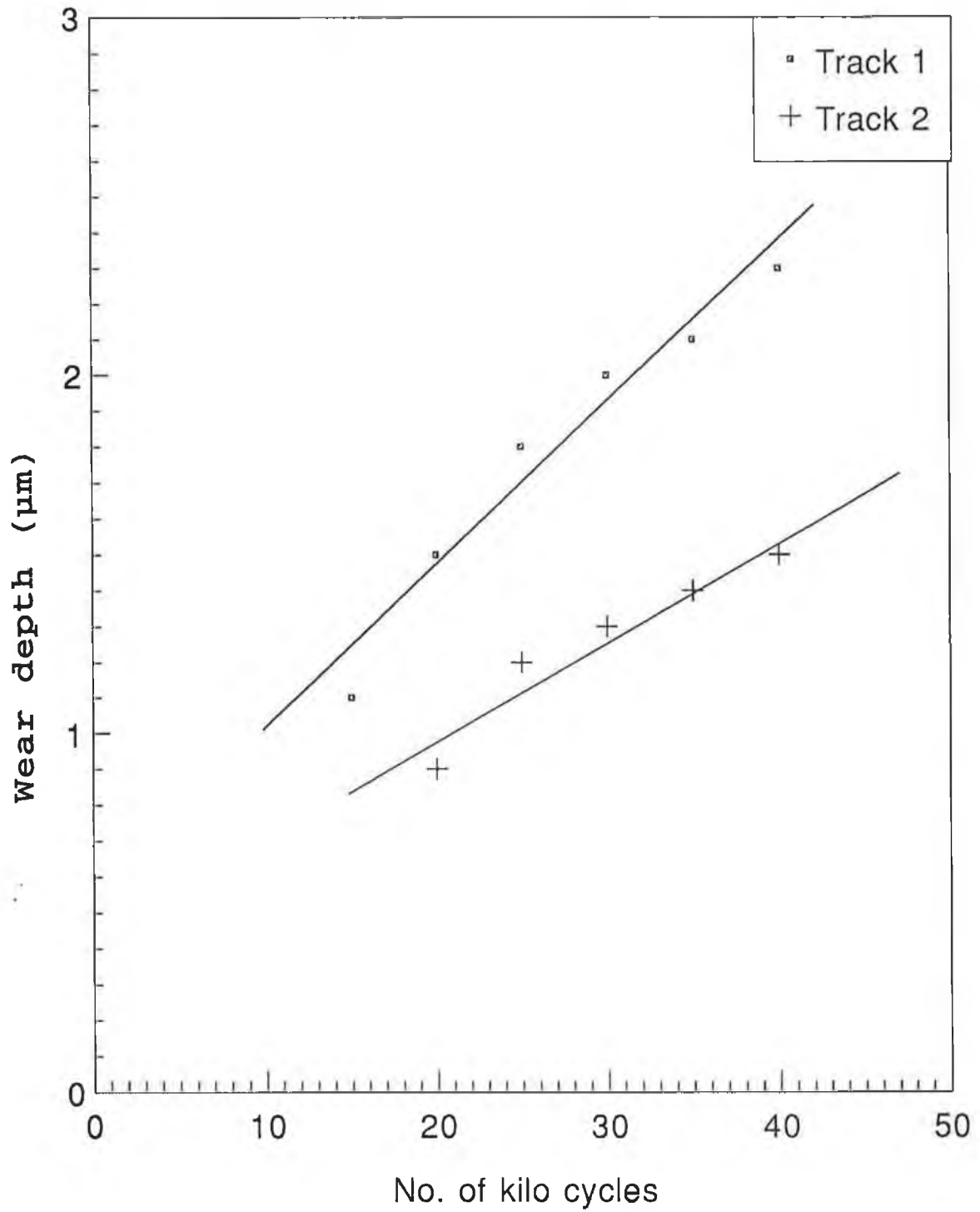


Fig.4.32 Wear depth of Uncoated V10 specimen.

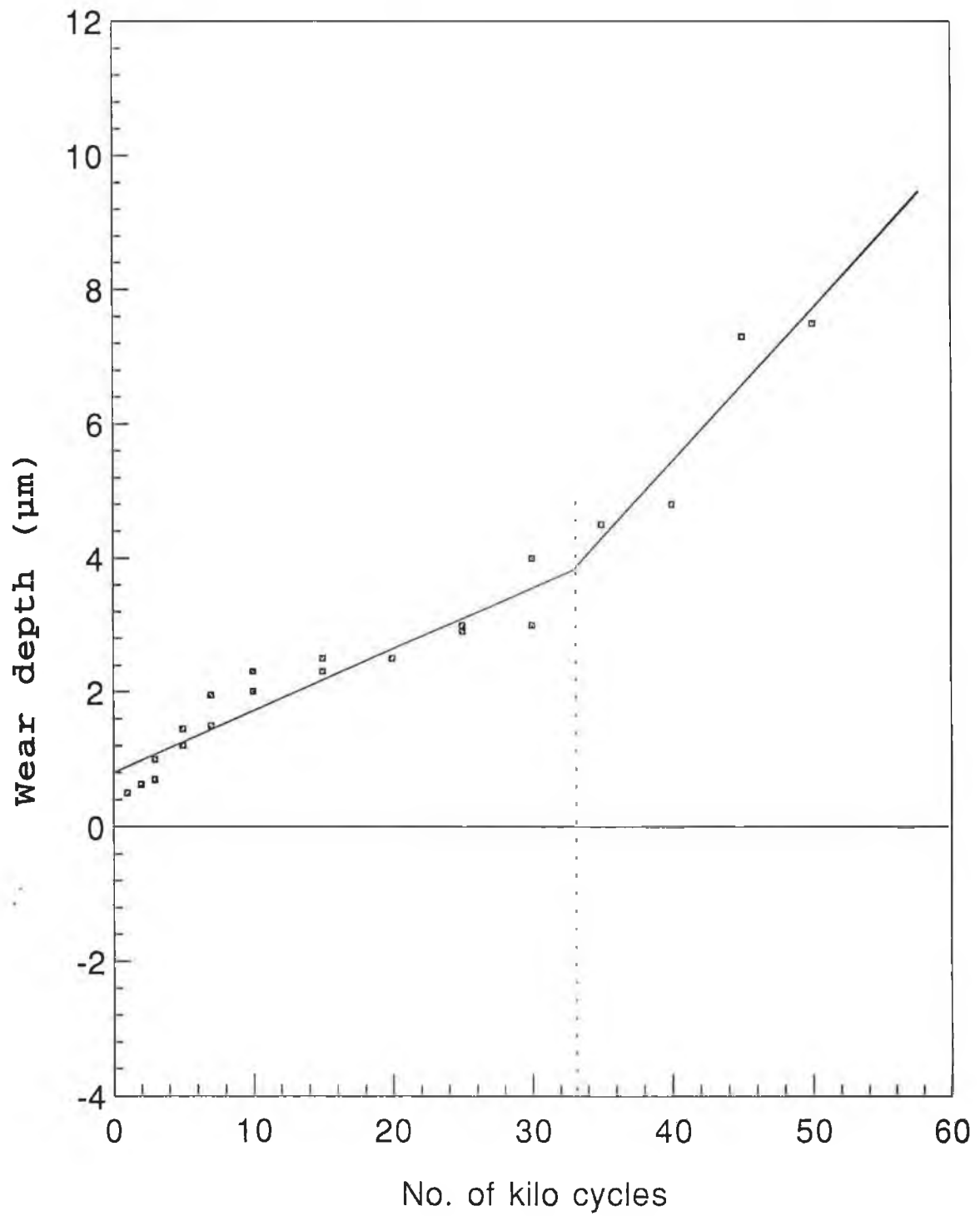


Fig.4.33 Average wear depth of Ti_xC coated D2 specimen.

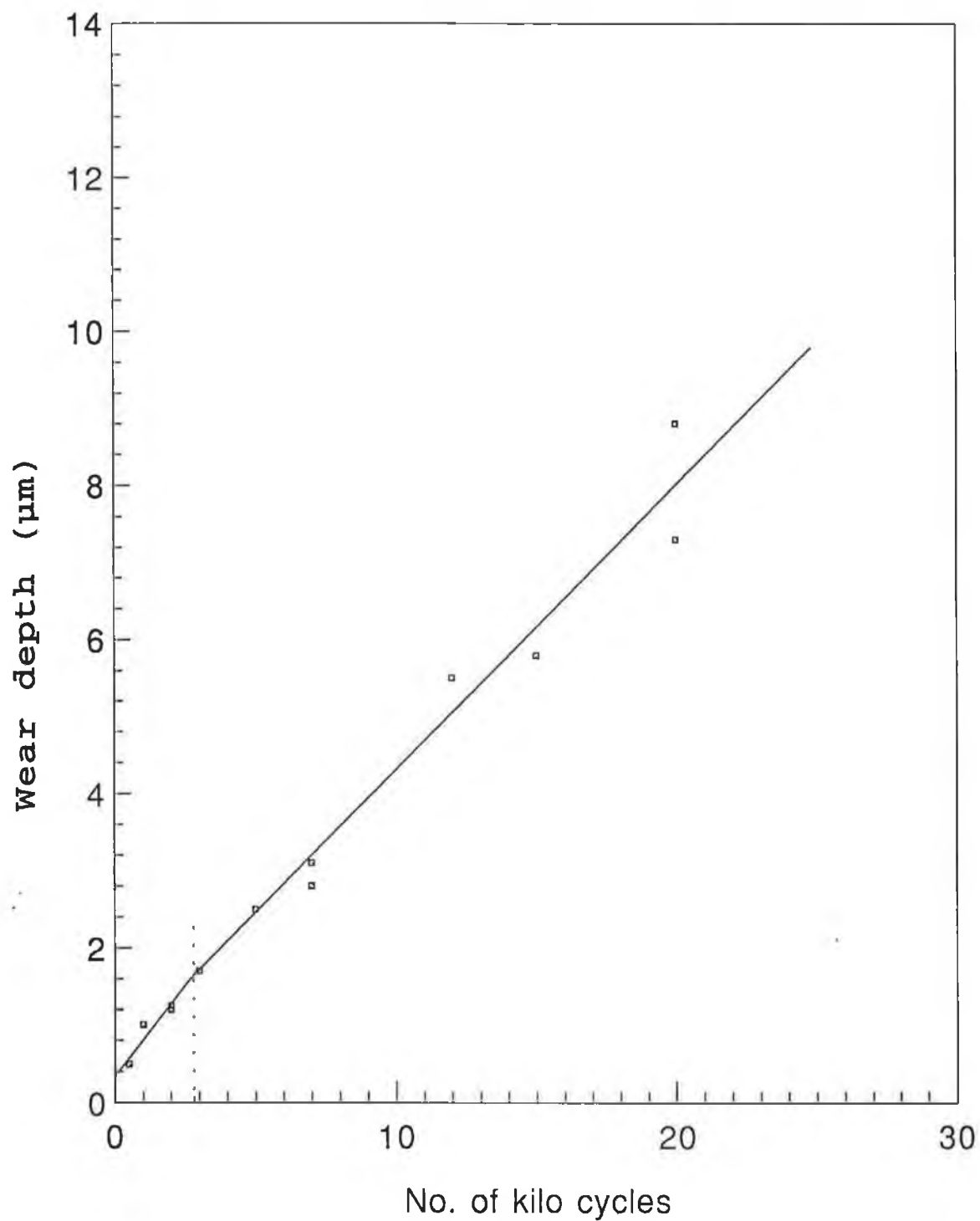


Fig.4.34 Average wear depth of TiN coated D2 specimen.

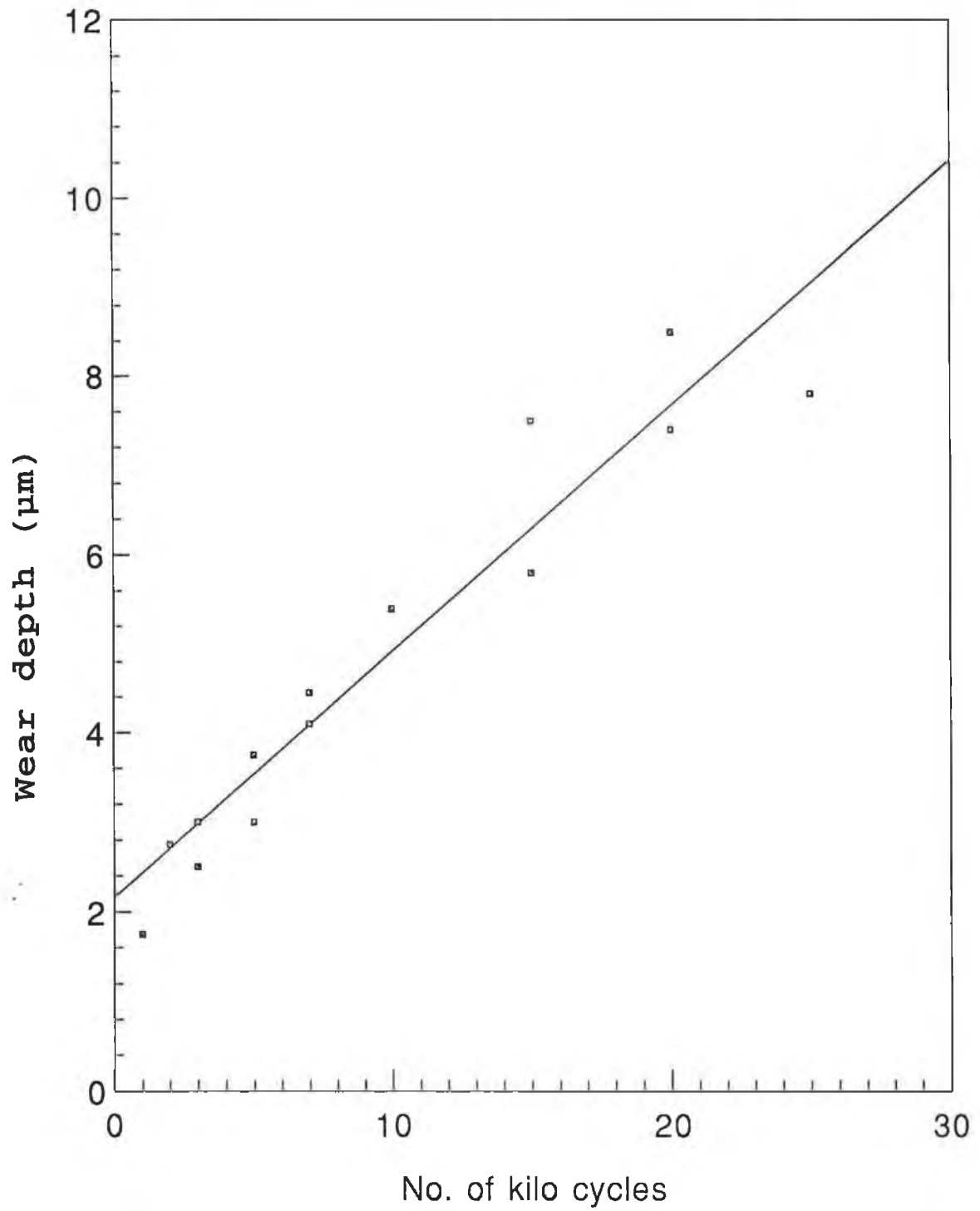


Fig.4.35 Average wear depth of Uncoated D2 specimen.

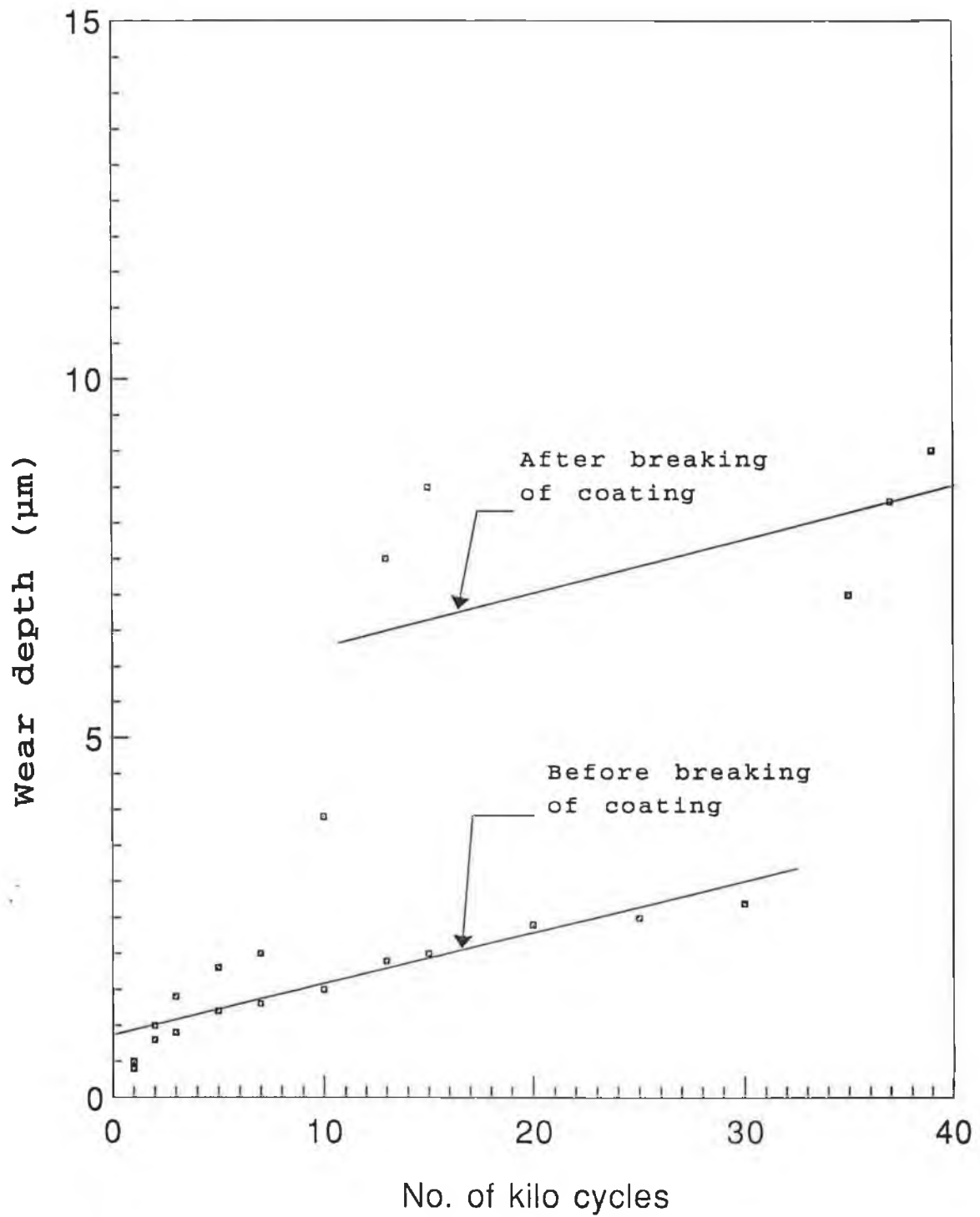


Fig.4.36 Average wear depth of Ti_xC coated D3 specimen.

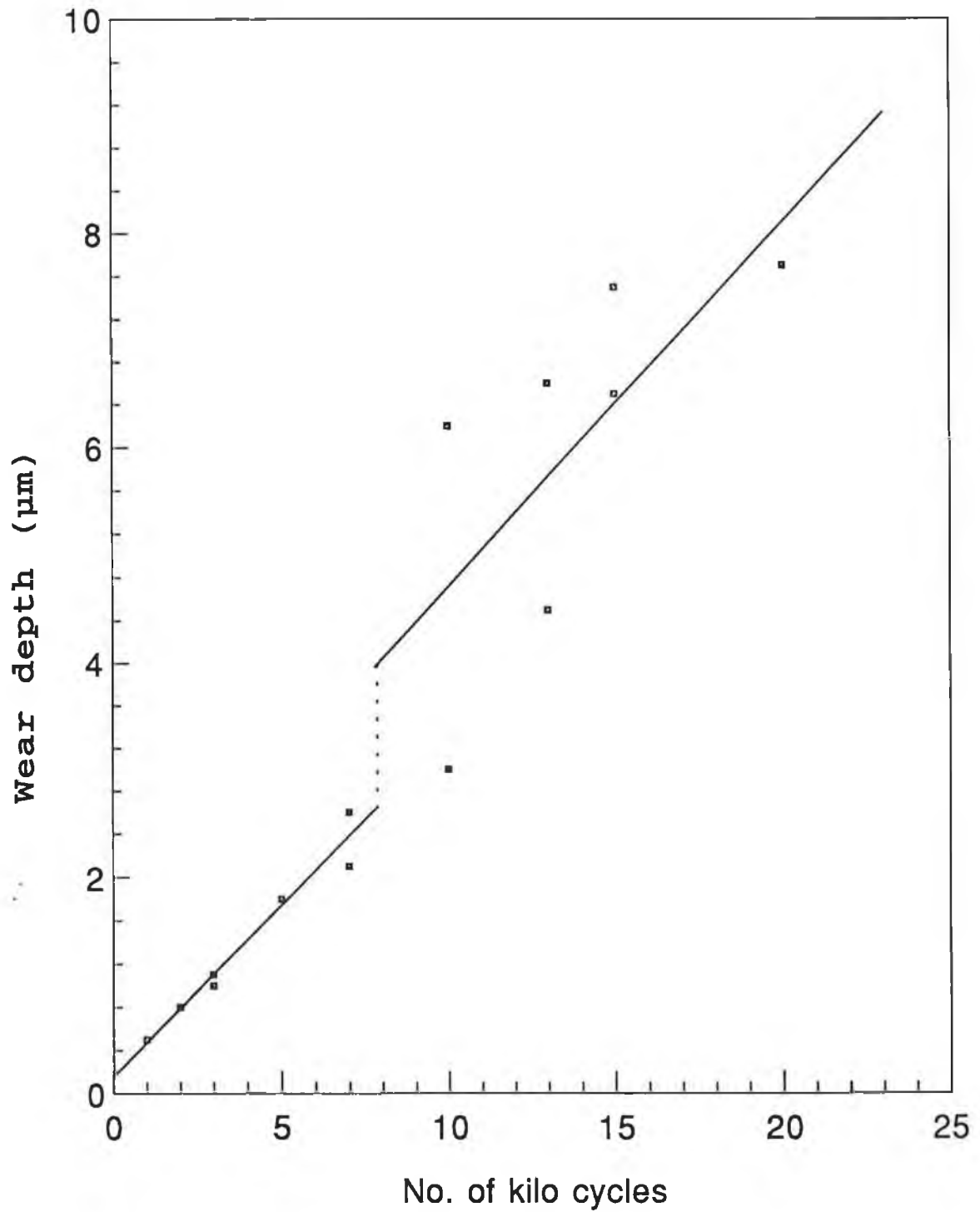


Fig.4.37 Average wear depth of TiN coated D3 specimen.

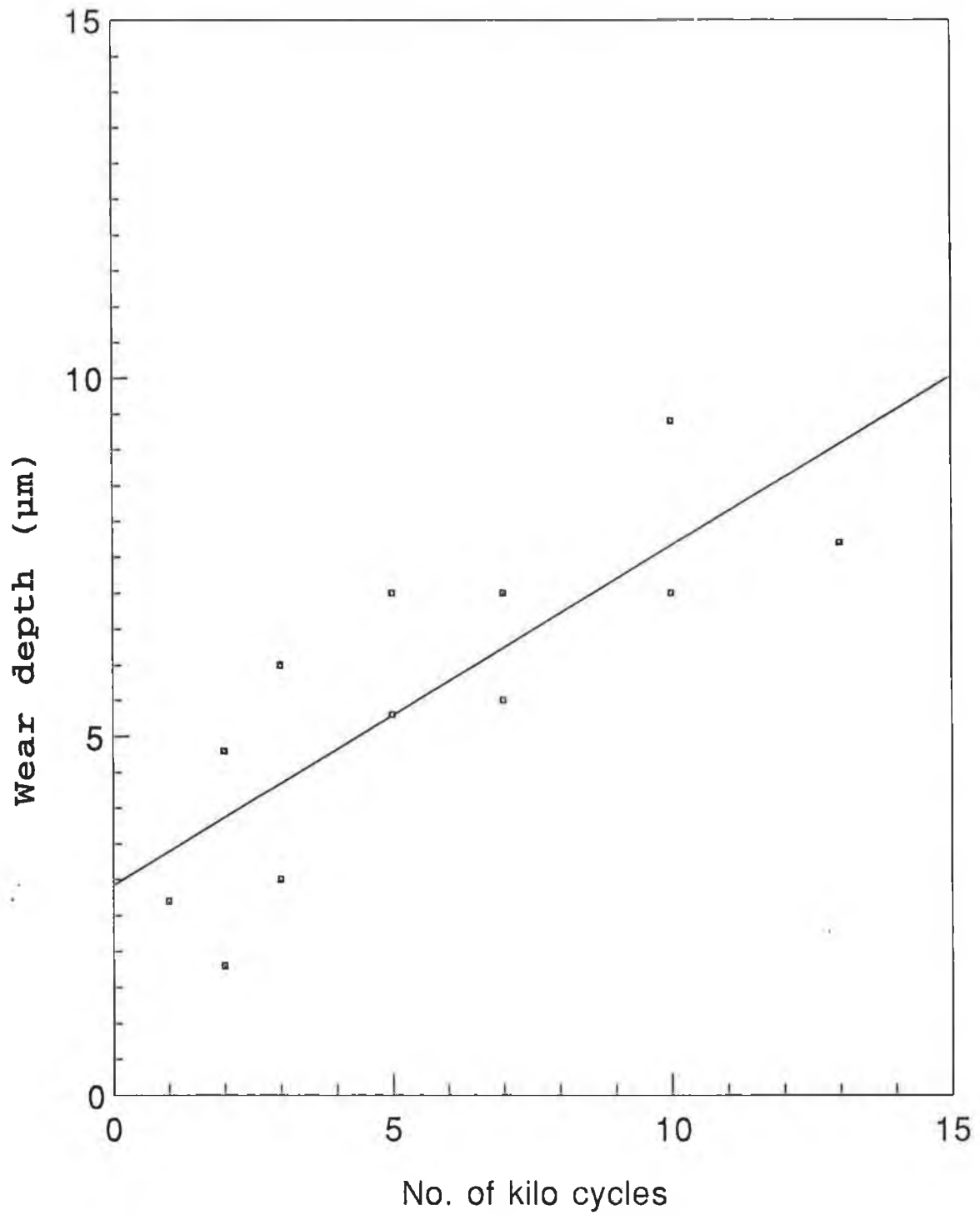


Fig.4.38 Average wear depth of Uncoated D3 specimen.

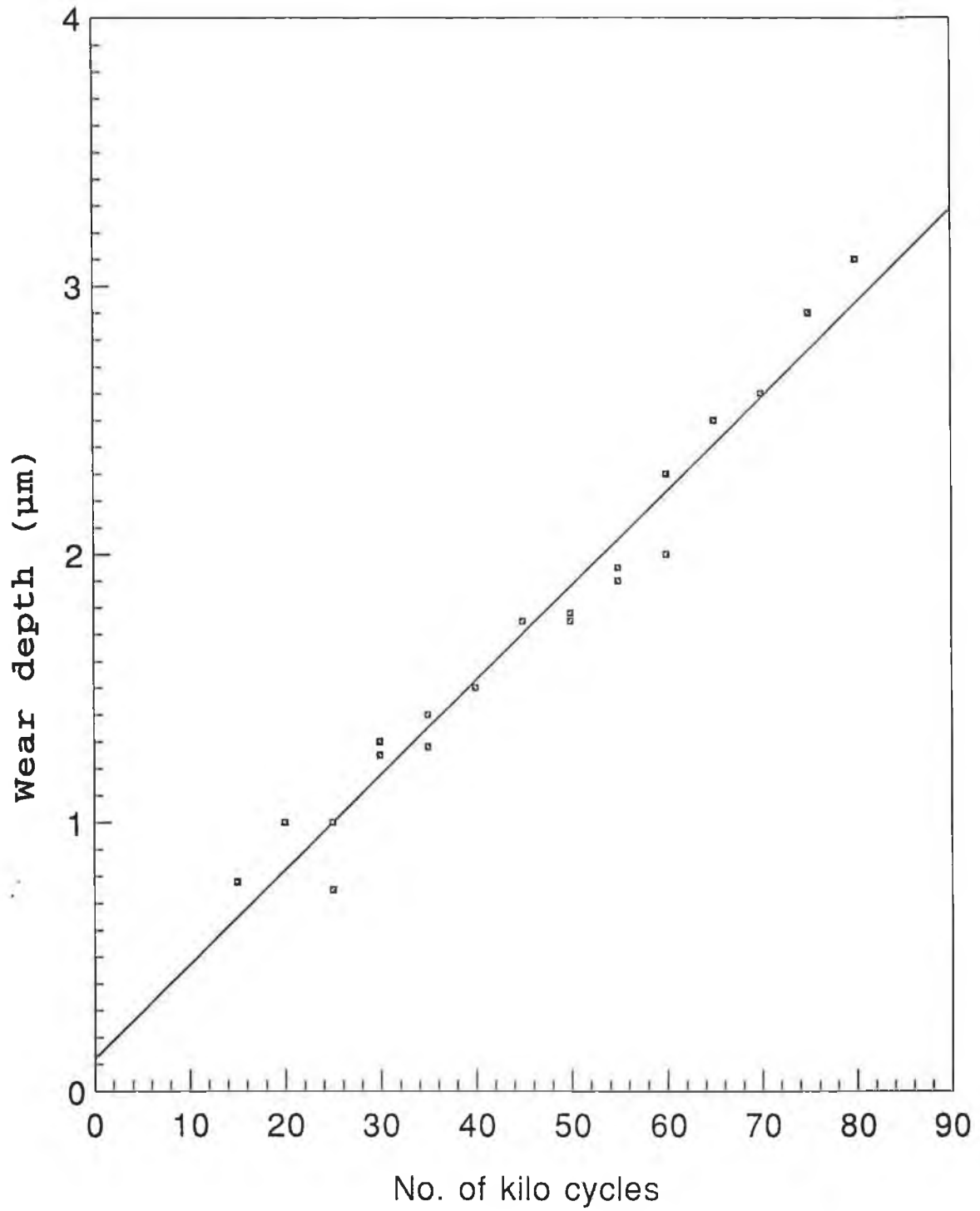


Fig.4.39 Average wear depth of Ti_xC coated V4 specimen.

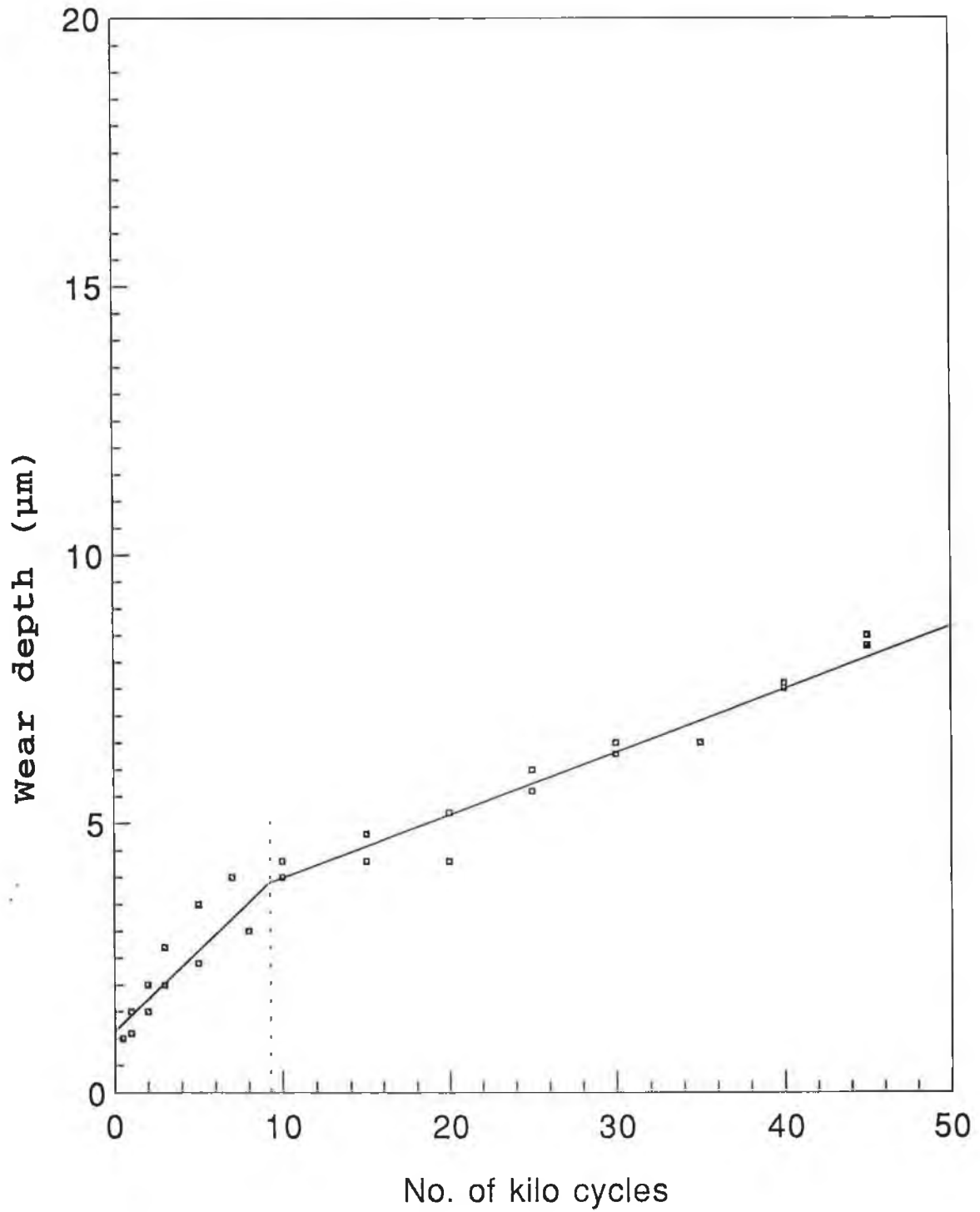


Fig.4.40 Average wear depth of TiN coated V4 specimen.

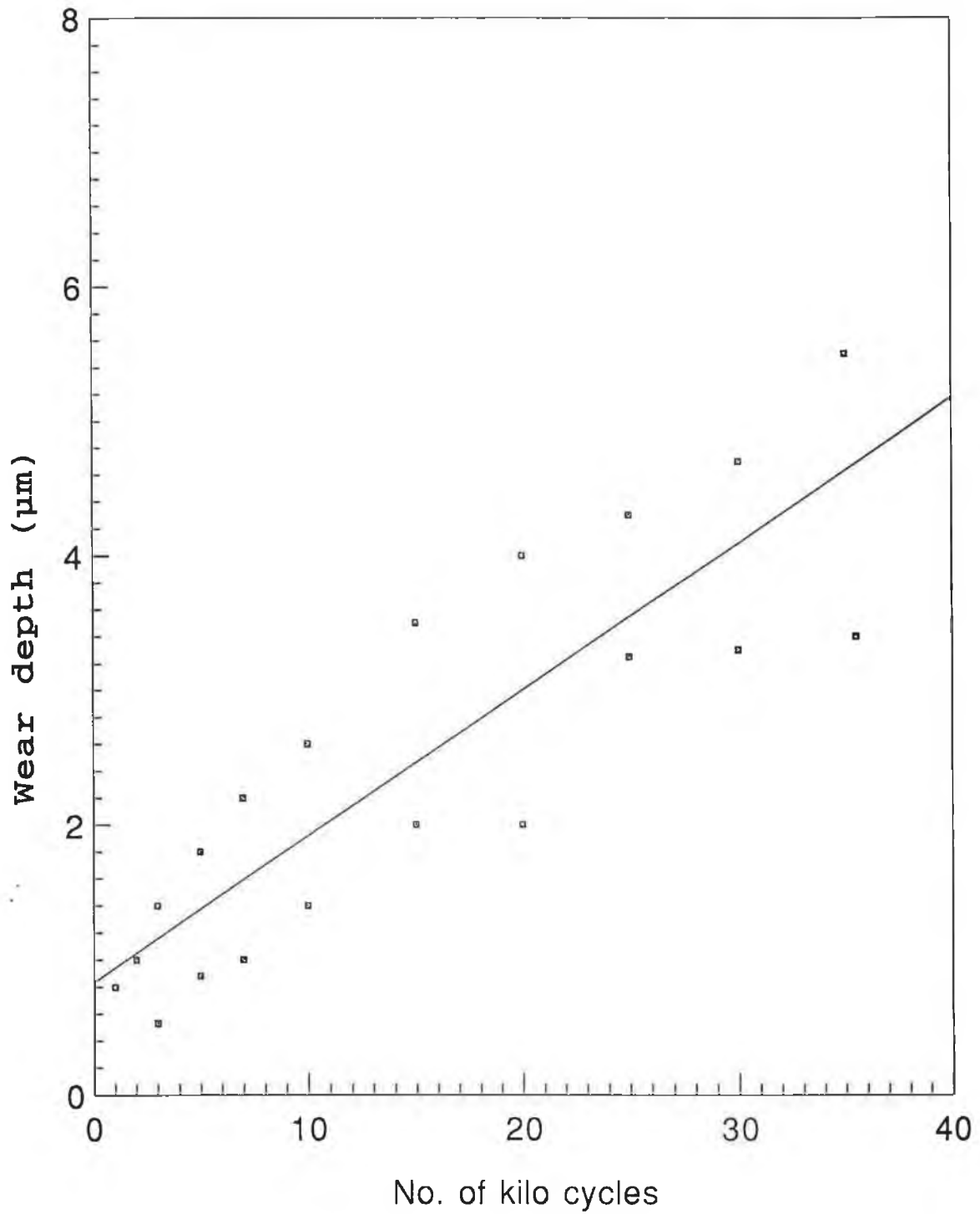


Fig.4.41 Average wear depth of Uncoated V4 specimen.

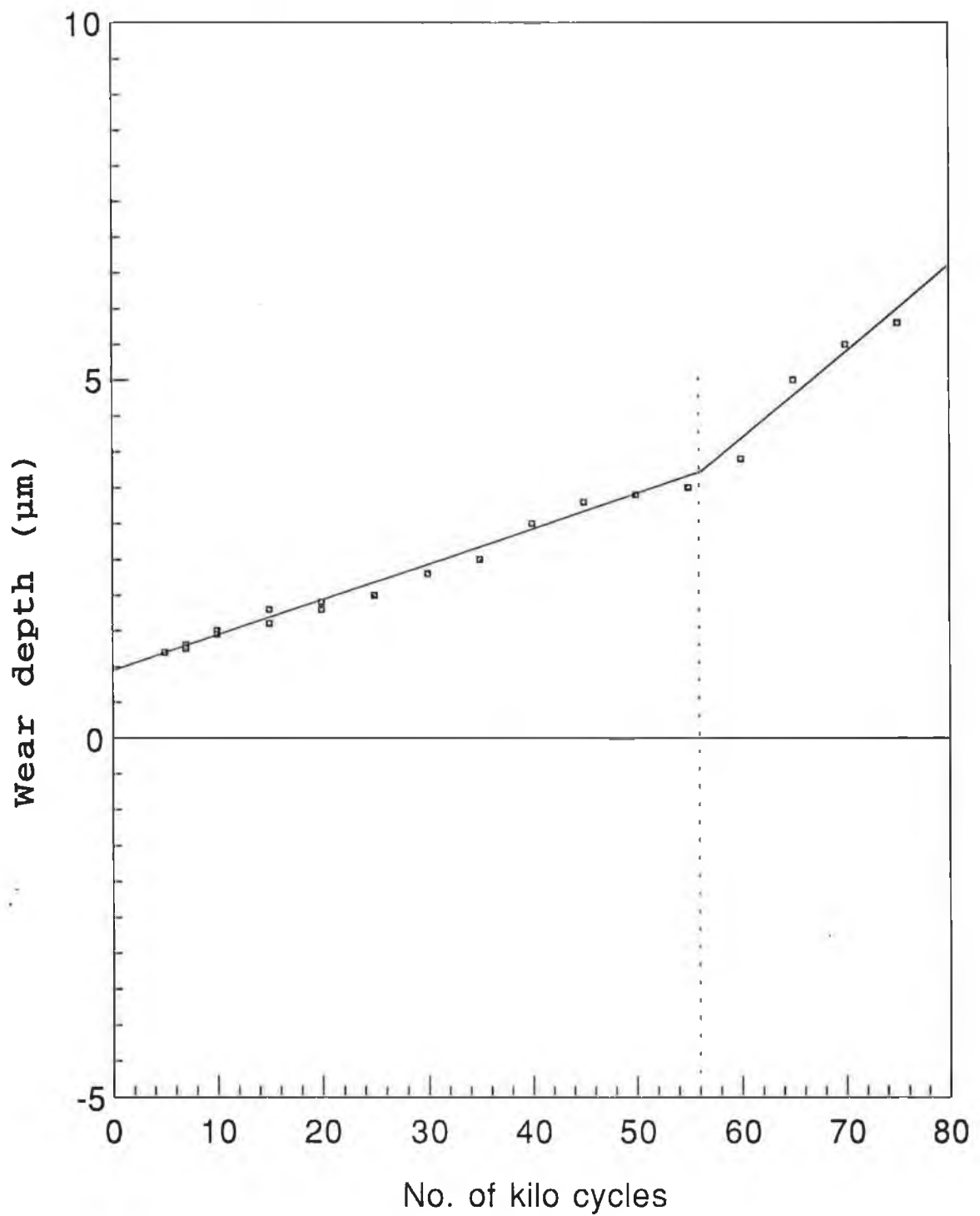


Fig.4.42 Average wear depth of Ti_xC coated V10 specimen.

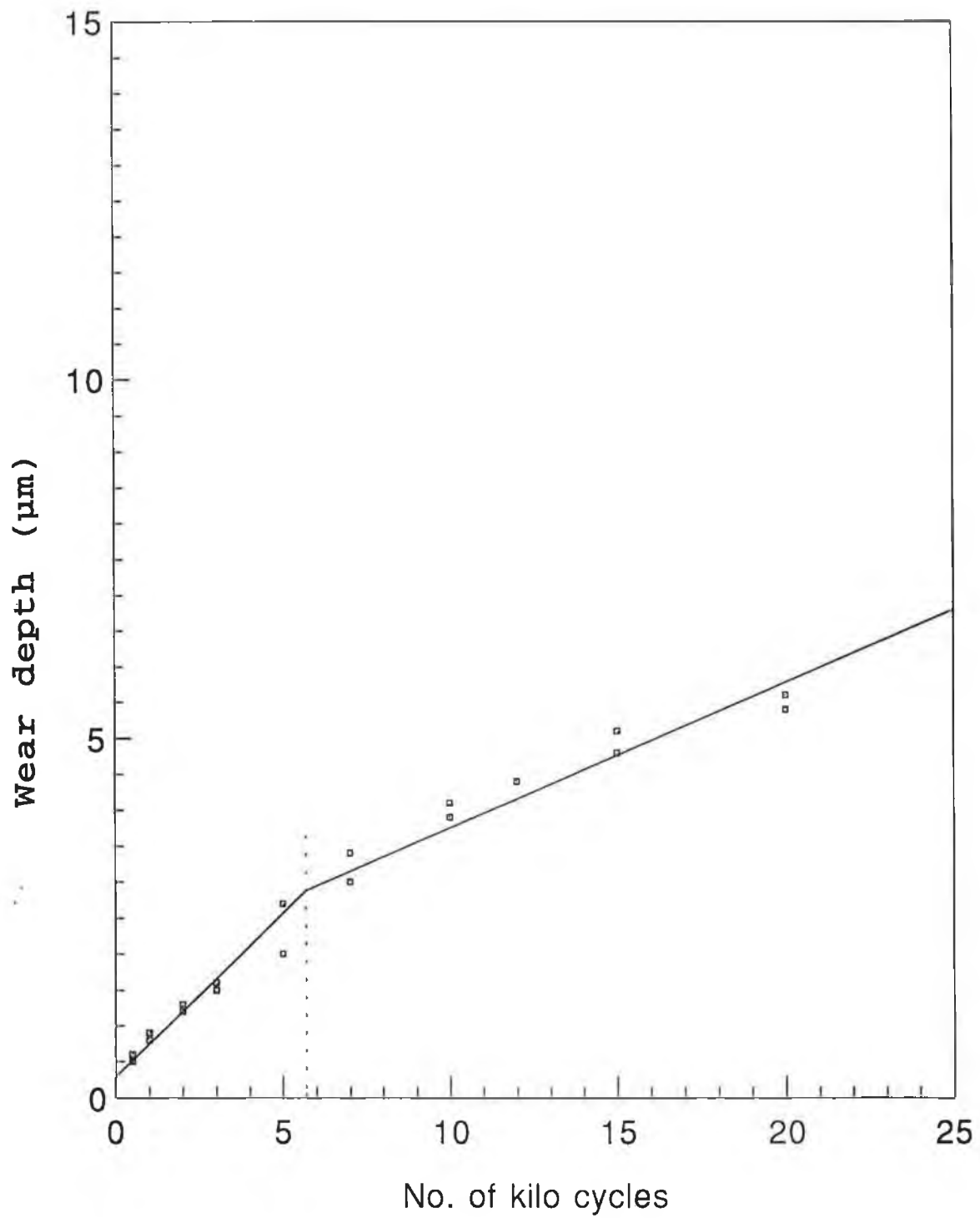


Fig.4.43 Average wear depth of TiN coated V10 specimen.

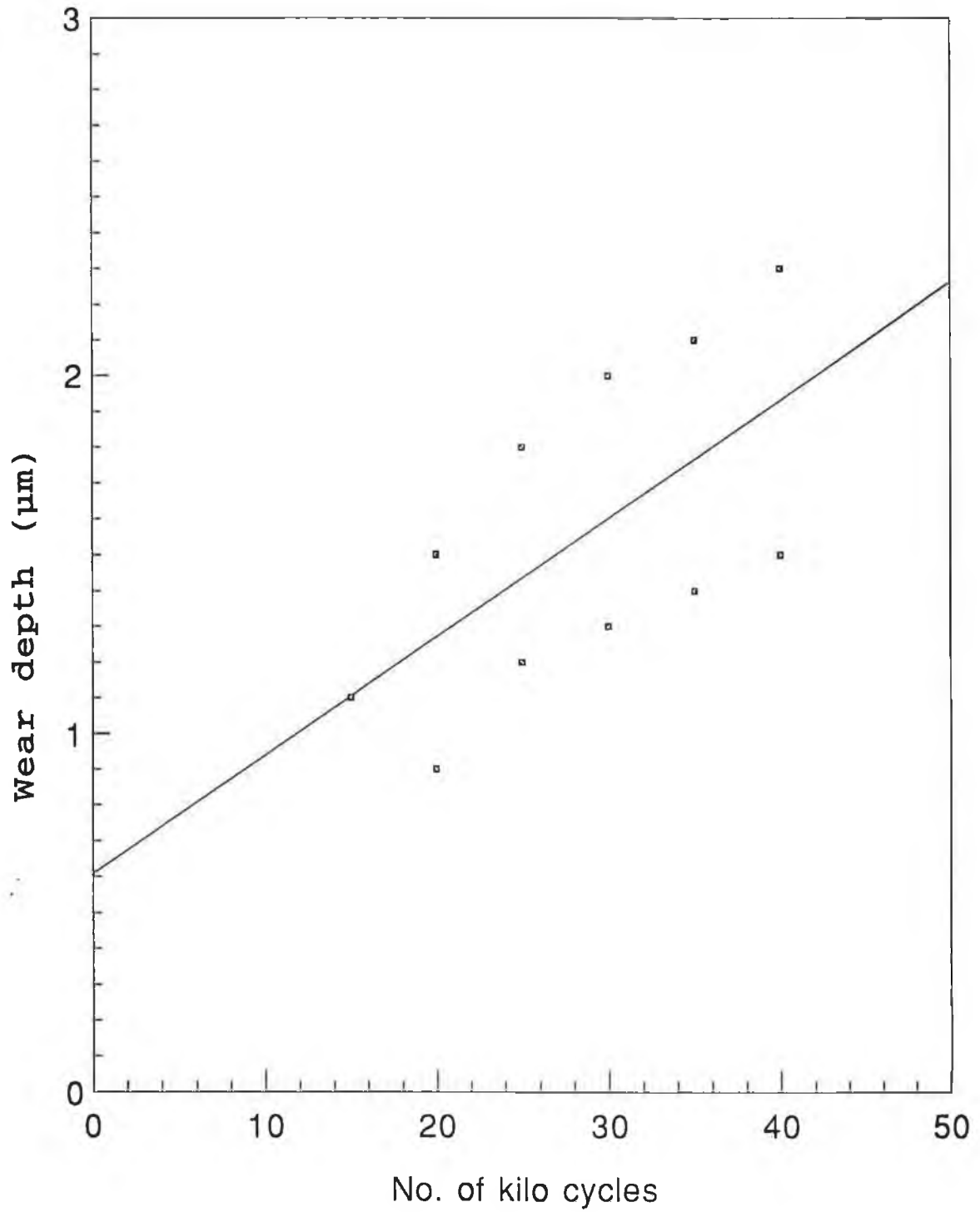


Fig.4.44 Average wear depth of Uncoated V10 specimen.

4.3.3 Wear of Coated and Uncoated Surfaces

Mostly coating is applied on the surface to increase its wear resistance. An improvement in wear resistance of the coated surface over the uncoated surface is indicated if there is less wear of the coated surface than on the uncoated surface. In the present study wear depth of the first wear track on coated and uncoated surfaces are shown as a function of number of cycles in Figs.4.45 to 4.48. Normalized wear of the first wear track on coated and uncoated surfaces are also shown as a function of number of cycles in Figs.4.49 to 4.52. Here normalized wear, d/w represents wear depth per unit wear width.

In Fig.4.45 it is shown that the TiN coated D2 tool steel surface experienced somewhat lower wear by comparison with the uncoated substrate. However the Ti_xC coated D2 tool steel surface experienced much lower wear than the uncoated D2 tool steel surface. In Fig.4.46 it is observed that the TiN coated D3 tool steel surface experienced lower wear and the Ti_xC coated D3 tool steel surface experienced much lower wear than the uncoated D3 tool steel surface. From Figs.4.47 and 4.48 it is observed that in both the cases of V4 and V10, TiN coated surfaces experienced much higher wear but Ti_xC coated surfaces experienced lower or nearly the same wear as uncoated surfaces. In this study, it is observed that wear resistance did not improve by the application of coating on the surface as a general case.

4.3.4 Comparative Wear of Different Coatings

Wear depth of the first wear track on Ti_xC coated, TiN coated and uncoated specimens of each of the substrate materials are shown as a function of number of cycles in Figs.4.45 to 4.48. Normalized wear of the first wear track on Ti_xC coated, TiN coated and uncoated specimens of each of the substrate materials are also shown as a function of number of cycles in Figs.4.49 to 4.52.

In Fig.4.45 it is shown that Ti_xC coated D2 tool steel surfaces wear out more slowly than uncoated D2 tool steel surfaces. When the coating was removed the base material wears out faster than the coated surface and almost at the same rate as the uncoated surface. But in the

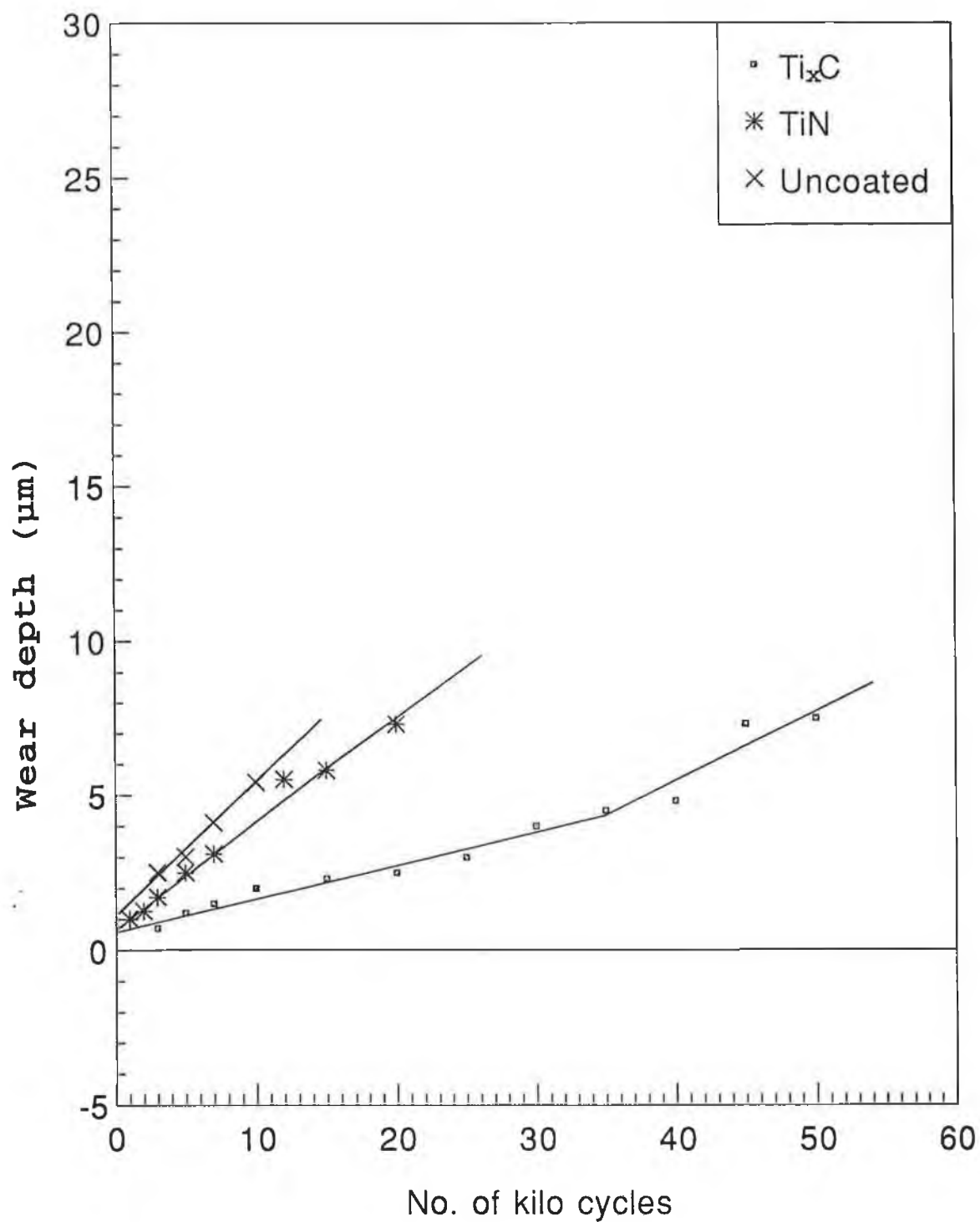


Fig.4.45 Wear depth of Ti_xC coated, TiN coated and Uncoated D2 specimen.

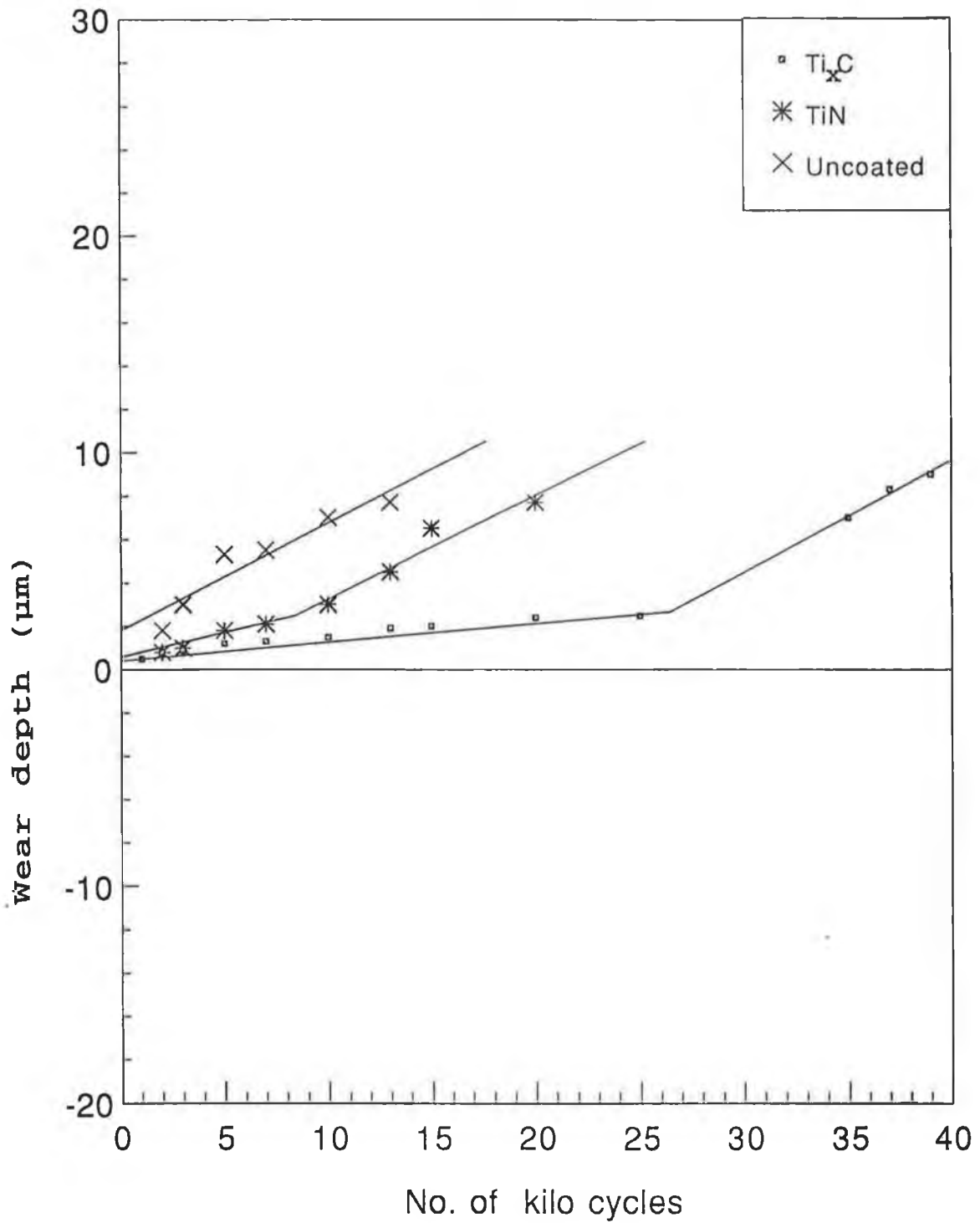


Fig.4.46 Wear depth of Ti_xC coated, TiN coated and Uncoated D3 specimen.

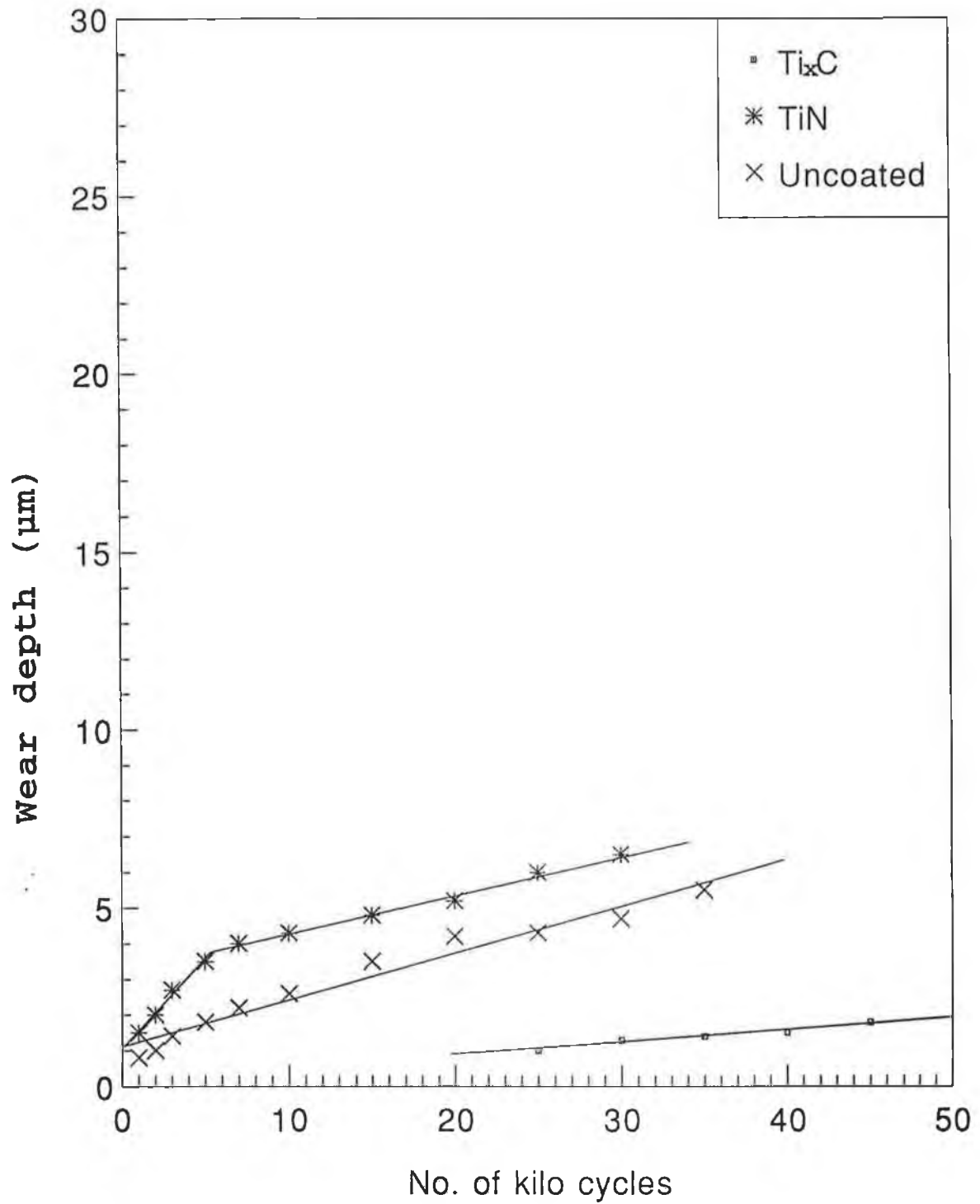


Fig.4.47 Wear depth of Ti_xC coated, TiN coated and Uncoated V4 specimen.

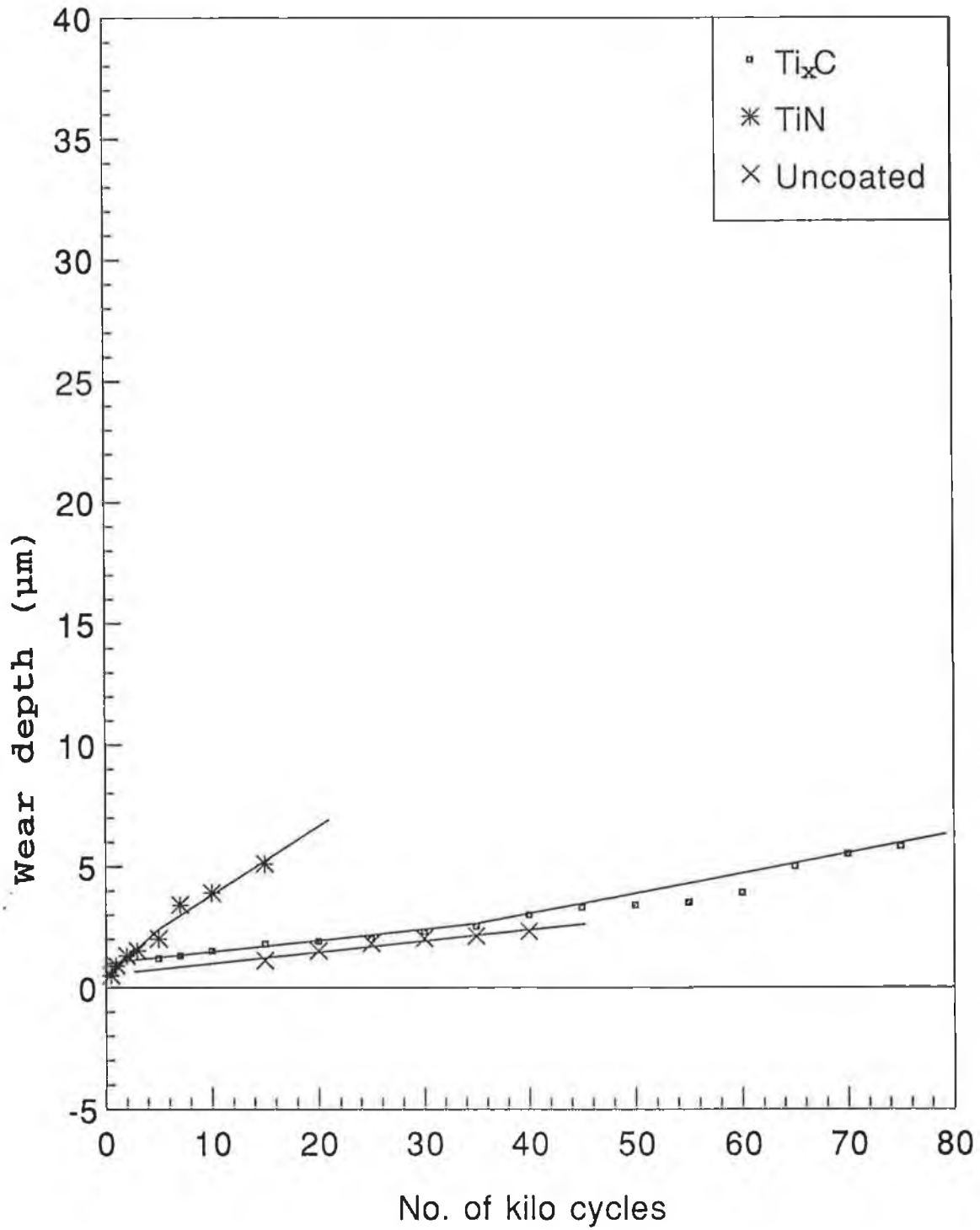


Fig.4.48 Wear depth of Ti_xC coated, TiN coated and Uncoated V10 specimen.

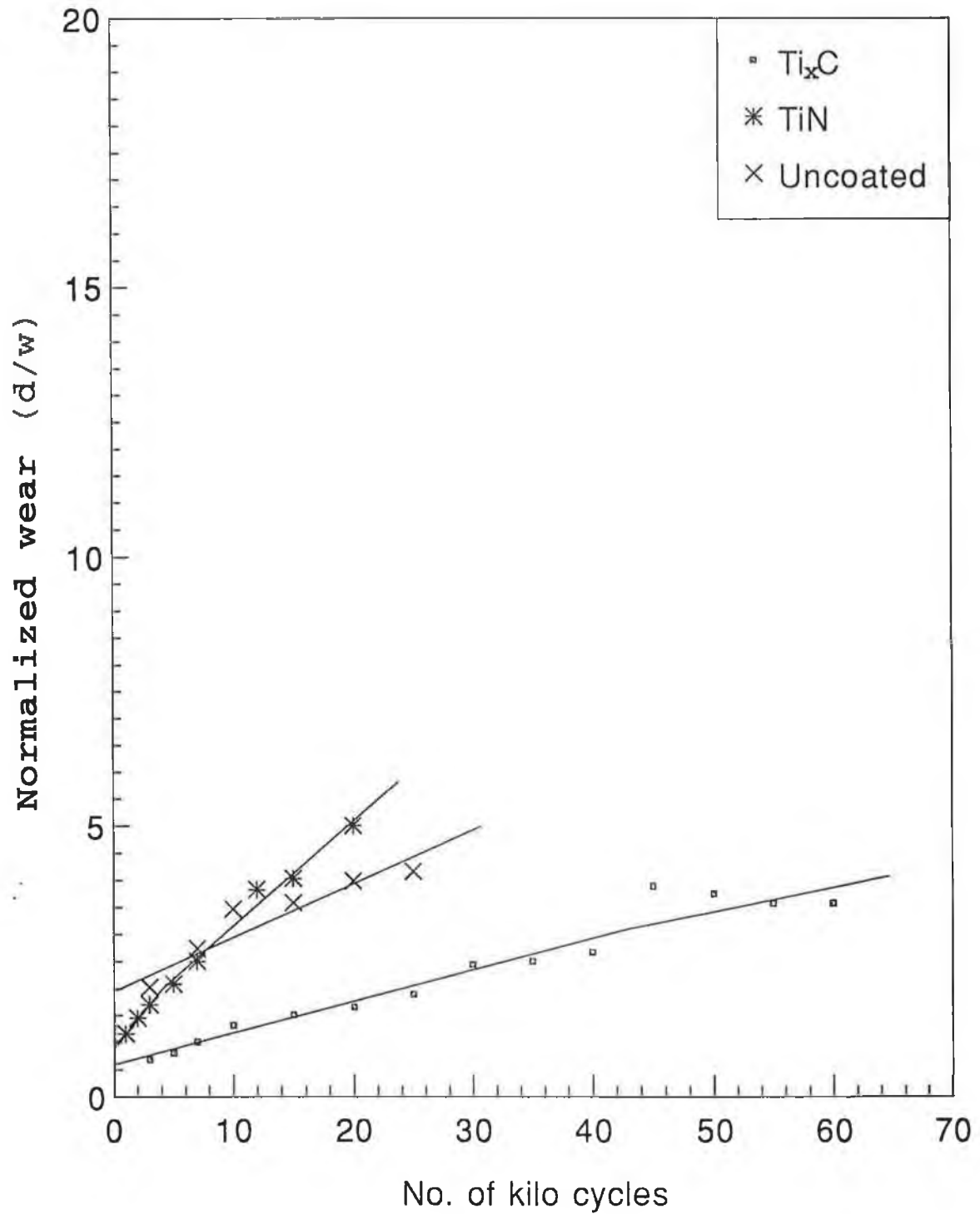


Fig.4.49 Normalized wear of Ti_xC coated, TiN coated and Uncoated D2 specimen.

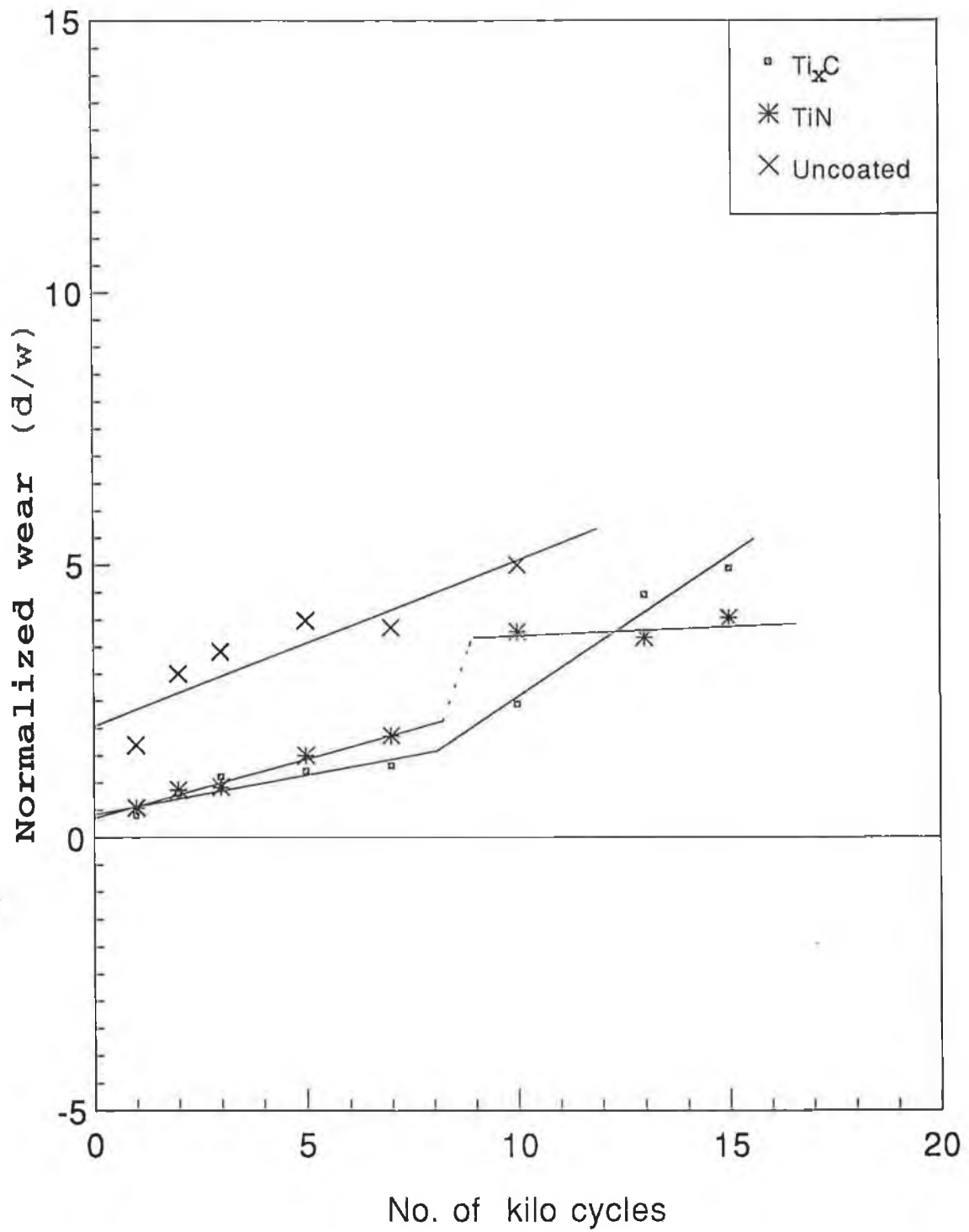


Fig.4.50 Normalized wear of Ti_xC coated, TiN coated and Uncoated D3 specimen.

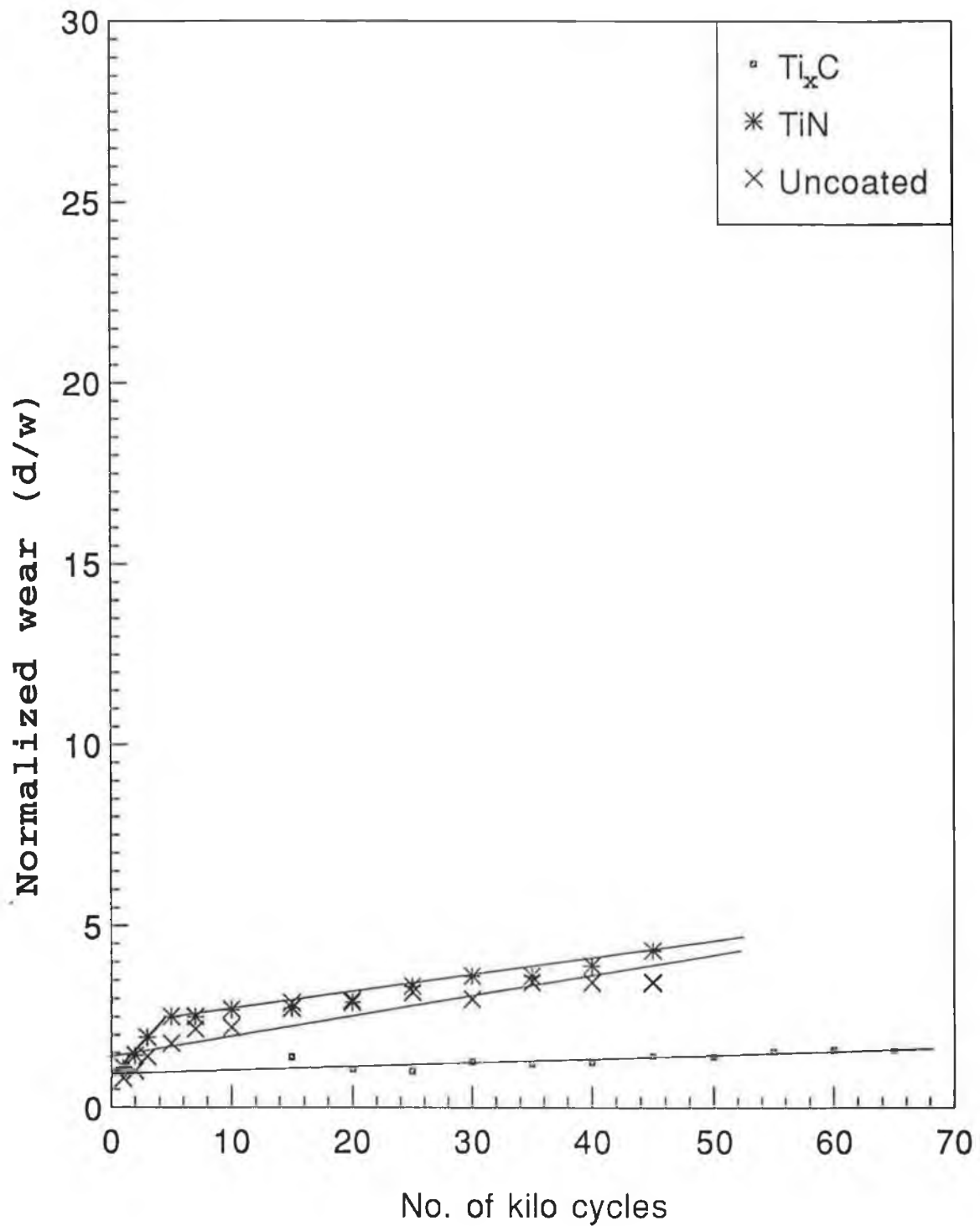


Fig.4.51 Normalized wear of Ti_xC coated, TiN coated and Uncoated V4 specimen.

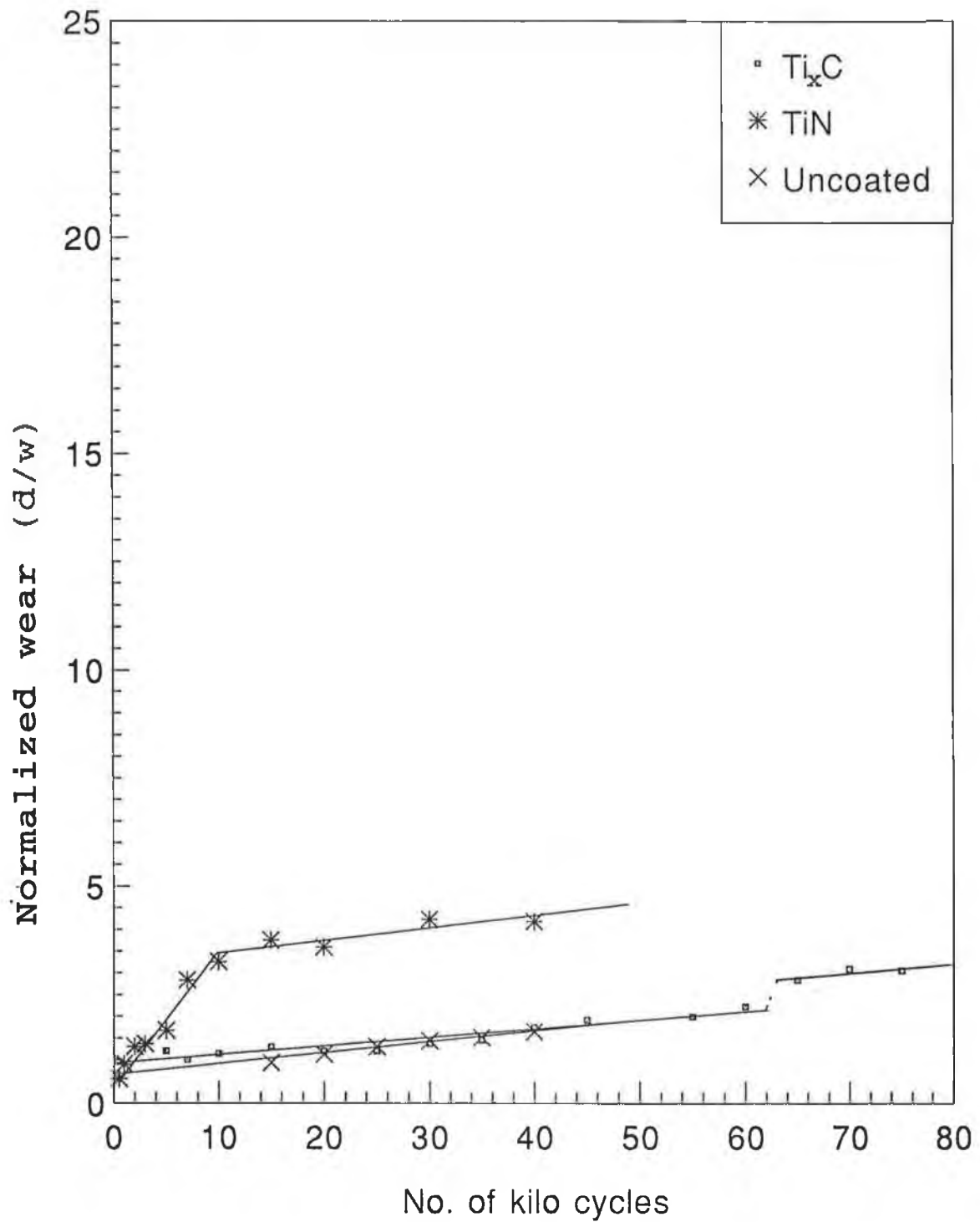


Fig.4.52 Normalized wear of Ti_xC coated, TiN coated and Uncoated V10 specimen.

case of the TiN coated D2 tool steel, the coated surface, the base material after the coating was removed and the uncoated surface wear out nearly at the same rate.

In Fig.4.46 it is shown that the Ti_xC coated D3 tool steel surface wears out more slowly than the uncoated D3 tool steel surface. When the coating was removed the base material wears out faster than the coated surface and almost at the same rate as the uncoated surface. In the case of the TiN coated D3 tool steel, the coated surface wears out more slowly than the uncoated surface. When the coating was removed the base material wears at the same rate as the uncoated surface.

In Fig.4.47 it is shown that Ti_xC coated V4 surfaces wear out more slowly than uncoated surfaces. The wear rate of the Ti_xC coated surface was very slow and near to an equilibrium load condition. The load was increased and the coating was removed completely in the first step with increased load. In the case of TiN coated V4, the coated surface wears out faster than the uncoated surface which is an indication of ineffective coating. The TiN coated surface also wears out faster than the base material surface.

In Fig.4.48 it is shown that the Ti_xC coated V10 surface wears out at the same rate as the uncoated V10 surface. When the coating was removed the base material wears out a little faster than the coated surface. In the case of TiN coated V10, the coated surface wears much faster than the uncoated surface and slightly faster than the base material.

4.3.5 Effect of Substrate Materials on Wear

The wear depth of Ti_xC coated and TiN coated specimens of four substrate materials are shown as a function of number of cycles in Figs.4.53 and 4.54 respectively. In the case of a coated surface, the load applied to produce wear is supported through the coating by the base material. Thus the base material properties are responsible for wear resistance of the coated surface. The effect of base materials on wear can be observed in Fig.4.53 and 4.54.

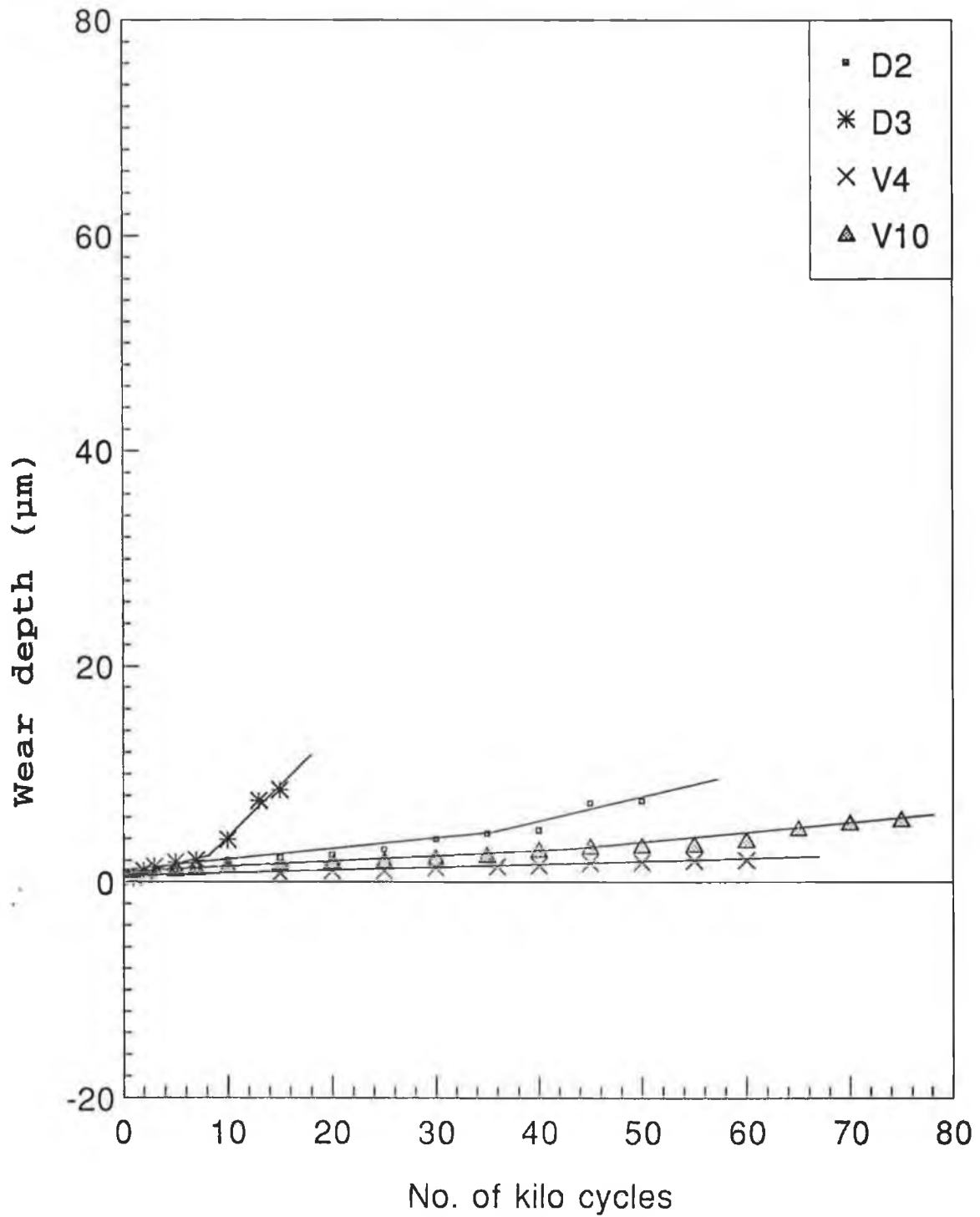


Fig.4.53 Wear depth of Ti_xC coated different substrate materials.

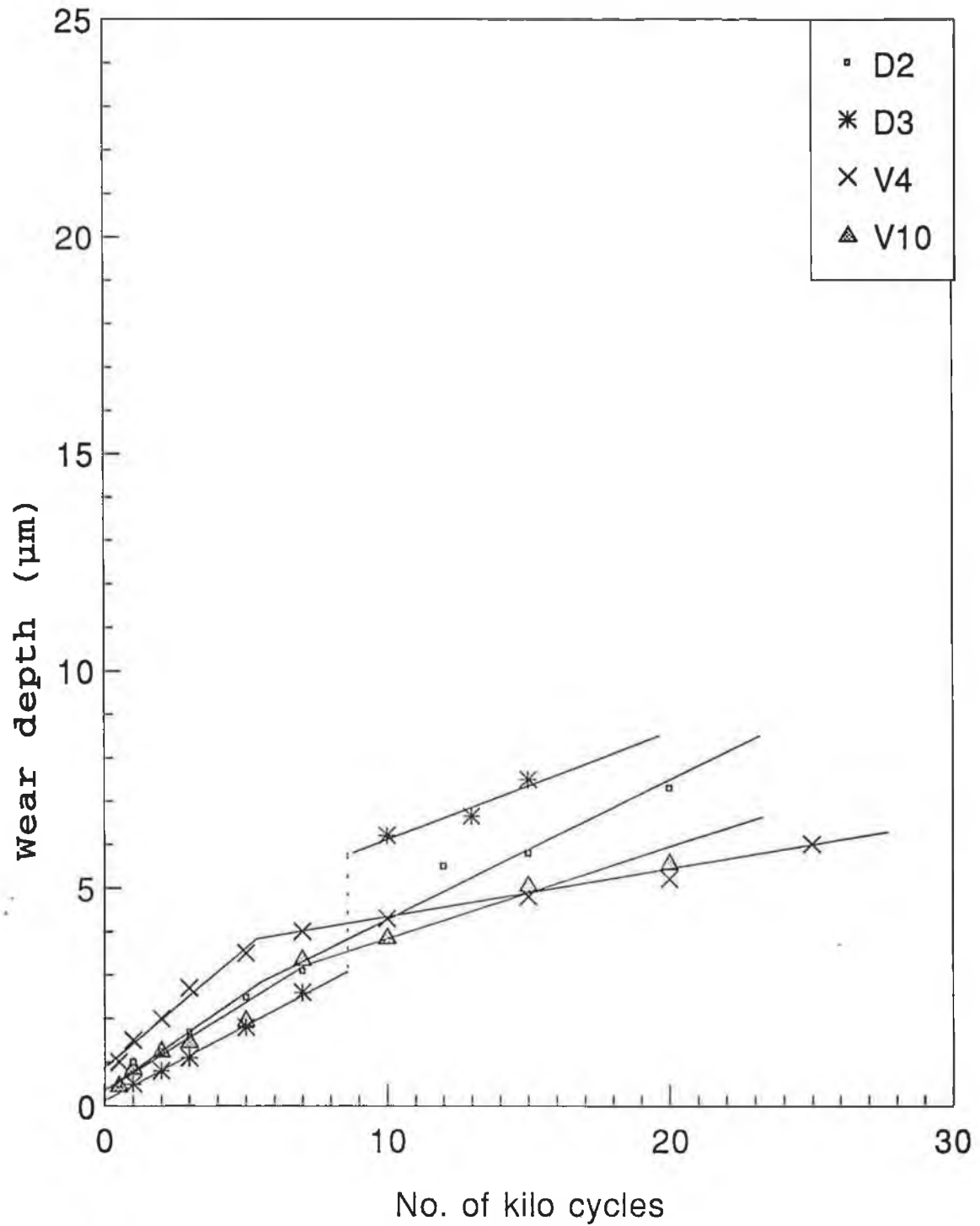


Fig.4.54 Wear depth of TiN coated different substrate materials.

4.3.6 Effect of Coating Hardness and Adhesion on Wear

The coating properties are responsible for wear resistance of the coated surface. In the well-known Archard equation [7], wear resistance is directly proportional to hardness of the specimen. But in the equation, there is a wear coefficient which depends on various properties of the mating materials. From Fig.4.55 it is observed that Ti_xC coating is harder than TiN coating. Thus it can be said that a Ti_xC coated surface is more wear resistant than a TiN coated surface when both the coatings are on the same base material.

The greater the difference in hardness between substrate and coating, the lower is the load required to produce appreciable surface contact. A lower load to produce appreciable surface contact indicates a lower real contact pressure. The hardness values of the coated specimens are not the hardness of the coatings but of the composites. In describing the difference in hardness between substrate and coating, the composite hardness is considered as the coating hardness. Wear resistance of Ti_xC and TiN coatings applied on different substrate materials are shown in Fig.4.53 and Fig.4.54 respectively. The greater the difference in hardness between coating and substrate the lower is the wear. This can be studied from Figs.4.53 to 4.54 in relation to Fig.4.55.

An adherent coating makes the surface more wear resistant. In Fig.4.56 adhesion of different coatings on different substrate materials is shown as bar graph. The above fact can be studied from Figs.4.53 and 4.54 in relation to Fig.4.56.

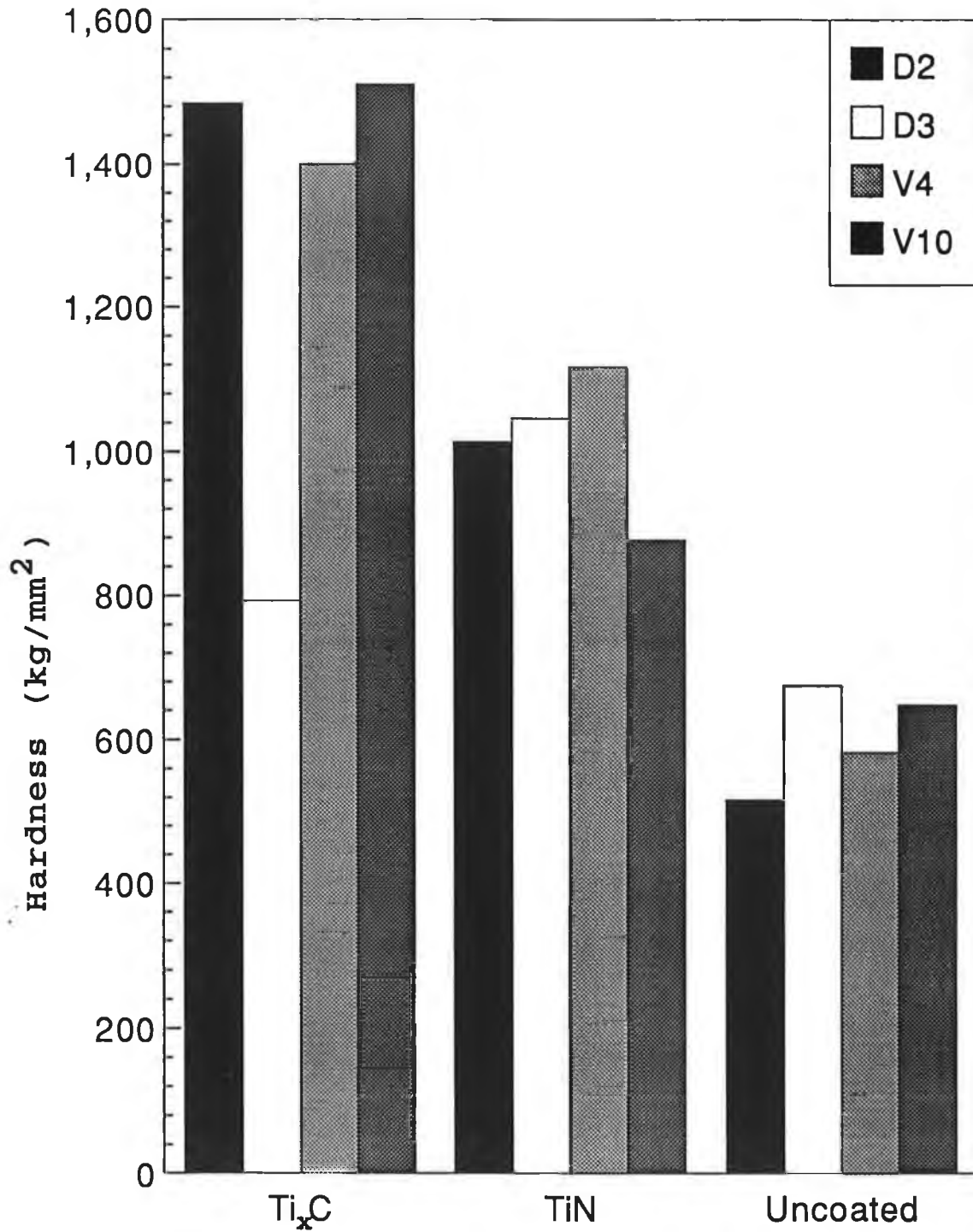


Fig.4.55 Hardness of coatings on different substrate materials.

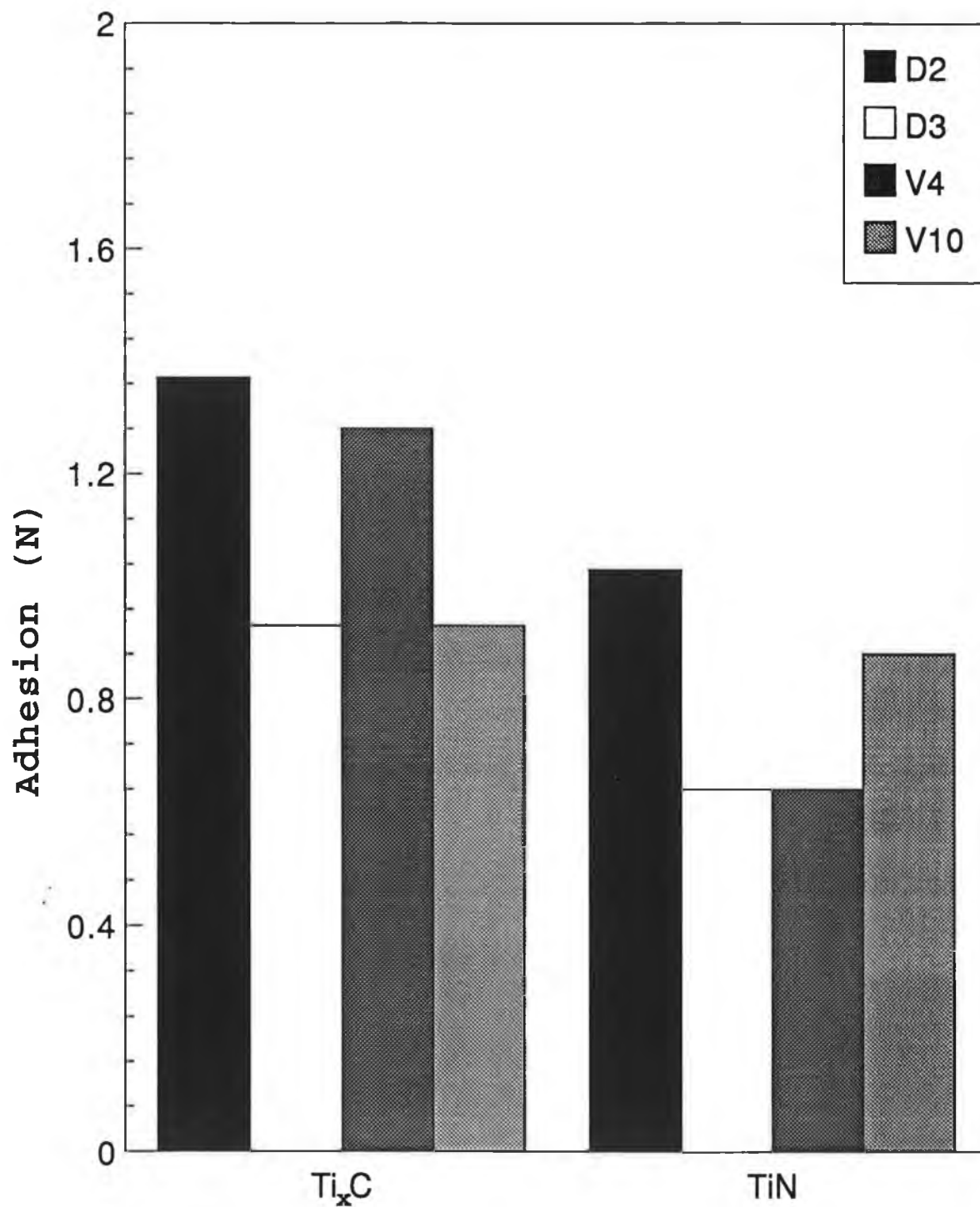


Fig.4.56 Adhesion of different coatings on different specimen materials.

Chapter 5

**Conclusions and Suggestions
for Further Work**

5.1 Introduction

Thickness and hardness of molybdenum nitride films have been studied using interferometry and microhardness test respectively. Hardness and adhesion of the films deposited under conditions specified to the external supplier have also been studied using microhardness and scratch tests respectively. Progressive wear measurements of these coated specimens obtained from external supplier and also of uncoated specimens were performed using the profilometer.

5.2 Conclusions

The results of characterization of films from deposition of MoN_x were analyzed to study the operating condition for deposition. The results of progressive wear on specimen coated under specified conditions and also on uncoated specimens have been analyzed to study the effect of number of cycles on wear, improvement of wear resistance of coated surface over uncoated surface, comparative wear of different coatings, effect of substrate materials on wear, effect of coating hardness on wear and effect of coating adhesion on wear.

5.2.1 Deposition of MoN_x Films

The formation of a molybdenum layer before the deposition of MoN_x films onto the substrate was allowed because such an interlayer enhance the adhesion of the films. But this molybdenum interlayer contributed to the measured deposition rate and hardness of the MoN_x coatings, the extent of which was difficult to assess.

It has been observed that adhesion of the deposited MoN_x films was poor regardless of the deposition parameters.

Deposition rate and hardness of the deposited films were in good agreement with existing work.

5.2.2 Wear Tests on Specimens Coated by External Supplier

In most cases, increase of wear depth in the second wear track was less than that in the first wear track with increasing number of cycles. This was most likely due to progressive wear in the stylus itself during the wear test in the first track.

In case of TiN coated surfaces for all the substrate materials, microscopic observation revealed the presence of pits over the surfaces. But Ti_xC coated surfaces for all the substrate materials were devoid of such pits. This was mainly responsible for the poor adhesion and poor wear performance of TiN coatings.

Application of TiN coatings did not improve the wear resistance of almost any of the four substrate materials. On the otherhand, Ti_xC coatings improved the wear resistance significantly of all the four substrate materials.

5.3 Suggestions

A well-designed fractional experiment can substantially reduce the number of experiments, with this in mind an experimental design and conditions may be developed. The design should be broad because a narrow set of parameters could produce very misleading results.

5.3.1 Deposition of MoN_x Films

The actual thickness of MoN_x films should be determined by subtracting the thickness of molybdenum interlayer. The thickness of molybdenum interlayer should be measured before the deposition of MoN_x films. Hence, the measured deposition rate of MoN_x films will be devoid of contribution from molybdenum interlayer. Time permitting this would have been done by the author.

When $D/t < 0.1$, where D is the depth of indentation and t is the thickness of MoN_x films alone, then the measured hardness of MoN_x films is free of contribution from molybdenum layer. If D/t varies between

0.1 and 1, the correction formula given in reference[49] cannot be applied to determine the hardness of MoN_x films because the effect of the molybdenum interlayer is not considered in the formula.

Part of the substrate bias arrangement, which is inside the deposition chamber, gets coated during deposition. This caused a short circuit. This part of the substrate bias arrangement should be shielded to avoid getting coated during deposition. This was not done at the design stage but is planned to be rectified later.

5.3.2 Wear Tests on Specimens Coated by External Supplier

More or even an additional wear track on each specimen could give better insight into the scatter of results over a sample surface. An additional wear track could be made at the centre of the sample surface if the sample did not have fixed offset from the centre of the tool holder block. Existing two wear tracks could be made by offsetting the sample with a spacer in between the sample and fixed locating edge along the wear track. Time permitting this would have been done by the author. It is suggested that the next researcher should undertake this modification.

When wear load was increased at the occurrence of equilibrium load situation, the load blocks did not remain in the horizontal plane. It was observed on the chart that tilt of the load blocks caused the trough of wear profile (across the wear track) to drift. This will require some modification of the apparatus which is due to be carried out by another researcher.

Selection of wear resistant materials is important in the industries where wear occurs in a wide variety of manners. Based on the results, all 4 substrates (both coated and uncoated) are listed in order of their wear resistance from high to low as follows. For the Ti_xC coated specimens: i) Vanadis 4, ii) Vanadis 10, iii) D2 tool steel and iv) D3 tool steel. For uncoated specimens: i) Vanadis 10, ii) Vanadis 4, iii) D2 tool steel and iv) D3 tool steel. As such should wear resistance be of most importance then the use of Vanadis 4 with Ti_xC would be recommended. However, if the cost of coating is unacceptably high then the use of Vanadis 10 would be recommended.

References

References

- [1] W. R. Grove, On the Electro-Chemical Polarity of Gases, *Phil. Trans. Roy. Soc. London*, 142, 87 (1852).
- [2] J.J. Thomson, *Rays of Positive Electricity*, Longmans, Green & Co., Ltd., London, (1921).
- [3] W. Tonn, Beitrag zur Kenntnis des Verschleißvorganges beim Kurzversuch, *Ztsch. f. Metallkunde*, Bd.29, 6, 196(1937).
- [4] S. Tolansky, *Multiple-beam Interferometry of Surfaces and Films*, Oxford University Press, London (1948).
- [5] D. Tabor, *The Hardness of Metals*, Clarendon Press, Oxford, England (1951).
- [6] J.T. Burwell and C.D. Strang, On the Empirical Law of Adhesive Wear, *J. Appl. Phys.*, 23, 18 (1952).
- [7] J.F. Archard, Contact and Rubbing of Flat Surfaces, *J. Appl. Phys.*, 24, 981(1953).
- [8] J.F. Archard and W. Hirst, The Wear of Metals Under Lubricated Conditions, *Proc. Roy. Soc. Lond., Ser A*, 236, 397 (1956).
- [9] I.V. Kragelsky, Some Concepts and Definitions which Apply to Friction and Wear, *Acad. Sci. USSR, Moscow*, 12 (1957).
- [10] G. Yoshimoto and T. Tsukizoe, On the Mechanism of Wear Between Metal Surfaces, *Wear*, 1, 472 (1958).
- [11] I. V. Kragelsky, Wear as a Result of Repeated Deformation of Surface Layers (Special case of contact with a deformable surface of absolutely fixed roughness), *Izv. Vyssh. ucheb. zavedeniy, Fizika*, 5, 119 (1958).
- [12] D.V. Keller, Adhesion Between Solid Metals, *Wear*, 6, 353(1963).
- [13] L. Rozeanu, Fatigue Wear as a Rate Process, *Wear*, 6, 337 (1963).
- [14] R.G. Bayer, W.C. Clinton and J.L. Sirico, Note on the Application of the Stress Dependency of Wear, *Wear*, 7, 282 (1964).
- [15] K. Endo and Y. Fukuda, A Role of Fatigue in Wear of Metals, *Proc. 8th Jap. Congr. Test. Mater. (1964)*, Kyoto, *Kyote Soc. Mater. Sci. Jap.*, 69 (1965).
- [16] D. Onderdelinden, F. W. Saris and P. K. Rol, The Validity of the Transparency Model for Single Crystal Sputtering, *Nucl. Instr. Methods*, 38, 269 (1965).
- [17] E. Rabinowicz, *Friction and Wear of Materials*, Wiley, New York, (1965).

- [18] I. V. Kragelsky, Calculation of Wear Rate, Trans. ASME, J. of Basic Engng. Ser D, 87, 785 (1965).
- [19] K. Endo, Y. Fukuda and O. Takamia, Influence of Internal Stress on the Wear of Steel, Bull. JSME, 4, 17 (1965).
- [20] C.N.Rowe, Some Aspects of the Heat of Adsorption in the Function of a Boundary Lubricant, ASLE Trans., 9, 101 (1966).
- [21] D. Onderdelinden, F. W. Saris and P.K. Rol, Proc. 7th Int. Conf. Phenomena in Ionized Gases, Vol.1, Belgrade, (1966).
- [22] T. W. Snouse and L. C. Houghney, Sputtering of Single Crystal Copper, J. Appl. Phys., 37, 700 (1966).
- [23] T. Spalvins, J. S. Przybyszewski and D. H. Buckley, Deposition of Thin Films by Ion Plating on Surfaces Having Various Configurations, NASA TND-3707 (1966).
- [24] E. Rabinowicz, Variation of Friction and Wear of Solids Lubrication, ASLE Trans., 10, 1 (1967).
- [25] D.H. Buckley and R.L. Johnson, The Influence of Crystal Structure and Some Properties of Hexagonal Metals on Friction and Adhesion, Wear, 11, 405(1968).
- [26] G. Polzer, Ein Beitrag zu den Problemen - Reibung und Verschleiß, Verlag der Technischen Hochschule, Karlmarxstadt, 176 (1968).
- [27] I. V. Kragelsky, E. F. Nepomnyashchy and L. M. Kharatsch, Lubrication and Wear, Fundamentals and Application to Design, Proc. Inst. Mech. Eng., 182, 3A, 396 (1957-1968).
- [28] P. Sigmund, Sputtering Efficiency of Amorphous Substances, Can. J. Phys., 46, 731 (1968).
- [29] B.A. Movchan and A.V. Demchishin, Study of the Structure and Properties of Thick Vacuum Condensates of Nickel, Titanium, Tungsten, Aluminum oxide and Zirconium oxide, Fiz. Met. Metalloved, 28, 653 (1969).
- [30] K. Endo, Y. Fukuda and H. Togata, The Wear of Steel in Lubricating Oil Under Varying Load, Bull. JSME, 12, 539 (1969).
- [31] G.K. Whener and G.S. Anderson, in L.I. Maissel and R. Glang (eds.), Handbook of Thin Film Technology, McGraw-Hill, New York, Chap.3, (1970).
- [32] D. Henderson, M. H. Brodsky and P. Chaudhari, Simulation of Structural Anisotropy and Void Formation in Amorphous Thin Films, Appl. Phys. Lett., 25, 641 (1974).
- [33] M.M. Khrushchov, Principles of Abrasive Wear, Wear, 28, 69 (1974).

- [34] E. Hornbogen, The Role of Fracture Toughness in the Wear of Metals, *Wear*, 33, 251 (1975).
- [35] T. Abe and T. Yamashina, The Deposition Rate of Metallic Thin Films in the Reactive Sputtering Process, *Thin Solid Films*, 30, 19 (1975).
- [36] A. G. Dirks and H. J. Leamy, Columnar Microstructure in Vapor Deposited Thin Films, *Thin Solid Films*, 47, 219 (1977).
- [37] J.A. Thornton, High Rate Thick Film Growth, *Ann. Rev. Material Sci.*, 7, 239 (1977).
- [38] A. H. Elthouky, B. R. Natarajan, J. E. Greene and T. L. Barr, A General Phenomenological Model for Reactive Sputtering, *Thin Solid Films*, 69, 229 (1980).
- [39] E. Rabinowicz in M. B. Peterson and W.O. Winer (eds.), *Wear Coefficients - Metals*, in *Wear Control Handbook*, ASME, New York, 475(1980).
- [40] N. Ohmae, T. Okuyama and T. Tsukizoe, Influence of Electronic Structure on the Friction in Vacuum of 3d Transition Metals in Contact with Copper, *Tribol. Int.*, 13, 177(1980).
- [41] T. Hata, E.Noda, O. Marimoto and T.Hada, High Rate Deposition of Thick Piezoelectric ZnO Films Using a New Magnetron Sputtering Technique, *Appl. Phys. Lett.*, 37, 633 (1980).
- [42] D.H. Buckley, *Surface Effects in Adhesion, Friction, Wear and Lubrication*, Elsevier, Amsterdam, (1981).
- [43] I.V. Kragelsky, M.N. Dobyichin and V.S. Kombalov, *Friction & Wear: Calculation Methods*, Pergamon Press Ltd., England (1982).
- [44] K.-H. Zum Gahr, *Abrasive Wear of Ductile Materials*, *Z.F. Metallkd*, 73, 267 (1982).
- [45] K.Stenbeck, E.Steinbeiss and K.-D. Uferz, The Problem of Reactive Sputtering and Cosputtering of Elemental Targets, *Thin Solid Films*, 92, 371 (1982).
- [46] R. Adachi and K. Takeshita, Magnetron Sputtering with Additional Ionization Effect by Electron Beam, *J. Vac. Sci. Technol.*, 20, 98 (1982).
- [47] R.F. Bunshah, *Deposition Technologies for Films and Coatings: Developments and Applications*, Noyes Publications, U.S.A. (1982).
- [48] T.R. Thomas, *Rough Surfaces*, Longman, London (1982).
- [49] B. Jönsson and S. Hogmark, Hardness Measurements of Thin Films, *Thin Solid Films*, 114, 257 (1984).

- [50] G. Lemperière and J. M. Poitevin, Influence of the Nitrogen Partial Pressure of the Properties of DC Sputtered Titanium nitride Films, *Thin Solid Films*, 111, 339 (1984).
- [51] R. Meissier, A.P. Giri and R.A. Roy, Revised Structure Zone Model for Thin Film Physical Structure, *J. Vac. Sci. Technol.*, A2, 500 (1984).
- [52] B. Bhushan and M. Gordon, Metallurgical Reexamination of Wear Modes: I. Erosive, Electrical Arcing and Fretting, *Thin Solid Films*, 123, 93 (1985).
- [53] D.G. Teer and R.D. Arnell, Recent Developments in Surf. Coat. and Modi. Processes, Organized by Prof. J. Hallig, Seminar at IMechE, 21 (1985).
- [54] B. Window and N. Savvides, Charged Particle Fluxes from Planar Magnetron Sources, *J. Vac. Sci. Technol.*, A4, 196 (1986).
- [55] D.S. Rickerby, Internal Stress and Adherence of Titanium nitride Coatings, *J. Vac. Sci. Technol.*, A4, 2809 (1986).
- [56] J. J. Cuomo and S. M. Rossnagel, Hollow-Cathode-Enhanced Magnetron Sputtering, *J. Vac. Sci. Technol.*, A4, 393 (1986).
- [57] U. Helmersson, J.E. Sundgren and J. E. Greene, Microstructure Evolution in TiN Films Reactively Sputtered Deposited on Multiphase Substrates, *J. Vac. Sci. Technol.*, A4, 500 (1986).
- [58] Z.S. Xing, Proc. Int. Conf. on Plasma Sci. Tech., Beijing, China, Published by Sci. Press and VCH (1986).
- [59] D.S. Rickerby, G. Eckold, K.T. Scott and I.M. Buckley-Golder, The Interrelationship between Internal Stress, Processing Parameters and Microstructure of Physically Vapour Deposited and Thermally Sprayed Coatings, *Thin Solid Films*, 154, 125 (1987).
- [60] K.H. Müller, Role of Incident Kinetic Energy of Adatoms in Thin Film Growth, *Surf. Sci.*, 184, L375 (1987).
- [61] P.J. Burnett and D.S. Rickerby, Experimental Studies and Interpretation of Hardness, *Thin Solid Films*, 148, 51 (1987).
- [62] S. Berg, H.-O. Blom, T. Larsson and C. Nender, Modelling of Reactive Sputtering of Compound Materials, *J. Vac. Sci. Technol.*, A5, 202 (1987).
- [63] T. Fukami, F. Shintani and M. Naoe, Observations on the Operation of a Planar Magnetron Sputtering System by Target Erosion Patterns, *Thin Solid Films*, 149, 373 (1987).

- [64] A.G. Spencer, K.Oka, R.W. Lewin and R.P. Howson, Activation of Reactive Sputtering by a Plasma Beam from an Unbalanced Magnetron, *Vacuum*, 38, 857 (1988).
- [65] D.S. Rickerby and P. J. Burnett, Correlation of Process and System Parameters with Structure and Properties of Physically Vapour Deposited Hard Coatings, *Thin Solid Films*, 157, 195 (1988).
- [66] S.K. Ghosh and T.K. Hatwar, Reactively Sputtered SiN Thin Films, *Thin Solid Films*, 166, 359 (1988).
- [67] V. Valvode, R. Cerny, R. Kuzel, J. Musil and V. Poulek, Dependence of Microstructure of TiN Coatings on their Thickness, *Thin Solid Films*, 158, 225 (1988).
- [68] Y. Imai, K. Osato and H. Nakauchi, Plasma CVD Molybdenum Film Formation, *Corr. Engg.*, 37, 11 (1988).
- [69] D. S. Rickerby, A. M. Jones and B. A. Bellamy, X-ray Diffraction Studies of Physically Vapour Deposited Coatings, *Surf. Coat. Technol.*, 37, 111 (1989).
- [70] J. Musil, S. Kadlec, J. Vyskočil and V. Poulek, Reactive Deposition of Hard Coatings, *Surf. Coat. Technol.*, 39/40, 301 (1989).
- [71] J. Vyskočil, J. Musil, S. Kadlec and W. D. Münz, in E. Brozeit et al (eds.), *Plasma Surface Engg.*, DGM Informations Gesellschaft, Oberasel, Vol.1, 661 (1989).
- [72] B. Bhushan, *Tribology and Mechanics of Magnetic Storage Devices*, Springer-Verlag, New York, (1990).
- [73] A. F. Jankowski and L. R. Schrawyer, Reactively Sputtering of Molybdenum, *Thin Solid Films*, 193/194, 61 (1990).
- [74] D.P. Upton, The Performance of New PVD Coatings on Cutting Tools, *Trans. of the Inst. of Metal Finishing*, Vol.68, No.4, 118 (1990).
- [75] J. Michalski and T. Wierzchoń, Formation of TiN Layers by Plasma-Assisted Chemical Vapour Deposition at Temperatures Greater than 823°K, *Materials Sci. Engg.*, A140, 499 (1990).
- [76] B. Bhushan and B.K. Gupta, *Handbook of Tribology: Materials, Coatings and Surface Treatments*, McGraw-Hill, Inc., U.S.A. (1991).

- [77] M. Benmalek, P. Gimenez, J. P. Peyre and C. Tournier, Characterization and Comparison of TiN Layers Deposited by Difference Physical Vapour and Deposition Processes, Surf. Coat. Technol., 39/40, 487 (1991).
- [78] P.J. Rudnik, M.E. Graham and W.D. Sproul, High Rate Reactive Sputtering of MoNx Coatings, Surf. Coat. Technol., 49, 293 (1991).
- [79] R.T. Carson, J.H. Givens, H.S. Savage, Y.W. Lee and J.M. Rigsbee, Reactively Ion Plated TiN: Effects of R.F. Power Density on the Structure and Electrochemical Properties, Thin Solid Films, 204, 285 (1991).
- [80] W. Olbrich, J. Fessmann and G. Kampschulte, Improved Control of TiN Coating Properties, Surf. Coat. Technol., 49, 258 (1991).
- [81] A. F. Jankowski and L. R. Schrawyer, Working Gas Pressure and Flow Effects on Reactively Sputtered Molybdenum oxide Thin Films, Surf. Coat. Tech., 54/55, 349 (1992).
- [82] F. Hohl, H.-R. Stock and P. Mayr, Properties of Sputtered TiN Films, Surf. Coat. Technol., 54/55, 160 (1992).
- [83] M. Maoujoud, L. Binst, P. Delcambe, Offergeld-Jardinier and F. Bouillon, Deposition Parameter Effects on the Composition and the Crystalline State of Reactively Sputtered Molybdenum nitride, Surf. Coat. Technol., 52, 179 (1992).
- [84] A.J. Perry, A.W. Baouchi, J.H. Petersen and S.D. Pozder, Crystal Structure of Molybdenum nitride Films Made by Reactive Cathodic Arc Evaporation, Surf. Coat. Technol., 54/55, 261 (1992).
- [85] P. V. Kola, Magnetron Sputtering of Protective Coatings for Mechanical and Biomedical Use, Report of Transfer from M.Eng. to Ph.D., School of Mech. & Manuf. Eng., D.C.U., Dublin 9, Ireland (1993).

Appendix A

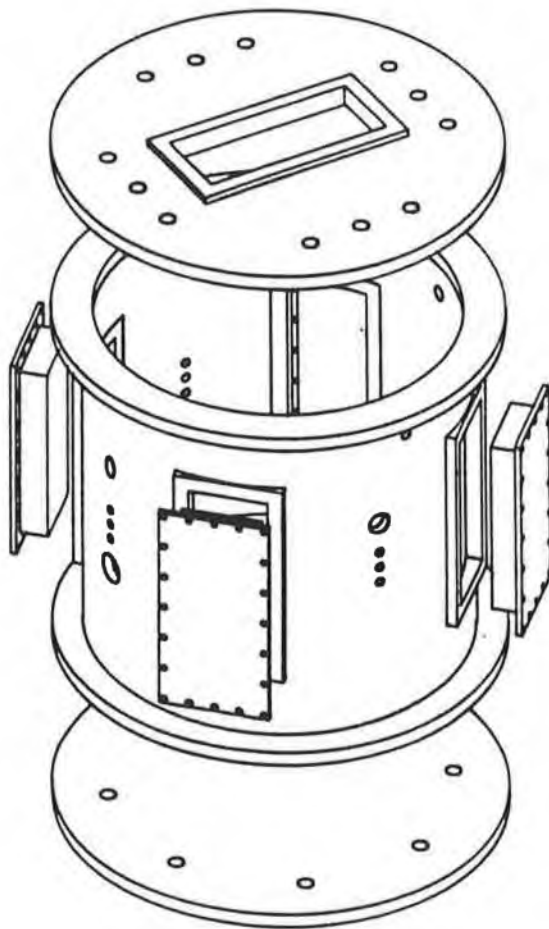


Fig.A.1 Assembly of the deposition chamber [Drawn by: L. Domican].

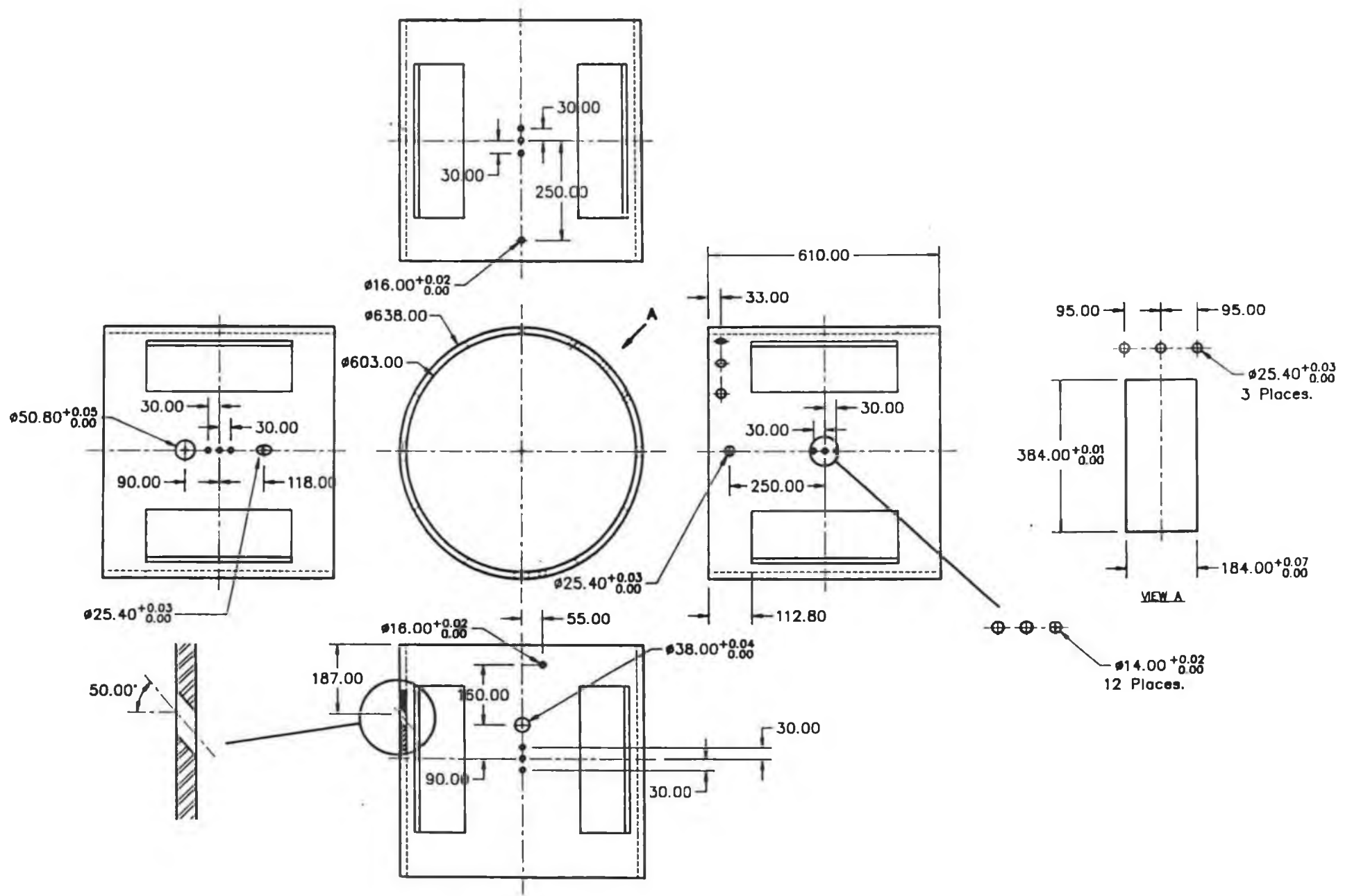


Fig.A.2 Deposition chamber [Drawn by: L. Domican].

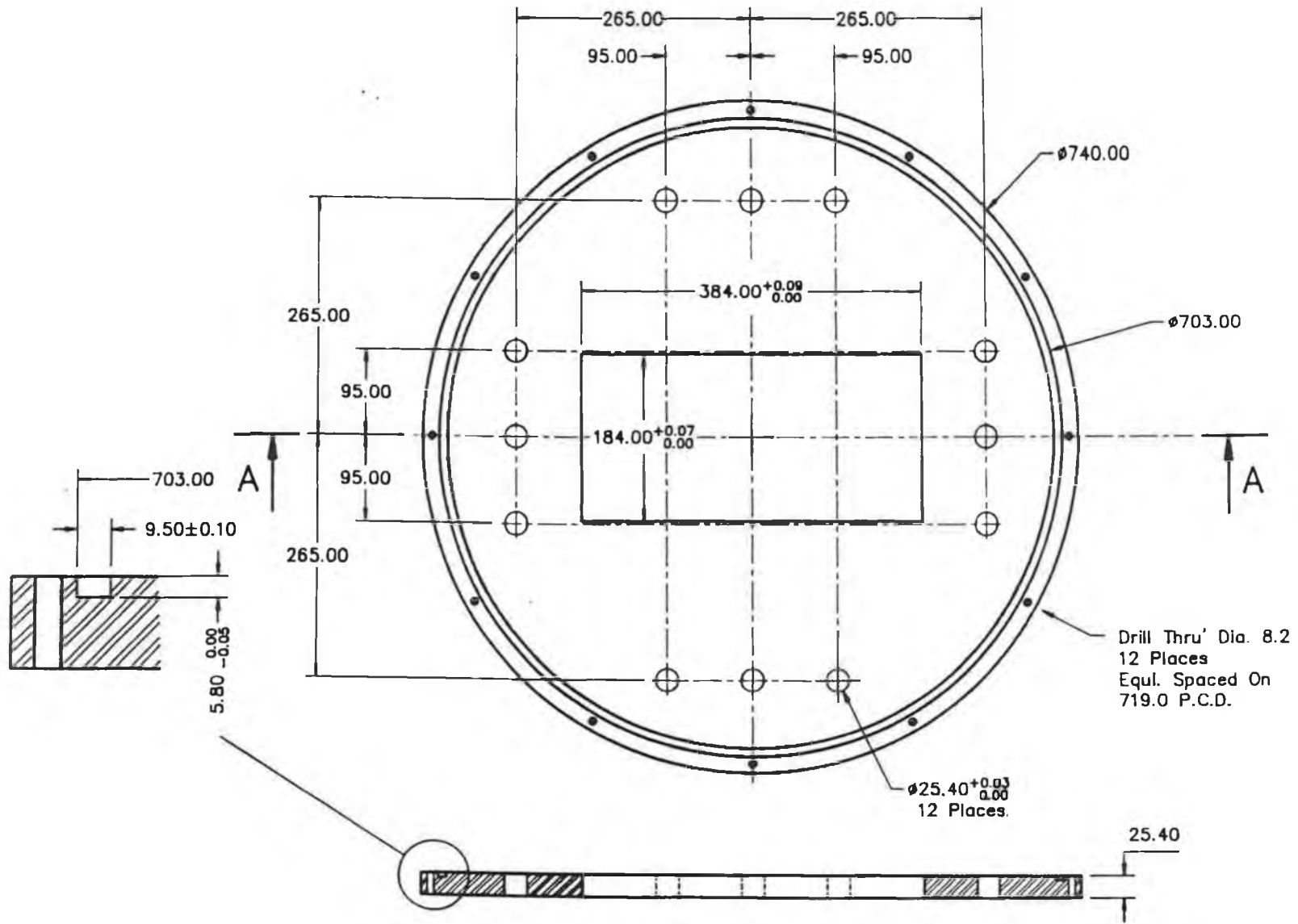


Fig.A.3 Top plate of the chamber [Drawn by: L. Domican].

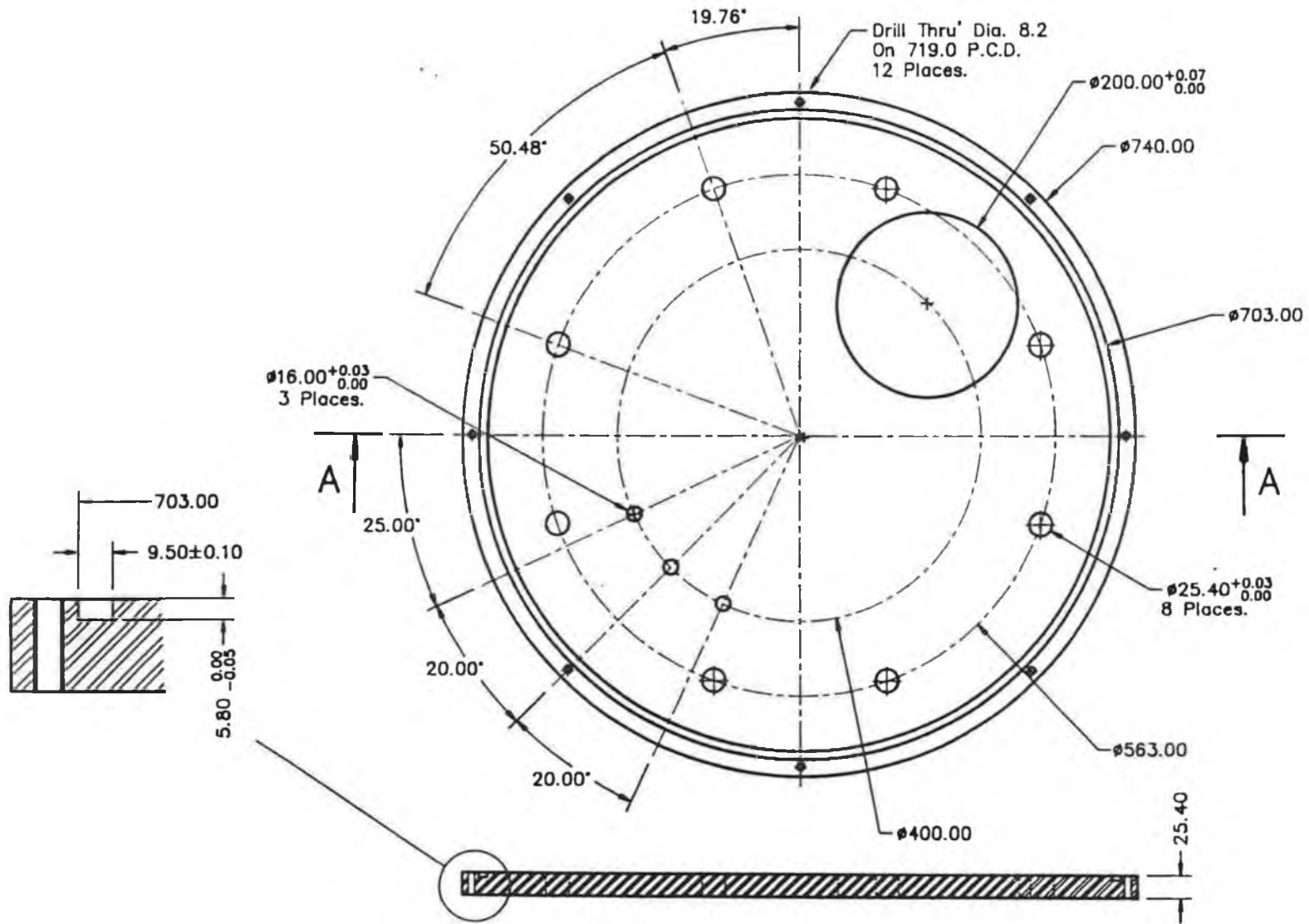


Fig.A.4 Bottom plate of the chamber [Drawn by: L. Domican].

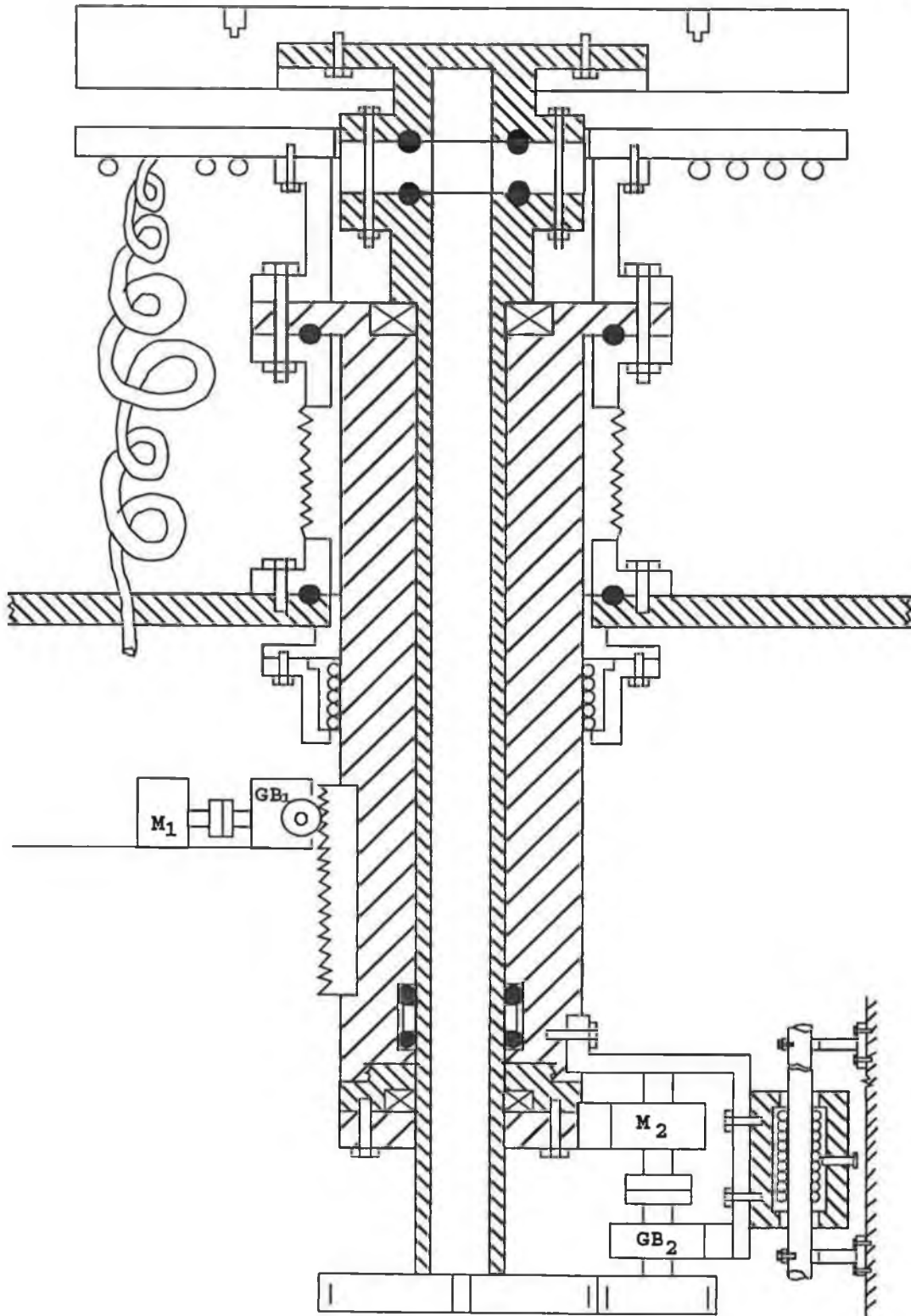


Fig.A.5 Assembly of the substrate table (section).

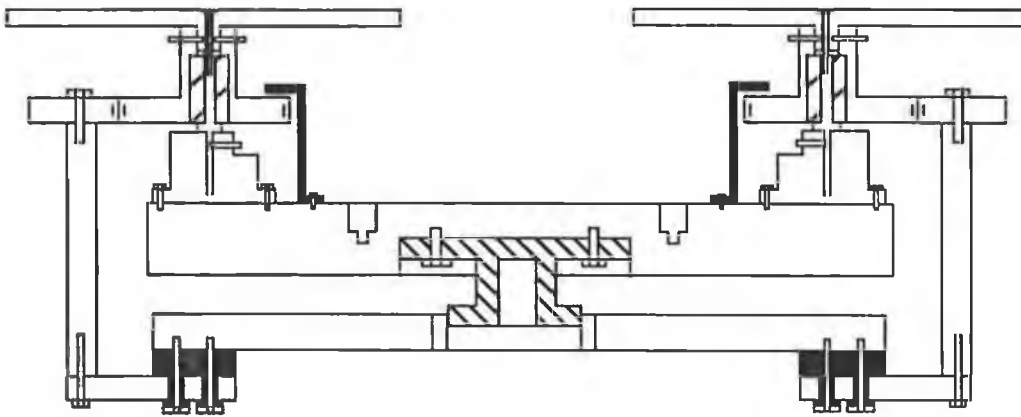


Fig.A.6 Assembly for substrate motion (section).

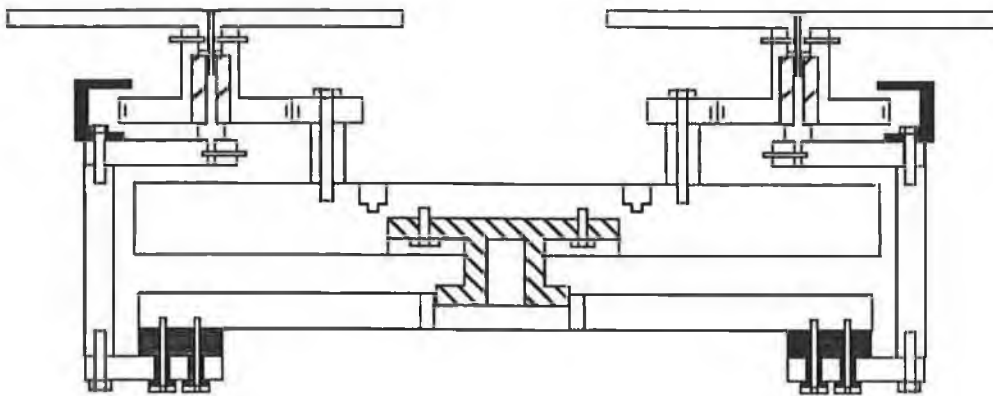


Fig.A.7 Assembly for substrate motion (section).